USGS NEHRP Final Technical Report

Project Title:

Improving earthquake locations along the Juan De Fuca Plate Boundary System

USGS Cooperative Agreement:

05HQGR0174

Principal Investigator:

Charles J. Ammon
Department of Geosciences, Penn State
440 Deike Building
University Park, PA 16802
Email: cja12@psu.edu / FAX: 814-863-7823

Graduate Student Assistants:

Mr. Thomas Van DeMark, January-May, 2005
Ms. Minoo Kosarian, June-December, 2006.

Time Period:

January 2005 - December 2006

Nontechnical Summary

Precisely locating earthquakes in regions outside dense regional networks remains a challenging problem. The PI proposes to apply and to refine a method to incorporate regional and teleseismic surface waves to provide precise relative locations of moderate-size earthquakes off the west coast of California, Oregon, and Washington (the Juan de Fuca Plate Region). Preliminary applications of the method show substantial improvements over standard USGS National Earthquake Information Center (NEIC) body-wave travel time based locations (as well as other global catalogs). The major objective of this proposal - improved relative earthquake locations for several hundred moderate-size events across the JFPR will help more clearly delineate tectonic structures in the region and provide important constraints on the relationships between aseismic and seismic slip, between moderate-size seismicity and geometric heterogeneities in faults, and between mainshock slip and aftershock processes across the region. The work has implications for improved global locations and could provide a useful tool for the NEIC.

Investigation Undertaken

The goal of this project is to provide precise relative earthquake locations along the boundaries of the Juan de Fuca Plate. These boundaries and the southern (Gorda region) are the most seismically active regions adjacent to the conterminous United States. Understanding this activity is important to the tectonic framework associated with the Cascadia subduction zone and the northern San Andreas Fault system - two important sources of seismic hazard in the United States. Knowing the locations of these earthquakes is also important for understanding their causes (in detail). From a more general perspective, precise relative locations can provide insights into such fundamental phenomena as earthquake interaction (such as Coulomb & dynamic stress triggering), which relates to important problems in earthquake physics.

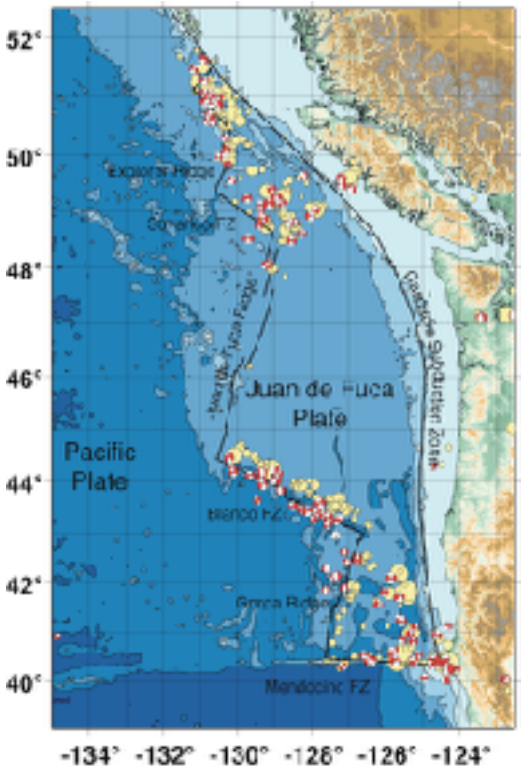

Target events for relocation using surface waves. Events are shown only for the time period from 01 January, 1990 to the present. Focal mechanisms for the approximately 128 events with GCMT solutions in the study region. The region contains clusters of strike-slip and normal faulting events. For the same time period the NEIC catalog contains just under 350 events with magnitudes larger than 4.5.

Scientific Results

We collected and analyzed data from the moderate-to-large magnitude strike-slip faulting earthquakes along the oceanic transforms within the Juan de Fuca Plate boundary system. The transform with the largest data set that we have collected exists for the Blanco Fracture Zone. The scientific results are summarized in the attachment, which is the 2006 M.S. Thesis of Tom Van DeMark and in the manuscript cited on the next page - Cleveland, Van Demark, and Ammon (2016). The 2016 publication included and improved on my and Tom's initial efforts.

In addition to our work on the Juan DeFuca Boundary System, Tom Van DeMark completed a study of earthquake locations along six other transforms to explore potential biases in the algorithm. The work is documented in his Penn State Master's Thesis, which is listed in the publications list below. Since that time, with other funding I had a PhD student more fully develop the theory behind the ideas and we later published several papers related to the methodology. In 2016, with Tom VanDeMark, we extended the 2006 work to include much of the northeast Pacific Region - the work is documented in Cleveland et al. (2016)

Publications Acknowledging This Contract:

Manuscripts:

Ammon, C. J., H. Kanamori, T. Lay, and A. A. Velasco, The 17 July 2006 Java Tsunami Earthquake (Mw = 7.8), *submitted to Geophys. Res. Letters, August, 2006*.

Velasco, A. A., C. J. Ammon, and T. Lay, A search for seismic radiation from late slip for the December 26, 2004 Sumatra-Andaman (Mw = 9.15) earthquake, Geophys. Res. Lett., 33, L18305, doi: 10.1029/2006GL027286, 2006.

Ammon, C. J., A. A. Velasco, and T. Lay, Rapid estimation of first-order rupture characteristics for large earthquakes using surface waves: 2004 Sumatra-Andaman earthquake, *Geophys. Res. Lett., 33*, L14314, doi:10.1029/2006GL026303, 2006.

Student Theses

Van DeMark, Thomas, Moderate and Large Earthquake Activity Along Oceanic Transform Faults, Penn State, June, 2006.

Publications Building Directly on This Work:

I could not attach this document to the current report because of file-size limitations. However, the work documented in the citation below (the article is available from the American Geophysical Union and) is the most recent (and in many ways the completion) of the work of this project.

Cleveland, K. M., T. F. VanDeMark, and C. J. Ammon (2015), Precise relative locations for earthquakes in the northeast Pacific region, J. Geophys. Res. Solid Earth, 120(10), 6960–6976, doi:10.1002/2015JB012161.

The Pennsylvania State University
The Graduate School

MODERATE AND LARGE EARTHQUAKE ACTIVITY ALONG OCEANIC TRANSFORM FAULTS

A Thesis in
Geoscience
by
Thomas F. VanDeMark

Submitted in Partial Fulfillment
of the Requirements
for the Degree of

Master of Science

May 2006

Thomas F. VanDeMark

The thesis of Thomas F. VanDeMark was reviewed and approved* by the following:

Charles J. Ammon
Associate Professor of Geosciences
Thesis Advisor, Chair of Committee

Kevin P. Furlong
Professor of Geosciences

Eliza Richardson
Assistant Professor of Geosciences

Katherine H. Freeman
Professor of Geosciences
Associate Head of the Graduate program in Geosciences

*Signatures are on file in the Graduate School.

Abstract

I analyze precise relative locations for moderate magnitude oceanic transform earthquakes derived using Ammon's (2003) adaptation of the double-difference location method, which exploits information contained in intermediate period (30 - 80 s) Rayleigh waveforms. Utilizing seismograms from events during the last 25 years, I focus on the Romanche, Chain, Blanco, Chile, Eltanin, Udintsev, and Balleny transform systems and explore spatio-temporal patterns in moderate-magnitude oceanic transform earthquake activity. Seismicity patterns along these seven active transforms exhibit a range of behavior. Specific short-term earthquake interactions occur, but do not dominate the moderate magnitude activity. Events larger than $M_W \sim 6.0$ appear to interact on most of the transforms, but their small numbers make a quantitative statistical analysis difficult. Moderate-size activity appears to migrate along segments of several transforms at a rate of 10-30 km/yr, perhaps driven by slow deformation at depth. The existence of large events on each transform requires at least part of oceanic transforms to have relatively deep seismogenic zones. But low seismic coupling coefficients and the spread in moderate-size earthquake activity along most of the transforms, suggest that estimates of the seismogenic zone depth using a 600° isotherm (from simple thermal models) may be too large.

Table of Contents

List of Figures

List of Tables

Acknowledgments

I acknowledge W.H.F. Smith and P. Wessel, the authors of the GMT software used to compose many of the figures in the thesis, IRIS and the IRIS Data Management Center for supplying the seismograms used in the relative location analysis. This work was partially supported by USGS Award Number 05HQGR0174.

I would also like to acknowledge my entire committee for their input and guidance during my time here at Penn State. I would like to especially thank Dr. Chuck Ammon for his expertise and being a hard, but fair advisor. He has shown me that doing good science is indeed hard work and that it is okay to work a week to write two sentences.

Finally I would like to acknowledge my friends and family who have supported me physically and mentally, especially during the last few weeks of the thesis writing process.

Thank you All!

Chapter 1

Oceanic Transform Faulting

1.1 An Overview

In this thesis I document my investigation of moderate-magnitude seismicity patterns along oceanic transform faults (OTFs). The thesis is composed of two main chapters and several appendices containing supporting material. In this chapter, I review a number of important OTF characteristics that have been investigated by other researchers. I have recomputed some quantities discussed in these earlier studies to take advantage of seismic activity that has occurred since the original publications. My goal is to provide the reader with some background on the current state of knowledge regarding OTF seismogenic "zones", including ideas on seismicity rates, aftershock sequences, and seismic coupling characteristics. Chapter 2 contains a description of the original work that I have performed to explore OTFs seismicity patterns using substantially improved earthquake epicentroid locations. The improved locations allows us to clarify some of the earlier ideas and to better explore temporal variations in OTF seismic activity. My thesis research is in many ways an observational study - the goal is not necessarily to test a specific hypothesis, but to help better characterize earthquake processes that occur on OTFs.

1.2 Earlier Studies of OTF Seismicity

Since the 1980's, a number of thorough investigations of the frictional state along subduction plate boundaries have been undertaken (*e.g.* Lay et al., 1982; Pacheco *et al.*, 1995, etc.). This work built on the efforts of many to establish reliable event magnitudes and locations in historical earthquake catalogs (*e.g.* Gutenberg and Richter, 1954; Duda, 1965; Abe and Kanamori, 1980; Pacheco and Sykes, 1992). The results were often expressed in terms of seismic asperity distributions or seismic coupling coefficients. Less frequent activity, along with poorer event location resolution, limited our ability to perform analogous studies along the oceanic transform faults. Only recently has a comparable analysis been completed (Boettcher and Jordan, 2004), although a number of earlier investigators have used the available data to explore descriptive statistics of activity along OTFs (*e.g.* Burr and Solomon, 1978; Okal and Langenhorst, 2000; Frohlich and Apperson, 1992; Bird *et al.*, 2002). And several more focussed investigations have provided our best glimpses into seismic activity along these important plate boundaries. In this chapter I review the key results of earlier studies and where appropriate, update the work by re-applying the same analysis methods to the growing catalog of oceanic transform earthquakes.

Bird *et al.* (2002) identified approximately 500 oceanic transform fault segments, with a total length of approximately 44,400 km. Unlike their continental strike-slip counterparts direct study of OTFs is expensive and difficult, so we rely on seismologic methods and remote sensing (gravity, sonar, *etc.*). Our efforts are limited by scarce oceanic sea floor instrumentation, historically short and incomplete earthquake catalogs, and no geodetic observations. Focussed investigations using hydrophone arrays (*e.g.* Forsythe *et al.*, 2003; McGuire, 2003) have provided some high-resolution information on small-magnitude seismicity processes, and multi-beam imaging of high-resolution bathymetry (*e.g.* Ligi *et al.*, 2002) have provided valuable geomorphic constraints on surface tectonics and transform structure. These and other studies have provided important insight into transform processes, but generalizations from these efforts are hindered by their spatial and temporal limitations.

Arguing from analogy with continental and subduction seismicity, we can iden-

tify a number of factors that may affect patterns in seismic activity along OTFs. Earthquake static stress interaction, where stress changed induced by one event may advance or retard rupture on nearby OTF segments (*e.g.* Stein, 1999). Working with many of the same earthquakes, Gomberg (2001) noted the potential for dynamic stresses associated with near-field shear waves may advance activity on nearby faults or fault segments and the triggering of small seismic events by large surface waves has been well documented (*e.g.* Kilb *et al.*, 200; Marone, 2000; Gomberg *et al.*, 2004; West 2005). Unlike most continental transforms, OTFs are also susceptible to stress perturbations from volcanic activity, including dike injections (*e.g.* Gudmundsson *et al.*, 2000) and aseismic deformation in the form of "slow earthquakes" is thought to be an alternate method of stress transfer on OTFs (*e.g.* Ihmle and Jordan, 1994) (Boettcher and Jordan, 2004) (*e.g.* McGuire *et al.*, 1996; Forsythe *et al.* 2003); although this theory remains controversial (Abercrombie and Ekström, 2001).

1.3 OTF Rheology

One important control on plate boundary system rheology is the thermal state, which for a Ridge-Transform-Ridge (RTR) OTF is governed by the thermal processes of the bounding ridges. Each transform has a separate tectonic history but a standard, albeit simplified, view of the RTR OTF thermal structure of the lithosphere can be constructed by averaging the thermal structure of oceanic lithosphere on either side of the fault. An example is presented in Figure 1.1, which was computed by averaging the thermal profiles for a standard oceanic half-space model (*e.g.* Stein and Wysession, 2003). The assumed thermal diffusivity was 10^{-6} m^2/s (Stein and Wysession, 2003; Boettcher and Jordan, 2004). The key feature of the increase in area available for earthquake activity on transforms separating slower moving plates (length also plays a role). In addition to the obvious fault length, the primary control on the seismogenic area is the depth to the unstable-stable sliding transition, which is assumed to occur near the 600°C isotherm, a value estimated seismically, and using simple models such as that shown in Figure 1.1 (Abercrombie and Ekström, 2001; Boettcher and Jordan, 2004).

The simple model used to construct Figure 1.1 omits a number of interesting

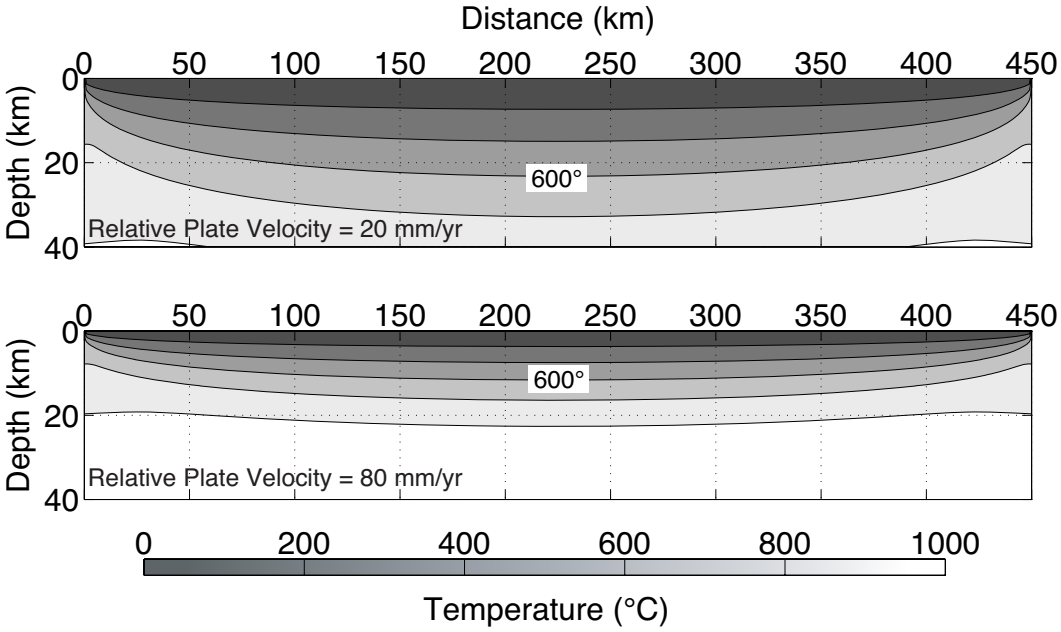

Figure 1.1. Approximate thermal structure for two 450 km long transforms with full relative plate velocities of 20 mm/yr and 80 mm/yr respectively. The contour interval is 200°C. The transition from unstable to stable sliding is believed to occur near the 600°C isotherm (based on seismic evidence, *e.g.* Abercrombie and Ekstrom, 2001). Figure courtesy of Charles J. Ammon.

aspects of OTF structure, foremost of which is the transfer of heat across the transfer. Furlong *et al.* (2001) presented calculations from coupled thermal-mechanical models that showed temperature perturbations along the the length of the transform of up to 100°C at depths just below the seismogenic region. Perturbations were largest near the ridge-transform intersection, where the plate boundary at depth grew more complicated. Ligi *et al.*, (2002) defined two classes of transforms: The classic, simple, narrow boundary envisioned by Wilson (1965) and a multi-fault system with a broad deformation zone, similar to continental strike-slip zones like the San Andreas and the North Anatolian Fault Systems. Detrick *et al.* (1993) studied the mid-Atlantic Ridge transforms and recognized two types of lithospheric structure with transforms: Type A is similar to regular oceanic intraplate crust, but it slightly thinner (4-5 km) with relatively lower seismic wave speeds; type B crust is thin (2-3 km) with seismic wave speeds much different than typical oceanic lithosphere. Along some transforms, the upper mantle may

only be 1-2 km beneath the seafloor due to an unusually thin or missing zone of sheeted dikes. The relatively hot lithosphere and the abundance of water creates an environment conducive to the serpentinization of the shallow mantle material, and such serpetinite has a low fracture strength and a low coefficient of friction. As little as 10% serpentinization of mantle rock can reduce rock strength by more than a factor of two (Escartin *et al.*, 2001). This relatively weak material is considered a key factor in the aseismic behavior of OTF systems. Ihmle and Jordan (1994) proposed that the stratification of oceanic lithosphere maybe responsible for the compound nature of some events. They suggested that fast ruptures in the seismogenic zone are triggered by slower episodes of smooth slip loading in the subjacent upper mantle. Abercrombie and Ekström (2001) countered this argument by presenting transform earthquakes with well-constrained depths as deep as 20 km. They suggested that aseismic slip does not have to occur at depth, but could occur within shallower serpentinized zones.

1.4 Earthquake Catalogs and OTF Seismicity

Mapping the moment deficit (essentially the difference in observed and expected slip from plate motions) on OTFs remains an unresolved fundamental issue. Unlike continental strike-slip faults, which show little or know moment deficit (Stein and Hanks, 1998), oceanic transform faults display a wide range of moment deficiency, with estimates ranging from nearly half to virtually no slip occurring seismically. Values appear to vary with relative plate motion velocities, transform length, and regional tectonic settings, but such broad scale moment deficit estimates are complicated by the short observing time of the more accurate earthquake catalogs, and high resolution estimates on particular fault segments are limited by imprecise earthquake locations.

I focus on the active transform fault along a fracture zone between two spreading ridges that accommodates shear between plates. More specifically I investigate only those boundaries for which the relative velocity vector of the plates (based on the NUVEL-1A model (DeMets et al., 1994)) is within 45° of the fault strike (after Bird et al., 2002). When mechanism information is available, oceanic transform earthquakes are identified as events with a b-axis plunge greater than or equal

to 45° and a location within 1° of the OTF. For broader analyses using observations from the last century events are assumed to be useable if they fall within the geographical area of known strike-slip mechanism events. Figure 1.2 is a map on which the OTFs investigated in this study are identified by the plotted focal mechanisms.

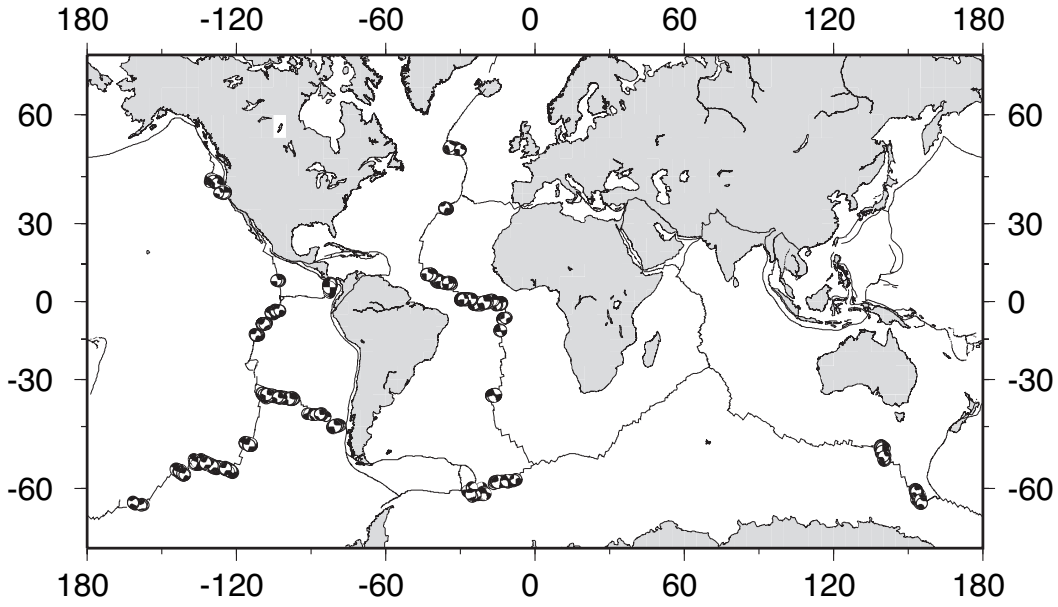

Figure 1.2. Focal mechanisms of earthquakes located on the oceanic transform faults investigated in this study. Mechanism information from the Harvard CMT catalog (1977-early 2006). Plate boundaries from UTIG are shown as solid lines.

For recent events (1977 to the early 2006) I use the Harvard Centroid Moment Tensor (CMT) Catalog (*e.g.* Dziewonski *et al.*, 1980) for moment rate deficiency calculations, and earthquake frequency-magnitude statistics. The availability of faulting geometry information in the CMT catalog eases identification of transform faulting earthquakes. A less detailed composite earthquake catalog spanning just under 90 years, from 1918 to early 2006, was used to look at broader scale patterns (a large event from January 2006 was important enough to include in the analysis). This composite catalog is an integration of information from several well known historical catalogs: Gutenberg-Richter (GR), International Seismic Summary (ISS), Coastal Geodetic Survey (CGS), Berkely Seismic Catalog (BRK), and the USGS earthquake catalog. The composite catalog facilitates our study of

moment-rate deficiency and foreshock/aftershock sequences.

1.5 Moment Rate Deficiency Analysis

In this section I describe my use of the Harvard CMT catalog to map the moment deficiency along a selection of the more active oceanic transform faults. I compare the seismic moment observed in earthquakes along 30 transform faults, estimated using the 28-year catalog of moderate-to-large earthquakes to the expected equivalent rate of moment release from a plate kinematic model (NUVEL-1A). The work is an update of the earlier effort by Okal and Langenhorst (2000). By summing the scalar moments of events from each transform and dividing by the total duration of the catalog we estimate the observed seismic moment release rate. We calculate an expected moment release rate using plate motions (essentially scaling the relative plate slip). A number of assumptions are necessary to make a comparison. The primary control on the area available for faulting are the transform length (at least to some minimum value) and seismogenic-zone depth extent. In most cases, the depth of unstable sliding is believed to be thermally controlled and correlated with the 600° isotherm (*e.g.* Engeln *et al.*, 1986; Stein and Wysession, 2003). We follow Okal and Langenhorst (2000) and estimate the OTF seismogenic contact area A^{pred} using:

$$A^{pred} = \frac{2}{3} \cdot L \cdot \sqrt{\frac{64 \text{ km}^2}{10^6 \text{ yr}} \frac{L}{v}} \tag{1.1}$$

where L is the fault length in km, v is the relative plate velocity across the OTF in km/yr, and 64 km^2/10^6 yr is a constant characterizing the thickening seismogenic lithosphere (Stein, 1978). The predicted equivalent seismic moment rate, $\dot{M}_0^{pred}$ can then be estimated using:

$$\dot{M}_0^{pred} = \mu v A^{pred} \tag{1.2}$$

where $\mu = 3 \times 10^{11} dyne/cm^2$, is the rigidity of the oceanic lithosphere. Using the ratio of observed to predicted seismic moment rate we can calculate the moment-

rate deficiency as a percent:

$$\dot{M}_0^{deficiency} = (1 - \dot{M}_0^{obs}/\dot{M}_0^{pred}) \times 100\%. \tag{1.3}$$

The observed seismic moment, $\dot{M}_0^{obs}$, is the sum of the seismic moments in the CMT catalog divided by the catalog duration.

Seismic coupling strength or χ (Scholz, 2002) is similar to our calculation of $\dot{M}_0^{deficiency}$ and is calculated as:

$$\chi = M_0^{obs}/M_0^{pred} \tag{1.4}$$

Previous researches have used χ to infer fault strength and the amount of aseismic slip that occurs on a fault (*e.g.* Boettcher and Jordan, 2004. By multiplying the $\dot{M}_0^{obs}$ and the $\dot{M}_0^{pred}$ individually by the duration of the catalog we can determine M_0^{obs} and M_0^{pred} and therefore χ. I compare my results of χ to that of Boettcher and Jordan's study (2004) in Table 1.1.

The resulting deficiencies are approximately corrected for the variation in the depth of the seismogenic zone with plate speed. Thus, the first order differences between the thermal structure of the slow and fast spreading plates are at least approximately accounted for in the moment rate deficiency estimation. If one assumes that no seismicity is missing (not always a good assumption), you can interpret the moment-rate deficiency (MRD) as the component of aseismic slip occurring in the system at seismogenic depths. MRD's for the 30 individual OTFs are tabulated in Table 1.1. Here I focus on trends in the values as a function of relative plate velocity across the boundary. Figure 1.3 is a chart showing the estimated moment rate deficiencies for the investigated transforms. Diamonds indicate those transforms that have hosted events with moment magnitudes larger than M_w 6.5 in the last 28 years.

A number of cautions are necessary before interpreting the CMT-based observations. The short duration of the catalog is a serious limitation - over the CMT time interval slower moving transforms are unlikely to have accumulated sufficient slip to insure the occurrence of the largest earthquake possible in the system. Simple estimates for slow plate motions suggest large event recurrence intervals should be much longer than the catalog length. This point was well illustrated by

Table 1.1. Predicted and observed rates of moment release.

Transform	L (km)	Full Rate (cm yr^{-1})	M_w (max)	Fault Area (km^2)	$\dot{M}_0^{pred}$*	$\dot{M}_0^{obs}$*	$\dot{M}_0^{deficiency}$ (%)	χ V&A	χ B&J
Valdivia	650	5.7	5.9	11,700	2.000	0.018	99	0.01	0.01
PAR 62S	260	6.5	5.8	2,800	0.541	0.007	98	0.01	n/a
Acension	270	3.3	5.9	4,100	0.408	0.013	97	0.03	n/a
Wilkes	150	14	5.9	830	0.348	0.011	97	0.03	0.02
Garret	140	14	5.8	740	0.317	0.015	95	0.05	0.05
Eltanin	1,000	8.1	6.4	19,000	4.620	0.247	95	0.05	0.04
Quebrada	190	13	6.0	1,200	0.480	0.026	95	0.05	0.01
Bode Verde	210	3.2	6.2	2,900	0.275	0.016	94	0.06	0.08
Sequeiros	150	11	5.9	960	0.301	0.021	93	0.07	0.06
Chile	1,100	5.6	6.7	27,400	4.610	0.349	92	0.08	0.07
Udinstev	330	7.6	6.4	3,700	0.836	0.067	92	0.08	0.09
Charlie Gibbs	360	2.1	6.7	7,900	0.501	0.056	89	0.11	0.12
Doldrums	740	2.8	7.0	20,300	1.700	0.183	89	0.11	0.12
Bullard	530	1.7	6.6	15,800	0.805	0.095	88	0.12	0.08
St. Paul	530	3.0	6.6	11,900	1.100	0.136	88	0.12	0.12
Guafo	300	5.8	6.4	3,600	0.633	0.091	86	0.14	n/a
George V	420	6.9	6.5	5,500	1.140	0.157	86	0.14	0.10
Discovery	80	13	6.1	330	0.131	0.018	76	0.24	0.19
Blanco	420	5.4	6.4	6,200	1.010	0.091	81	0.19	0.10
Panama	470	6.5	6.8	6,700	1.310	0.254	81	0.19	n/a
Menard	210	8.7	6.4	1,740	0.454	0.087	81	0.19	0.15
Mendocino	270	5.3	7.0	3,300	0.517	0.102	80	0.20	n/a
Gofar	110	13	6.2	540	0.212	0.050	76	0.24	0.12
Balleny	340	6.5	6.7	4,100	0.809	0.214	74	0.23	0.25
Oceanographer	160	2.1	6.3	2,400	0.148	0.047	68	0.32	0.33
Romanche	900	3.1	7.1	25,900	2.410	0.779	68	0.32	0.27
Vema	300	2.7	6.9	5,300	0.432	0.182	58	0.42	0.37
Tristan da Cunha	250	3.4	6.6	3,600	0.369	0.160	56	0.44	0.37
Chain	250	3.1	6.8	3,800	0.352	0.196	45	0.55	0.38
S. Sandwich	340	1.6	7.4	8,400	0.401	0.620	0	1.00	n/a

*M_0($\times 10^{26}$ dyn cm yr^{-1})

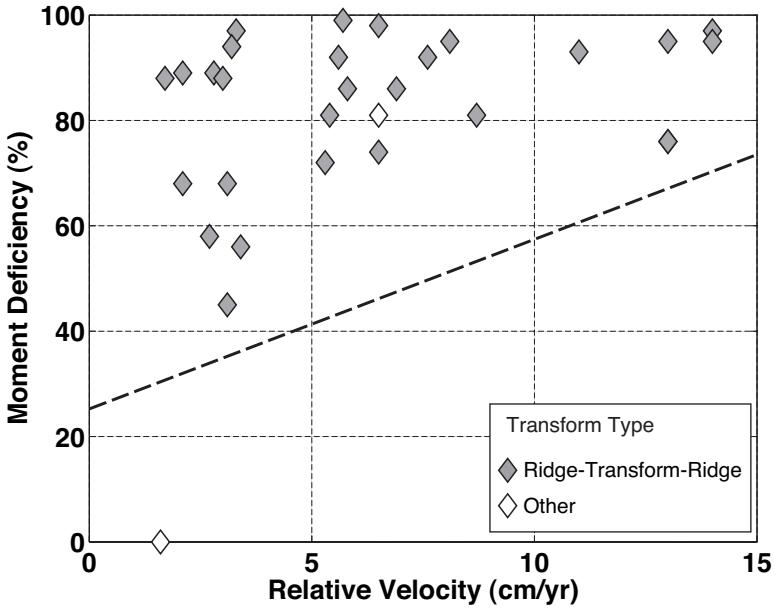

Figure 1.3. Moment deficiency as a function of relative plate velocity. A lower limit to moment deficiency in RTR transforms (the dashed line) is suggested by these data.

recent activity on the South Sandwich Transform, which has the lowest relative plate velocity in our study, 1.6 cm/yr. A major earthquake (M_w 7.4) ruptured the transform on 02 January, 2006. The MRD changed from approximately 60% to effectively 0% following this single event. Although the South Sandwich Transform is not a transform bounded by ridges, it connects the South Sandwich Trench and the Bouvet Triple Junction, the point is that one cannot draw any robust conclusions regarding specific transforms bounding plates with slow relative motions from a short catalog, but some inferences may be possible using the available ensemble of slow-moving transforms. The short catalog duration may explain the large range in moment deficiency seen for transforms with relative low relative plate speeds. Transforms bounding plates with faster relative velocities are a different story, some should have recurrence intervals within the catalog duration.

Previous studies noted that observed total seismic moment along an OTF decreases as relative plate velocity increases (*e.g.* Burr and Solomon, 1978; Frohlich and Apperson, 1992). The simplest inference is that more slip occurs aseismically at depth because the seismogenic area decreases with increasing plate speed. Our data support this observation. The computation of the moment deficiency

includes a correction for the decreasing area with the intention of focussing on the component of aseismic slip occurring within the seismogenic zone. Examination of Figure 1.3 shows that transforms bounding relatively fast moving plates such as the East Pacific Rise have a uniformly high moment deficiency but the lower bound of Figure 1.3 decreases systematically with decreasing plate speed. If the approximate area available for rupture correction used to compute the predicted moment is correct, then this pattern can be attributed to the higher velocities also limit the area frictionally unstable at seismogenic depths. However, slower transforms have a wide range of moment deficiency values even though it would seem that they would have large areas of frictionally unstable lithosphere to fracture, which should increase their ability to produce seismic moment (e.g. Abercrombie and Ekström, 2001).

No transform with a relative plate velocity greater than 7 cm/yr has hosted an event with $M_w \geq 6.5$. This is consistent with a thermally controlled, thinner seismogenic zone expected along these regions (*e.g.* Boettcher and Jordan, 2004). The slower transforms (relative plate velocities less than 7 cm/yr) may likely host a large event in the future. However, it is common to assume that the strength of coupling across the transform is characterized by the percentage of moment rate deficiency and the size of the earthquakes on the transform (*e.g.* Lay *et al.*, 1982; Boettcher and Jordan, 2004). So we may suggest from this observation that separate older (on average), slower moving plates have a higher coupling strength than those separating faster, younger plates (on average).

1.6 Gutenberg-Richter Analysis

In this section I investigate the size distribution of transform fault earthquakes using the Gutenberg-Richter relationship:

$$log_{10}N = \alpha - \beta M_w \tag{1.5}$$

where M_w is the moment magnitude, N is the cumulative number of earthquakes greater than M_w, α is the N-axis intercept, and β is the slope. I separated the transforms into three groups based on relative plate velocities, 0.0 to 3.9 cm/yr, 4.0

to 7.9 cm/yr, and greater than 7.9 cm/yr. The separation results in three populations with roughly the same number of earthquakes, which enables an exploration of patterns between relative plate velocity and earthquake magnitude distributions. I constructed a cumulative frequency-size distribution for each group (Figure 1.4). The threshold magnitude (m_t) and corner magnitude (m_c) for each distribution were estimated by visual inspection. The slope (β) for the each distribution was estimated using the magnitude range bounded by m_t and m_c. The threshold magnitude is simply an estimate of the catalog completeness, which as evident from Figure 1.4, has a value approximately equal to 5.5 for the Harvard CMT on OTFs.

In subduction zones, the corner magnitude, m_c, can be related to the size of the seismogenic zones and interpreted as indicating the size earthquake that ruptures the vertical extent of the seismogenic zone (*e.g.* Pacheco and Sykes, 1995). Earthquakes with a larger magnitude begin rupturing more along strike of the structure than vertically. Using the same ideas on the transform faults produces results consistent with this idea. As relative plate velocity decreases the corner magnitude and the size of the largest earthquake on a given transform increases (*e.g.* Burr and Solomon, 1978; Bird *et al.*, 2002). Estimated values of m_c are tabulated in 1.2. We see a clear increase in m_c with decreasing relative plate velocity (Figure 1.4). The 0.0 to 3.9 cm/yr group has a $m_c \approx 6.5$, while the 4.0 to 7.9 cm/yr group has a $m_c \approx 6.2$, and the greater than 7.9 cm/yr group has an $m_c \approx 6.0$. These observations support a fundamental concept that faster transforms have a thinner amount of frictionally unstable lithosphere that can be fractured. The first-order control on these values is likely the depth of faulting coinciding with an isotherm (often assumed to be 600°C), which remains relatively shallow on faster transforms (*e.g.* Engeln *et al.*, 1986).

Table 1.2. Gutenberg-Richter Relation Parameters

Relative Plate Velocity (cm/yr)	m_t	m_c	β	L_{Total}
$v < 4$	5.5	6.5	0.9	4,500
$4.0 \geq v < 8.0$	5.5	6.2	1.1	4,560
$v \geq 8.0$	5.5	6.0	1.5	2,030

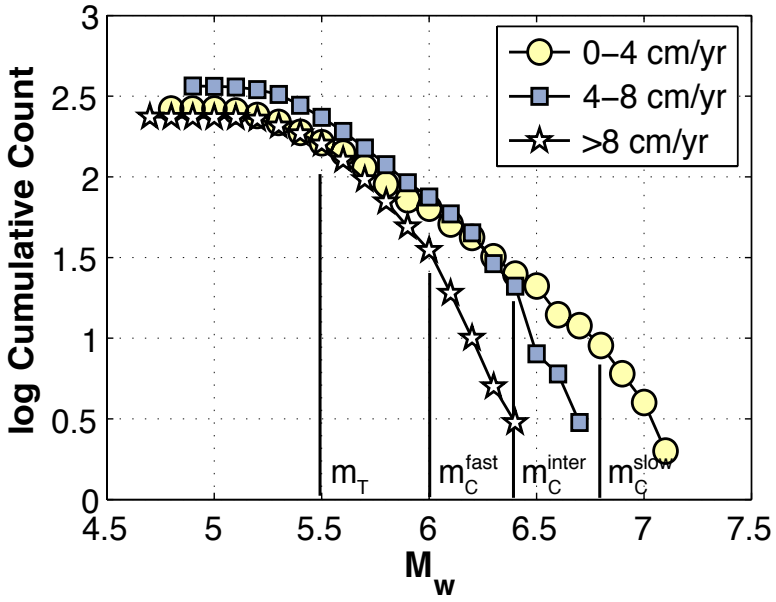

Figure 1.4. Gutenberg-Richter relationships for strike-slip CMT solutions globally. The event populations are sorted into velocity groupings (0-3.9 cm/yr, 4-7.9cm/yr, and 8 cm/yr) and all plots are cumulative counts. We note that as relative velocity increases, corner magnitude decreases, and beta decreases.

Between m_t and m_c, the Gutenberg-Richter distribution is an indication of the earthquake size distribution between large asperities within the seismogenic zone (the large asperities rupture in events with magnitudes larger than m_c). Typical global values for the slope are approximately unity (*e.g.* Stein and Wysession, 2003). A relatively steeper, more negative slope, $\beta > 1$, indicates a fault that favors small event activity, a more sub-horizontal slope, $\beta < 1$, indicates a fault that favors larger events compared with global patterns.

Okal and Langenhorst (2000) suggested that along transforms β correlates negatively with relative plate velocity (as velocity increases, β decreases), but those results were disputed by Bird *et al.* (2002). Bird *et al.* (2002) argued for the use of a tapered Gutenberg-Richter relationship, which assumes a constantly decreasing slope, which combats the limited range between m_t and m_c and the assumption that there is no portion of the frequency-magnitude relation that is not affected by m_c. Bird *et al.* (2002) suggested that the small event populations were the source of error in Okal and Langenhorsts (2000). In any event, we should be care-

ful of how much significance we place on such results since β values may vary from catalog to catalog and because the log number versus magnitude relation is rarely linear over the considered magnitude range. Furthermore, intuition and evidence suggests that the value of β changes with the tectonic regime (*e.g.* Frohlich and Davis, 1993; Theiner and Velasco, personal communication).

I repeated the simpler calculations of Okal and Langenhorst (2000) and assumed a linear frequency-magnitude law to calculate β (Figure 1.4) with a larger distribution of events than used in the original study. The three separate groups have a similar number of events, with a minimum of 234 events in the fastest plate velocity category. The total length of transform included in each category differs, which affects the total number of events in each category (Table 1.2), but does not affect the shape of the curves. Correcting the curves for total length would result in a shift of the > 8 cm/yr curve upward by about 0.3 log units. Although I did no formal statistical analysis, visual inspection of Figure 1.4 suggests that all three populations form a nearly linear frequency-magnitude relation from m_t to m_c. The β value for all events combined is 1.0, consistent with global observations. Estimated values of β are tabulated in Table 1.2. The results support Okal and Langenhorst's (2000) inference - I see a clear decrease in β as relative plate velocity increases. A 22% increase is observed between the slow and intermediate groups and a 36% increase is noted between the intermediate and fast group.

The results are consistent with the observation that the larger earthquakes occur along transforms separating plates moving at relatively slower rates. In general there is thought to be a relation between β and frictional heterogeneity on the fault (Kisslinger and Jones, 1991). As β increases, the fault becomes more heterogeneous. This agrees with the above observation that β increases as faults become slower, and coincides with Searles (1986) observation that faster transforms are usually simpler due to the thinness and the weakness of the fast spreading lithosphere, which lends itself to a homogeneous fault plane and a low β value.

1.7 Conclusion

Earlier investigations of OTF seismicity have produced a number of robust observations. As known for some time, large events are restricted to the trans-

forms bounding slower-moving plates. The cut-off in large-event activity appears relatively sharp at a relative plate velocity of about 7 cm/yr. The increase in moment-rate deficiency with increasing relative plate offset rates, which presumably indicates a larger fraction of aseismic slip in seismogenic depths, is consistent with a OTFs dominated by stable sliding friction. Large asperities and hence large events are absent along OTFs separating relatively fast-moving plates. Gutenberg-Richter relation slopes support these observations, as they are consistent with a heterogeneous frictional state distribution on OTFs bounding fast-moving plates. The corner magnitude cutoff for these same transforms are consistent with thermal ideas that predict a thinner seismogenic zone along OTFs separating fast moving plates.

In the next chapter, I describe my investigation of patterns in OTF seismicity using greatly improved relative locations for events predominantly from the last 15 years, at which time the establishment and growth of global seismic networks produced a rich collection of waveforms I use to improve locations. The ultimate goal of that effort is to better characterize OTF seismogenic zones and to explore temporal patterns in OTF earthquakes. I explore the patterns much the same way that earlier workers have explored seismicity statistics - looking for correlations with relative plate speed, transform length, the occurrence of large events, *etc.* Fewer transforms have hosted a sufficient number of events during the short 15 year time span, so I focus my relocation efforts on seven transforms with a relatively high level of moderate-magnitude seismic activity.

Chapter 2

Spatial & Temporal Patterns in Oceanic Transform Seismicity

2.1 Introduction

Substantial effort has been focussed on the study of strike-slip fault systems such as the San Andreas, North Anatolian, and central Asian systems. Study of these large, accessible structures is important to advance our understanding of fundamental plate-tectonic processes and to better resolve and mitigate natural hazards. OTFs have received less attention because in their remoteness they present no hazard and are much less accessible. They are, however, key components in the global plate-tectonic processes. While generally viewed to be structurally simpler than their continental counterparts, a number of the larger OTFs are substantially more seismically active than similar-size continental systems. Table 2.1 provides a comparison of the number of observation between two oceanic and continental shear zones and Figure 2.1 illustrates the point. Although of roughly equal lengths, the Chile OTF has hosted about six times as many moderate and larger earthquakes in the last 28 years. The more active OTFs are an excellent source of observations to draw conclusions and even construct fundamental hypotheses regarding faulting and shear zone deformation, as well as to understand earthquake physics more deeply.

For example, the limited number of data available from the continental systems hampers our ability to investigate such fundamental earthquake processes as

earthquake interaction. In contrast, active OTF systems produce a wealth of data regarding strike-slip faulting, but quantitative seismic investigations are generally limited by inaccurate and imprecise event locations. In this paper, we present and analyze precise OTF earthquake locations derived using Ammon's (2003) adaptation of the double-difference location method developed by (Waldhauser and Ellsworth, 2000). Specifically, we produce precise relative earthquake epicentroids along the Romanche, Chain, Blanco, Chile, Eltanin, Udintsev, and Balleny OTFs using intermediate-period Rayleigh waveforms. Our relocations are much more precise than body-wave locations available in standard earthquake catalogs, generally producing relative locations with a precision of a few kilometers.

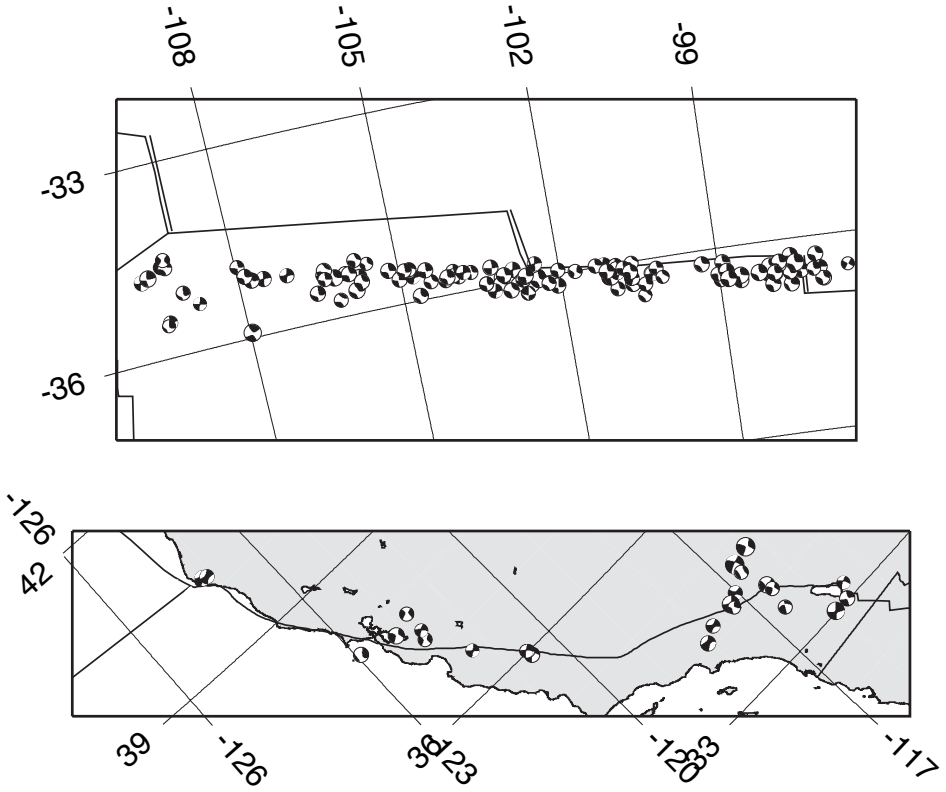

Figure 2.1. Oblique Mercator projection maps showing the moderate and large earthquakes that have occurred on the Chile OTF and the San Andreas Fault System of California. The Chile system has hosted almost 6 times as many recent (Harvard CMT) events in this magnitude range. The offset in the Chile transform system locations is partly the result of the biased and imprecise nature of catalog locations.

Table 2.1. Comparison of the number of events in the Harvard CMT (1977 to Present) on select continental and oceanic shear zones of similar length.

Type	Fault Zone	Length (km)	Plate Velocity (mm/yr)	Number of Events
Oceanic	Chile F.Z.	1,100	59	123
Oceanic	Eltanin F.Z.	1,000	83	92
Continental	San Andreas	1,100	40	21
Continental	N. Anatolian	1,300	65	21

2.2 Relative Epicentroid Location Using Rayleigh Waves

2.2.1 Observations

The fundamental observation used in the relocation scheme are vertical-component Rayleigh wave displacement seismograms. For nearby events with similar faulting geometries and depths, the Rayleigh waveforms are characteristic, and small shifts in the arrival time of the waves can provide valuable information on the relative positions of the sources (Figure 2.2). The large amplitude R1 waveforms are have a remarkably consistent shape from event to event, and the lower phase-velocities make these signals more sensitive to epicenter shifts than the corresponding teleseismic body waves.

We used the Harvard CMT catalog to identify OTF transform faulting events between 1980 to early 2006. Faulting geometry screening was performed by requiring that the b-axis plunge was greater than 45° and that the original event location was within 1° of the OTF. Furthermore, we only included events that are between the transform bounding spreading ridges. We selected the seven transforms based on the number of moderate and larger size events during the time spanned by the establishment (mid-1980's) and rapid expansion (1990's) of the Global Seismic Network (*e.g.* Butler *et al.*, 2004). Since we are working with Rayleigh waveforms, we ignore the effect of depth and focus on locating the faulting centroid, or epicentroid.

For each event, we acquired the raw vertical component signals from the IRIS

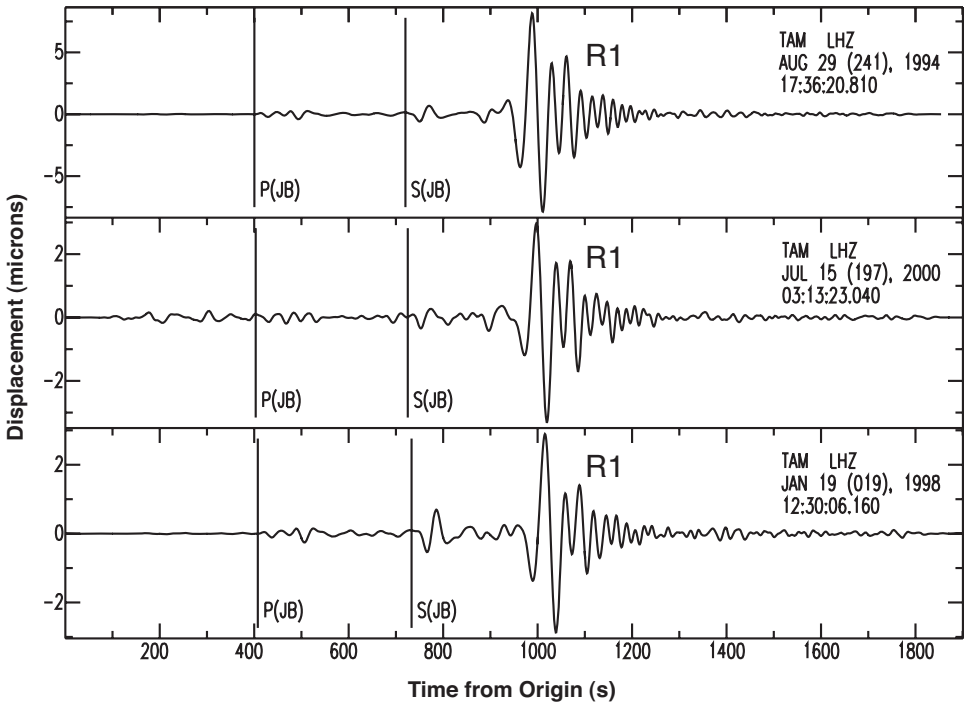

Figure 2.2. Characteristic Rayleigh waveforms recorded at Tamanrassett, Algeria, for three events located along the Romanche Transform in the equatorial Atlantic. The P and S arrival times, and the short-arc Rayleigh wave (R1) are labeled. The signals have been low-pass filtered with corners at 30 and 80 seconds period.

Data Management Center (DMC) and computed displacement seismograms. Each seismogram was visually inspected and assigned a quality rating (A-F) within a velocity group window of 2.75 to 4.00 km/s. Example waveforms and quality factors are shown in Figure B.1. Earlier events (*c.a.* 1980's) had as few as 12 waveforms but more recent events had upwards to 400 waveforms. The number of observations increased most rapidly around 1990. Only quality A-C signals were used in subsequent analyses, and then only when they met correlation and linking distance criteria described below.

As with all double-difference location methods (*e.g.* Waldhauser and Ellsworth, 2000) our fundamental assumption is that a cluster of events that are relatively close together in comparison to the event-station distance have similar ray-paths. The only place an earth model enters the problem is near the sources. Rayleigh-wave time shifts were measured using a straight-forward time-domain cross correlation signal computed across the period range from 30 to 80 seconds. The

observations in this signal band often retain a characteristic shape that minimizes problems associated with cycle-skipping on dispersed Rayleigh waves. We only included time shifts that correspond to signals producing a normalized correlation value of at 0.75 (maximum of 1.0), and only include events for which we have at least eight acceptable waveform correlations. The long wavelengths associated with the band-limited Rayleigh waves (>100 km) minimize the impact of sharp variations in seismic wave speeds on the analysis; in fact, the phase-velocity for typical oceanic lithosphere in this bandwidth is relatively constant (*e.g.* Nishimura and Forsyth, 1989), and corresponds to slowness values between 0.27 and 0.32 km/s. The slow variation in Rayleigh wave slowness allows us to work with a uniform slowness model across each OTF. We experimented with values across the expected range to assess the affect our assumption has on the results (which was minor). For particularly long transforms a gradual variation across the region could cause some distortion of the locations, but the same limitation applies to all the common location procedures and does not appear to be a strong factor in our results.

An important control parameter in double-difference inversions is the maximum distance over which allow events are allowed to link. We tested maximum link distances of 25, 50, and 125 km. All three values are comparable to one half a wavelength near the center of our bandwidth (about 50s period, or 200 km wavelength). A smaller linking distance insures that only events close by are included in the inversion, but depending on the initial spread in the locations, the small value may fail to link events that were simply originally grossly mislocated. After numerical tests we chose the 125 km maximum link distance because it compensated for large location errors in the original NEIC locations, and because we could not detect any substantial distortions in the overall pattern of seismicity as a result of the aggressive linking.

The relative insensitivity of the Rayleigh waves to depth allows us to examine the cross-correlation derived time-delays for consistency using a simple azimuthal display. We show four examples in Figure 2.3. In each panel, circles represent all time-shift estimates (including those from poorly correlated observations), the gray sinusoid is the pattern expected from the original NEIC locations, and the black sinusoid shows an L_1 fit of a sinusoid to the observations. The sinusoidal correlation is the last quality check applied to the observations. If an event fails to

show an expected sinusoidal pattern with any other events, it is removed from the double-difference inversion. In other words, we assume that events that correlate over a wide range of azimuths have mechanisms and source depths similar enough to allow a precise relative location.

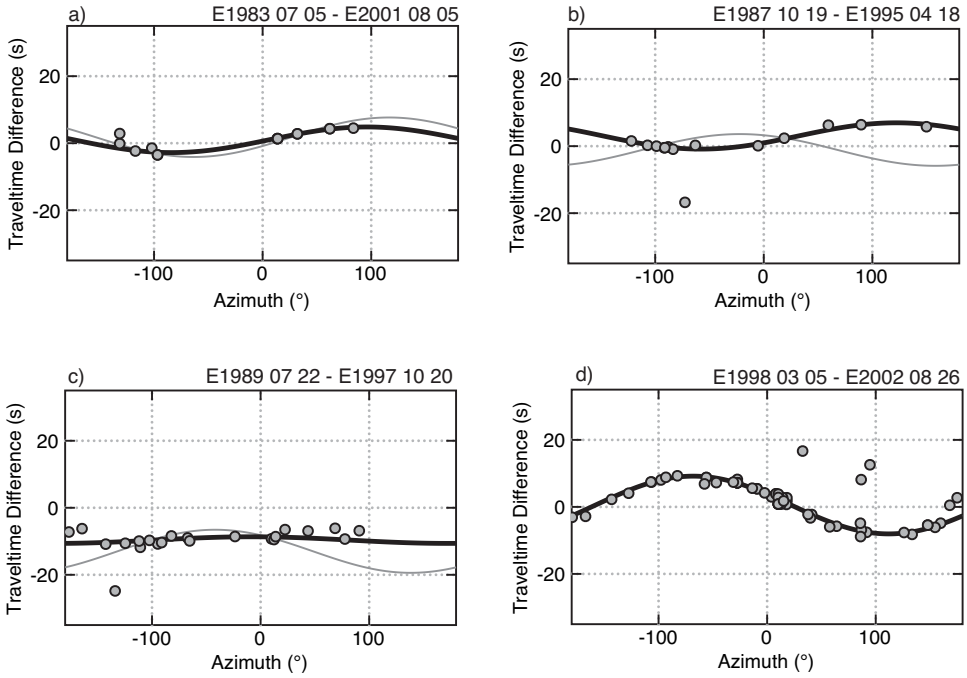

Figure 2.3. Examples of sinusoid patterns as a result of plotting phase shift residuals with azimuthal distribution. These examples show how the optimal shifts become better constrained through time and how the distance between linked events increases the amplitude of the sine curve. The link distance for (a) is 8 km, for (b) is 46 km, for (c) is 37 km, and for (d) is 17 km. The light gray line shows NEIC locations, the solid black line show our locations, and the symbols show the phase shift residual between the two linked events at a particular station.

2.2.2 Double-Difference Epicentroid Inversion

The double-difference inversion was performed using a spherical earth version of the double-difference equations of Waldhauser and Ellsworth (2000). A nonlinear estimation problem is set up linking the observed and predicted differences in Rayleigh-wave delay from all stations and events with the partial derivatives with

respect to position and time. Specifically,

$$\mathbf{P} \cdot \delta\mathbf{h} = \delta\mathbf{t} \tag{2.1}$$

where $\mathbf{P}$ is a matrix of double-difference partial derivatives for the epicentroid latitude, longitude, and the centroid time, $\delta\mathbf{h}$ is a correction vector for the epicentroid parameters, and $\delta\mathbf{t}$ contains the double-difference residual vector. Equation (2.1) is solved iteratively until convergence. The initial locations are the epicenters and origin times reported by the US Geological Surveys National Earthquake Information Center (NEIC). For larger events we expect some movement of the hypocenter simply because the epicenter and epicentroid are shifted relative to one another. For smaller magnitude events, ruptures are smaller and the difference may only be a few kilometers. A similar argument applies to the difference between origin time and centroid time, which is the temporal quantity that the Rayleigh waves sense. Equation (2.1) contains no information on absolute location or time, so we can only resolve relative locations and relative centroid time differences adjusted for the NEIC origin times.

We inverted the equations with a singular value decomposition using LAPACK routines (Anderson et al., 1999) and applied minimum length constraints on the correction vector (*e.g.* Waldhauser and Ellsworth, 2000). Each iteration includes three inversions with iteratively reweighted observations to reduce the sensitivity to outliers. The iterative weights were computed from the misfits - any misfit larger than 3.0 seconds was assigned a weight equal to — 3.0 / dt — where dt is the time shift residual. Otherwise the weight was unity. The cutoff at 3.0 seconds was chosen based on the fit of better data in early applications of the inversion (Ammon, 2003). The iterative algorithm produces a result that approaches an L_1 optimization of the fit to the observed arrival time differences. The inversions described below all converged within a few iterations and remained stable with further iteration.

The partial derivatives with respect to colatitude and longitudes have a very simple form (Stein and Wysession, 2003) but they require an estimate of the wave's horizontal slowness. We used an average value of 0.3 s/km for the Rayleigh waves. This slowness may be a little high for the period range but the true value is

certainly between 0.25 to 0.3 s/km (4.00 to 3.33 km/s phase velocity). An error in the assumed slowness value maps directly into the location uncertainty. If we assume that we can measure the time shift to within about 2 seconds (based on the observations), then our distance uncertainty is between 6 and 8 km. The uncertainty associated with choosing a single slowness from the range 0.25 to 0.30 s/km is less than about 20% of 8 km, which is less than 2 km. The RMS values from the double-difference inversion are closer to 1 second, so the above analysis is conservative. The small range in horizontal slownesses of the surface waves makes this method relatively insensitive to a reasonably chosen slowness. Although a formal estimate of our location uncertainty is difficult to demonstrate, direct examination of the observed time shifts and geometric consistency of the results along the relative simple transform structures suggest that many relative locations are accurate to better than five kilometers.

2.2.3 Precise OTF Earthquake Relative Locations

Relative epicentroid locations along the seven transforms were calculated using a 125 km linking distance, a minimum 75% cross-correlation value, and a uniform slowness of 0.30 s/km. Using these criteria and the data screening procedures described above, we have were able to relocate an average of 94% of the earthquakes included in the analysis. The lowest relocation success rate occurred along the Romanche Transform system, where only 76% of the events were relocated, the highest relocation success rate was along the Balleny transform, where all events were relocated. These success rates compare favorably with body-wave studies, but we are looking at much larger events. The majority of events that we could not relocate occurred prior to 1990, when station coverage was low. We summarize the inversion parameters and fits to the double-difference observations in Table 2.2. The weighted fits to the observed data were comparable to the sample rate of the long-period channels used in the analysis, which is about the best one should expect with the simple cross-correlation method employed. Pushing the results to sub-sample rate precision would produce fits much more precise than warranted given intrinsic variations in surface-wave slowness.

We first review the re-locations for each transform system and then follow

Table 2.2. Table of links, differences, and residuals for each OTF.

Transform	# Events	# Links	# Double Differences	Unweighted Residual	Weighted Residual
Balleny	36	298	10,479	10.09	1.36
Blanco	35	90	5,396	36.33	1.07
Chain	23	105	5,305	10.48	1.31
Chile	123	646	25,986	44.03	1.46
Eltanin	92	687	41,424	63.91	1.29
Romanche	51	110	646	22.06	1.55
Udintsev	32	220	12,104	62.71	1.43

with an analysis of the seismicity patterns observed with the high-resolution relative locations. Lists of all the relocated events are tabulated in the Appendices. Bathymetry shown on the maps is predicted from satellite altimetry and ship sounding (Smith and Sandwell, 1997). Throughout the discussion we distinguish between large and small events. We define a large event as one that would rupture a 10-15 km deep seismogenic zone, which assuming a stress drop of $3MPa$ and a simple scaling relation for the slip as a function of length (Boettcher and Jordan, 2003),

$$D = \frac{\Delta\sigma}{\mu} L^{1/2} W^{1/2} \tag{2.2}$$

where D is the slip, $\Delta\sigma$ is stress drop, L is the fault length and W is the fault width (depth of the seismogenic zone). If we assume that $L = W = 10$ km we estimate 1 m of slip and the associated moment magnitude for this slip and area is $M_W \approx 6.3$. Equation 2.2 allows us to place the boundary between "large" and "small' at $M_W \approx 6.3$. But the variation with moment is is continuous, and we caution the reader that the distinction between a M_W 6.2 and 6.3 cannot be considered substantial. We try to account for this subtlety in our discussions.

The Chain Transform. The Chain Transform system, located in the equatorial Mid-Atlantic Ridge, is approximately 250 km long and bounds plates more at a relative plate velocity of 3.1 cm/yr. Figure 2.4 shows the initial (NEIC) and final locations for the events along the system. This short transform includes two distinct seismicity clusters, both of which host moderate and large seismicity ($5 \leq M_W \leq 7$). These two clusters are separated by an approximately 30 km

section of sub-seismicity between them. Several seismic gaps are present at each end of the transform adjacent to the spreading ridges and perhaps one near the middle of the transform, possibly near a bend in the system. Finally, we observe that the largest seismicity ($M_W \geq 6$) is centered within each seismic cluster.

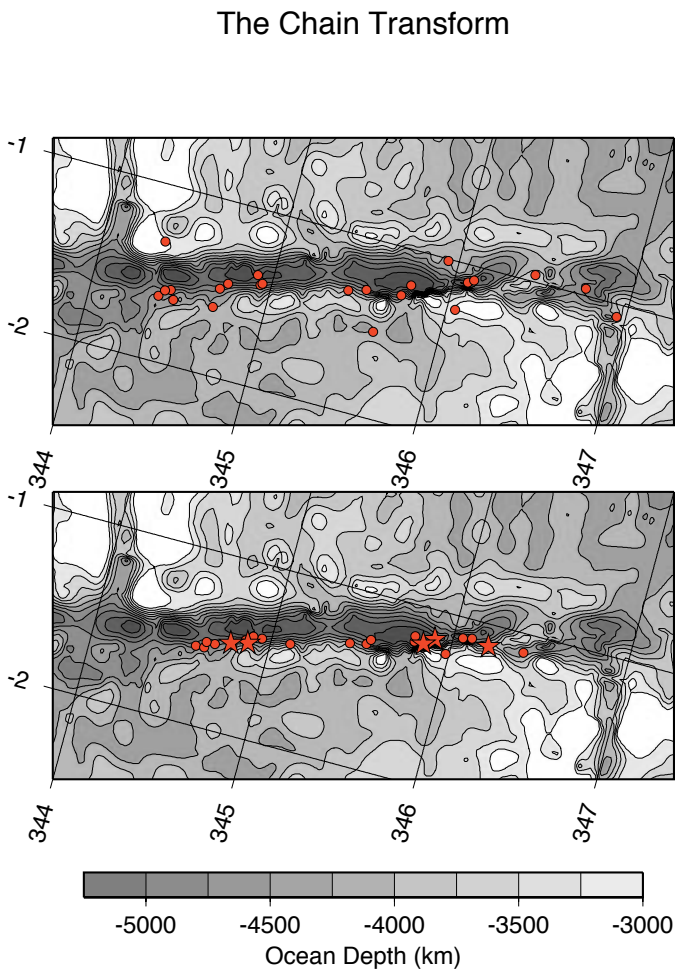

Figure 2.4. Event location maps for the Chain Transform system. The top panel shows the initial NEIC locations, the bottom the Rayleigh-wave relocations. Stars are events of $M_W \geq 6$ and circles identify smaller magnitude events. Bathymetry from ETOPO 02 is shown with shading. The schematic plate boundaries are interpreted from the bathymetric profiles shown.

The Udintsev Transform. The Udintsev Transform system, located on the Pacific-Antarctic Ridge, is approximately 320-330 km long and separates plates

moving with a relative plate velocity of 7.6 cm/yr. Figure 2.5 shows the initial (NEIC) and final locations for the events along the system. Initial locations show a large scatter, but the relocation are relatively tightly clusters along the length of the transform. No events with M_W larger than 6.3 have occurred west of -143E, but two events with M_W equal to 6.3 have occurred to the east. Londsdale (1994) suggested that the Udintsev system was split by a short offset ridge near -142.25E. We see some evidence for an offset across this longitude, events to the left on Figure 2.5 seem shifted slightly up relative to those on right. Some structure is evident within the relocations, including several subclusters. The transform system appears to have some extended width, perhaps indicative of several active, *en echelon* fault strands, consistent with Lonsdale (1994).

The Balleny Transform. The Balleny Transform system, located along the Australian-Antarctic Ridge, is approximately 350 km in length and bounds plates with moving a relative plate velocity of 5.1 cm/yr. Figure 2.6 shows the initial (NEIC) and final locations for the events along the system. Initial locations show a large scatter, but the relocation are relatively tightly clusters along the length of the transform. Initial locations in this remote part of the southern hemisphere are widely dispersed, but the relocations show a relatively simple structure. Two events are located off the main pattern, which has a concentration of large events along the southern section. The largest event was an $M_W = 6.7$. Events along the main trend include several tight clusters with substantial distance between. Shifting the entire pattern slightly northward would increase the correlation with the bathymetry.

The Blanco Transform. The Blanco Transform system is approximately 400 km in length and separates the Juan De Fuca and Pacific plates, which move with a long-term relative plate velocity of 5.4 cm/yr. The moment-rate deficiency for the entire system is about 80-90% (Chapter 1, Boettcher and Jordan, 2004). Morphologic investigations suggest that the system is separated into 5 segments with a total length of about 350 km (Dziak *et al.*, 1991). Figure 2.7 shows the initial (NEIC) and final locations for the events along this system. We inherit a northeastern bias from the initial NEIC locations; all the epicentroids are shifted

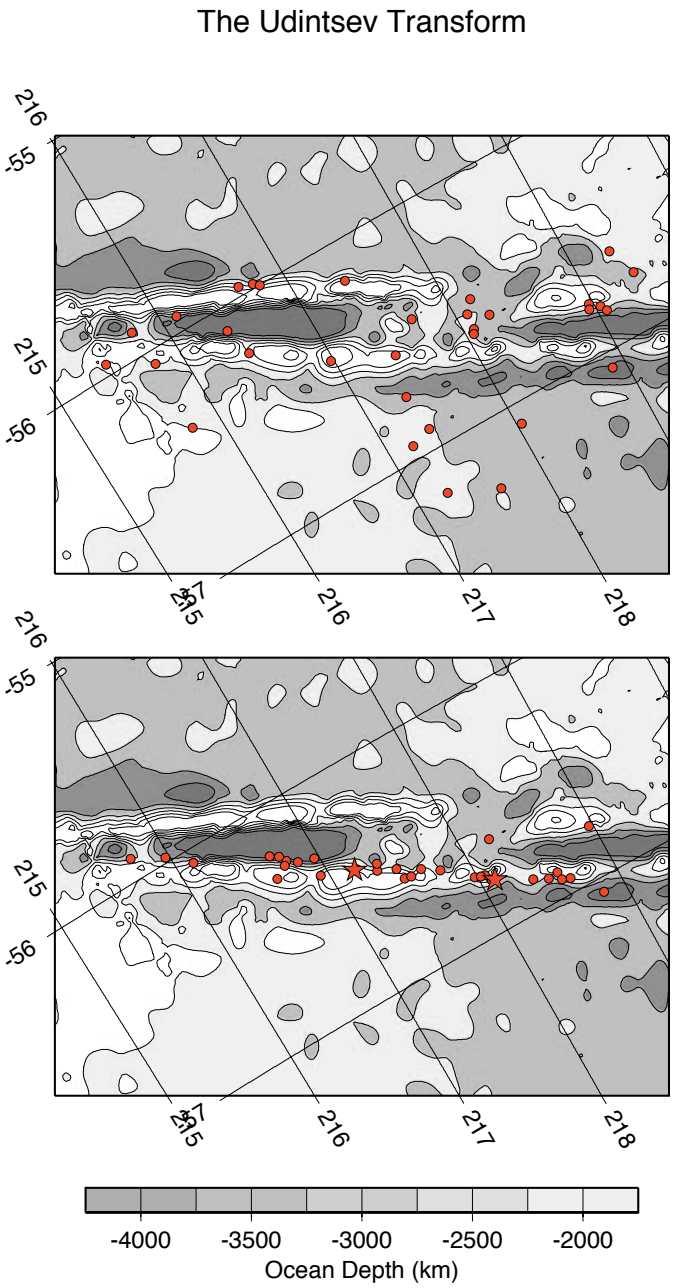

Figure 2.5. Event location maps for the Udintsev Transform system. The top panel shows the initial NEIC locations, the bottom the Rayleigh-wave relocations. Stars are events of $M_W \geq 6$ and circles identify smaller magnitude events. Bathymetry from ETOPO 02 is shown with shading. The schematic plate boundaries are interpreted from the bathymetric profiles shown.

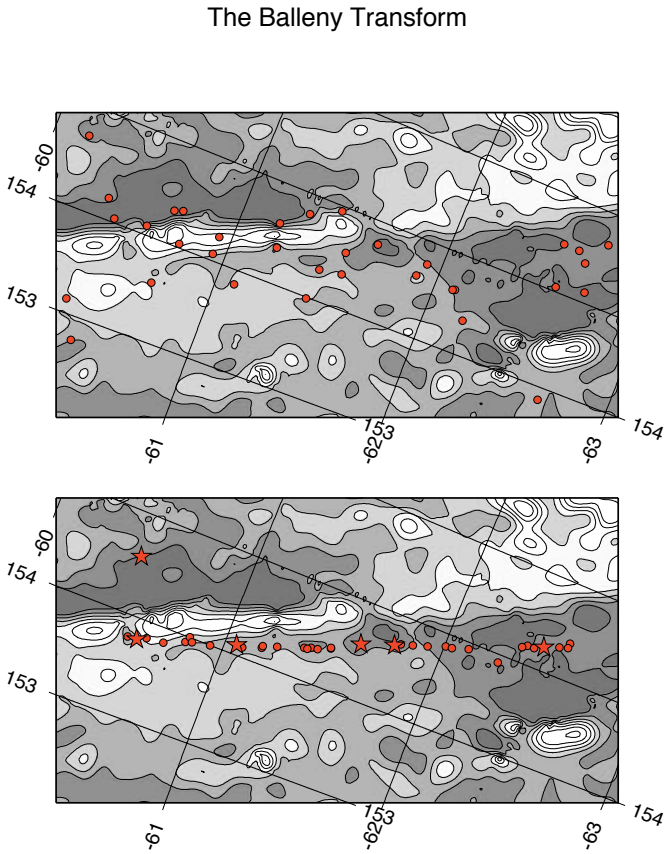

Figure 2.6. Event location maps for the Balleny Transform system. The top panel shows the initial NEIC locations, the bottom the Rayleigh-wave relocations. Stars are events of $M_W \geq 6$ and circles identify smaller magnitude events. Bathymetry from ETOPO 02 is shown with shading. The schematic plate boundaries are interpreted from the bathymetric profiles shown.

northward. As illuminated by moderate and large events, the system has two well-defined seismic segments which are separated by a roughly equal length region that has not had any recent, large transform ruptures. Dziak *et al.* (1991) suggested central area, which contains the Cascadia Depression, is an area of active spreading. Two moderate-size normal faulting events in the Harvard CMT catalog support this hypothesis.

The northwestern segment appears to be relatively simple single fault, but a slightly more complex faulting geometry is an appropriate characterization for the southeastern cluster. We do not see evidence for three segments in our northwestern event cluster, which Dziak *et al.* (1991) inferred from bathymetry. The

two larger events on the northwestern segment occurred after Dziak *et al.*, (1991) noted differences in Gutenberg-Richter *b*-values for the northwestern and southeastern segment (using a 25-year long catalog from 1963-1988). If the larger events occurred on different segments, they suggest that stress changes are felt across the small ridge separating the two segments (*e.g.* Forsyth *et al.*, 2003).

The southeastern segment has a small gap in moderate seismicity but we resolve little offset between the two segments, suggesting that they are on the same structure. Much of the northwestern end of the southeastern segment lacks moderate-size activity. The pattern is evident in Dziak *et al.*, (1991), so the gap appears as far back as the 1960's. Plate rates are such that strain sufficient to produce a magnitude 7 earthquake would have accumulated in the 40-45 year time frame. No events of that size have occurred on the Blanco, two large events occurred in the region in 1914 and 1917. Unfortunately, the locations for these events are poorly known. This southeastern segment also includes four relatively large events that recur approximately every five years and release enough slip to account for that accumulated during plate motions on the same time frame, which implies the segment has little or no moment deficiency. Although detection may play a role in the observation, the Blanco has a high percentage of aftershocks in comparison to other OTFs.

The Romanche Transform. The Romanche Transform system, located along the equatorial Mid-Atlantic Ridge, is approximately 900 km in length and separates plates moving with a relative plate velocity of 3.1 cm/yr. Figure 2.8 shows the initial (NEIC) and final locations for the events along the system. The initial NEIC locations are much less dispersed than along other more remote transforms and the location corrections are less than needed elsewhere, suggesting that original locations may be of higher quality here. Presumably this is related to the the transform proximity to North America and Europe, where data are plentiful. The transform has an even distribution of large events along its entire length. Two distinct moderate-magnitude event clusters occur along the eastern half of the transform and the region between the clusters has hosted a recent large event. Unlike some of shorter transforms, the events along the Romanche do not follow narrow features, the event clusters seem to spread perpendicular as well as

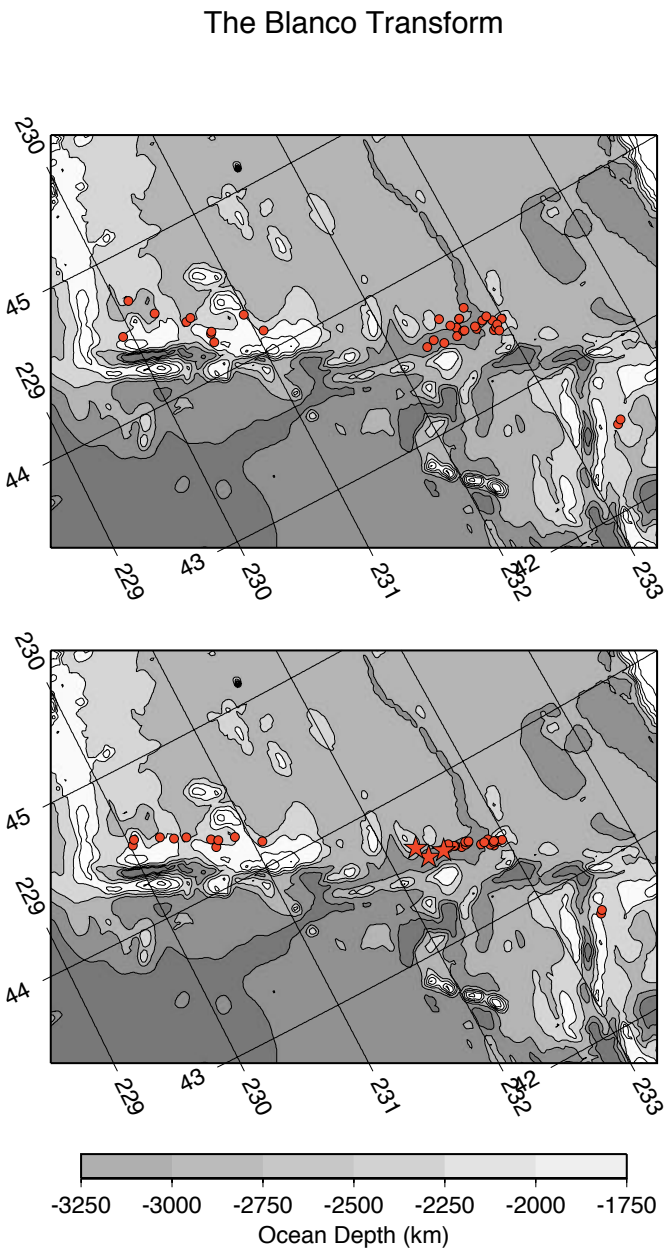

Figure 2.7. Event location maps for the Blanco Transform system. Stars are events of $M_W \geq 6$ and circles identify smaller magnitude events. The top panel shows the initial NEIC locations, the bottom the Rayleigh-wave relocations. Bathymetry from ETOPO 02 is shown with shading. The schematic plate boundaries are interpreted from the bathymetric profiles shown.

laterally to the transform trend. These patterns are consistent with parallel, *en echelon* and/or braided fault systems, which have been previously observed on the Romanche through the use of side scanning sonar (Parson and Searle, 1986). The Romanche can be characterized as a complex, well-coupled transform dominated by relatively large seismic activity.

The Eltanin Transform. The Eltanin Transform system, located along the Pacific-Antarctic Ridge, is approximately 1000 km in length and bounds plates moving with a relative plate velocity of 8.1 cm/yr. Figure 2.9 shows the initial (NEIC) and final locations for the events along the system. The Eltanin is a composite of three smaller transforms: The Hollister, Tharp, and Heezen, each of which are separated by segments of the Pacific-Antarctic Ridge. The Hollister, which is approximately 150 km in length, is dominated by moderate and large seismicity along its entire length; no gaps are apparent. The Tharp, which is approximately 450 km in length, contains two clusters of seismicity located at opposite ends of the transform. A nearly 100 km section of decreased seismic activity separates the clusters. The largest event on the transform is centered in the cluster adjacent to the southeast spreading ridge. The Heezen OTF, which is approximately 400 km in length and contains a large aseismic section approximately 150 km in length. The remaining length of the transform is contains four short seismic clusters separated by short gaps. One possibility is that the cluster of events off the right in Figure 2.9 may have absolute locations along the region with the strong bathymetric gradient. The two clusters of events between -128E and -127E lie in a region that should have a ridge. The transition from the Tharp to the Heezen segments may include some complicated deformation. Our relative locations illuminate a simple, single-strand fault geometry on all three segments, with an exception occurring at the far-east end where complications arise due to interaction with the East Pacific Rise (Lonesdale, 1994). Our locations also show clear separation between seismic clusters, delineating one substantial apparently aseismic segment or gap in the Heezen transform. The far-east cluster on the Tharp (middle transform) is 70% moment deficient - quite remarkable considering the number of events within the relatively short length of the cluster.

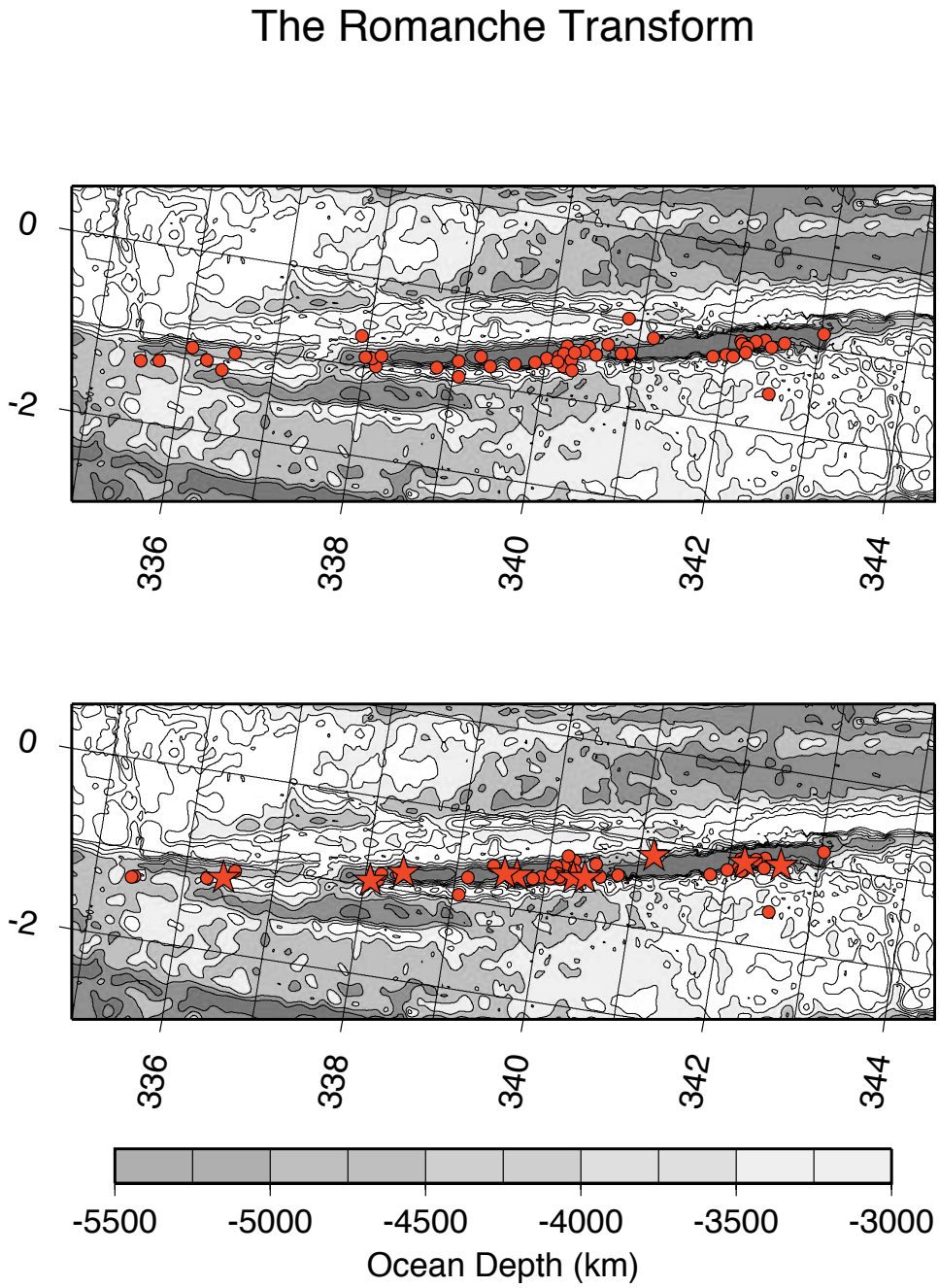

Figure 2.8. Event location maps for the Romanche Transform system. The top panel shows the initial NEIC locations, the bottom the Rayleigh-wave relocations. Stars are events of $M_W \geq 6$ and circles identify smaller magnitude events. Bathymetry from ETOPO 02 is shown with shading. The schematic plate boundaries are interpreted from the bathymetric profiles shown.

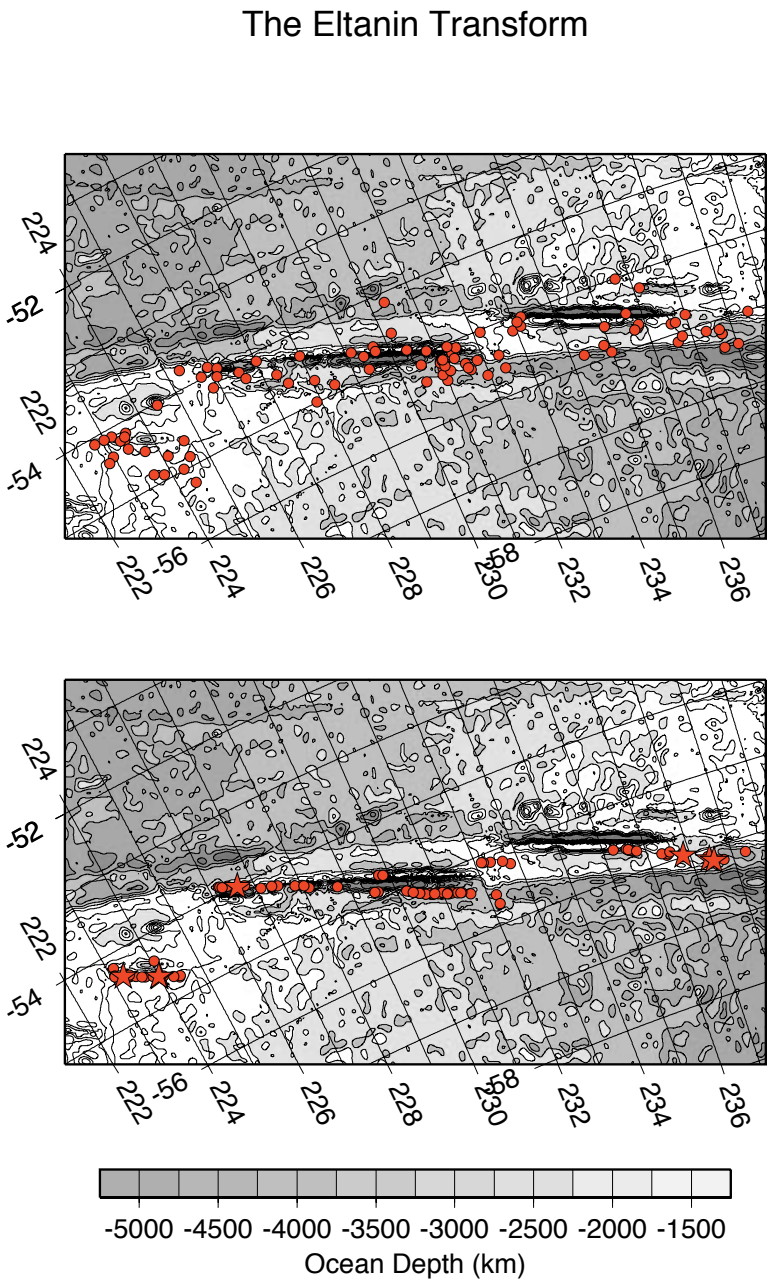

Figure 2.9. Event location maps for the Eltanin Transform system. The top panel shows the initial NEIC locations, the bottom the Rayleigh-wave relocations. Stars are events of $M_W \geq 6$ and circles identify smaller magnitude events. Bathymetry from ETOPO 02 is shown with shading. The schematic plate boundaries are interpreted from the bathymetric profiles shown.

The Chile Transform. The Chile Transform system, located along the East Pacific Rise, is approximately 1,100 km long and separates plates moving with a relative plate velocity of 5.6 cm/yr. Figure 2.10 shows the initial (NEIC) and final locations for the events along the system. The initial locations show increased scatter with distance from the South American coast, although the same is true of the relocated events, including one large nearby, but apparently off-transform event. Activity along the western half of the transform is less linear than that to the east, which trends includes sharply defined linear features between -104E and -102E, -101E and -100E, and -99E and -97E. We observe eight distinct clusters of seismicity along the transform. The clusters vary in length from approximate 50 km to 150 km and the largest separation between clusters is approximately 90 km, and this gap is adjacent to the longest seismic cluster. The Chile OTF is the longest and most seismically active transform in our study, 1,100 km in length, has hosted 123 moderate-size events since 1980, of which only three had $M_W \geq 6$. At least one large seismic gap or aseismic region is apparent along the eastern half of the transform.

2.3 Space-Time Seismicity Patterns Along OTFs

Space-time seismicity diagrams (STSDs) based on the new relative locations for each of the seven transforms are shown in Figures 2.11 through 2.15. All earthquake with $M_S \geq 6$ are denoted by a black star and all earthquakes $M_S < 6$ are denoted by gray circles. Surface rupture length is estimated for all events greater than $M \geq 6$ and a horizontal error bar is used to denote the rupture length. After Abe (1975) we use the scaling equation:

$$M_0 = 1.23 \times 10^{22} S^{3/2} \tag{2.3}$$

to estimate rupture area for these events; where M_0 is the scalar moment in dyne-cm and S is the rupture area in square kilometers. We assumed that the maximum depth of the seimogenic zone to be 10 km. The value may be a little low, but the rupture lengths scale linear with the assumption. If we assume a seismogenic zone thickness near large events to be about 20 km, then we would half the lengths

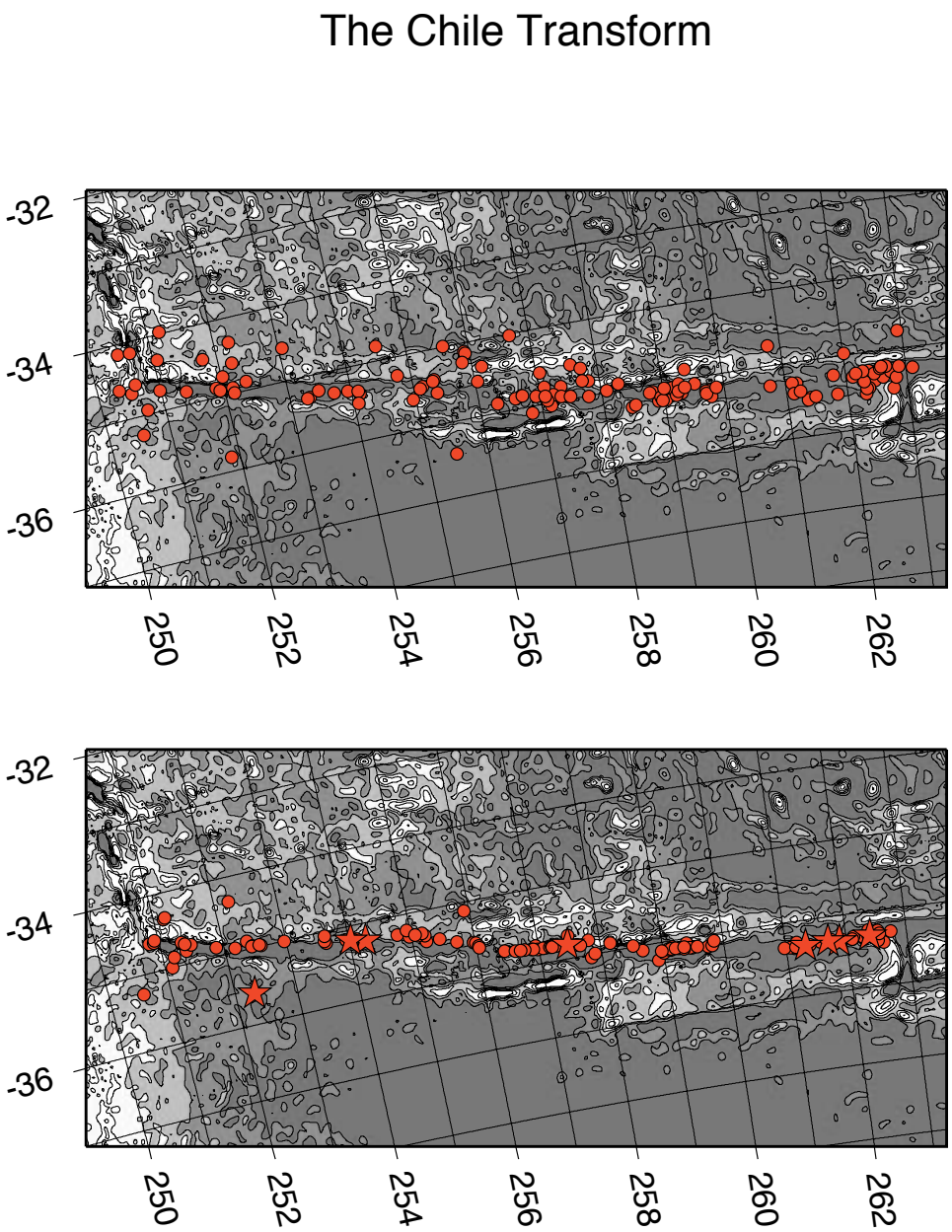

Figure 2.10. Event location maps for the Chile Transform system. The top panel shows the initial NEIC locations, the bottom the Rayleigh-wave relocations. Stars are events of $M_W \geq 6$ and circles identify smaller magnitude events. Bathymetry from ETOPO 02 is shown with shading. The schematic plate boundaries are interpreted from the bathymetric profiles shown.

shown. Previous researchers have calculated seismogenic zone widths from 0.1 to 8 km (Boettcher and Jordan, 2004) but moderate-size earthquake event depths on the Romanche and Chain OTFs have been estimated between 5 and 20 km (Abercrombie and Ekstrom, 2001). For simplicity we assumes that the ruptures were bilateral - many of the events have sparse aftershock sequences, so rupture direction is not well constrained.

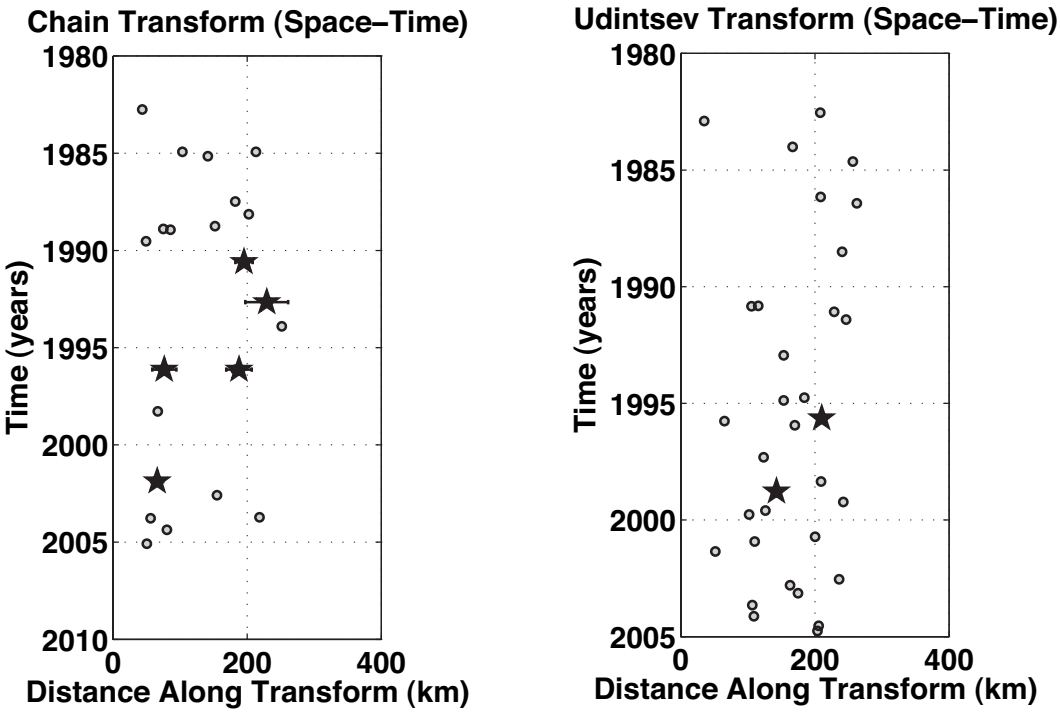

Figure 2.11. Space-time seismicity plots for the Chain and Udintsev OTFs.

Our improved relative locations provide an opportunity to explore a number of intriguing patterns in earthquake activity along OTFs. But a number of factors must be kept in mind while examining the seismicity patterns. First, the time span, limited by the availability of digital seismic data, is short. Even when we have good locations from 1980 on, that's only 26 years. And for some of the remote transforms, all events from the early part of the study may not have had sufficient correlatable waveforms because of sparse station coverage - effectively decreasing the time span. Drawing conclusions regarding the larger events is a particular problem to watch for regarding OTFs separating slow moving plates, where large event recurrence intervals may be much longer than a few decades.

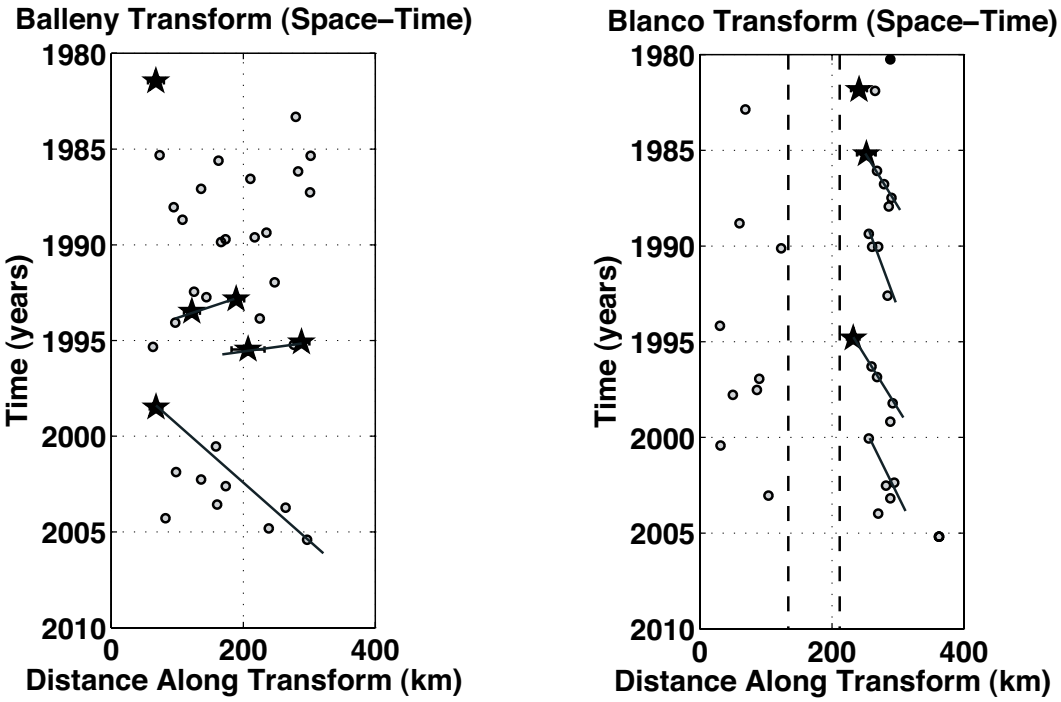

Figure 2.12. Space-time seismicity plots for the Blanco and Balleny OTFs.

To draw conclusions from such a short observing period requires that we look for unusual, repeatable patterns, which favors a focus on smaller events and/or OTFs separating faster moving plates. Despite these limitations, a space-time analyses help us investigate earthquake interactions and migrations along the OTFs in our study. While we don't expect moderate-size activity to interact in a static-Coulomb manner, patterns in the moderate-magnitude events may represent loading from more difficult to detect slower deformation that must occur along structures with such large moment-rate deficiencies.

Earthquake Interaction. Earthquake interaction became a subject of interest as soon as large earthquake catalogs became available (*e.g.* Lay et al., 1982). The $M_W \geq 6$ events seem to interact along adjacent segments of the fault more often than not, although their smaller number makes statistical assessment of the patterns difficult. Since the interaction of larger magnitude events has been carefully analyzed within subduction zones (*e.g.* Lay and Kanamori, 1980) and on continental transform systems (*e.g.* Stein et al., 1997), the idea that they would interact

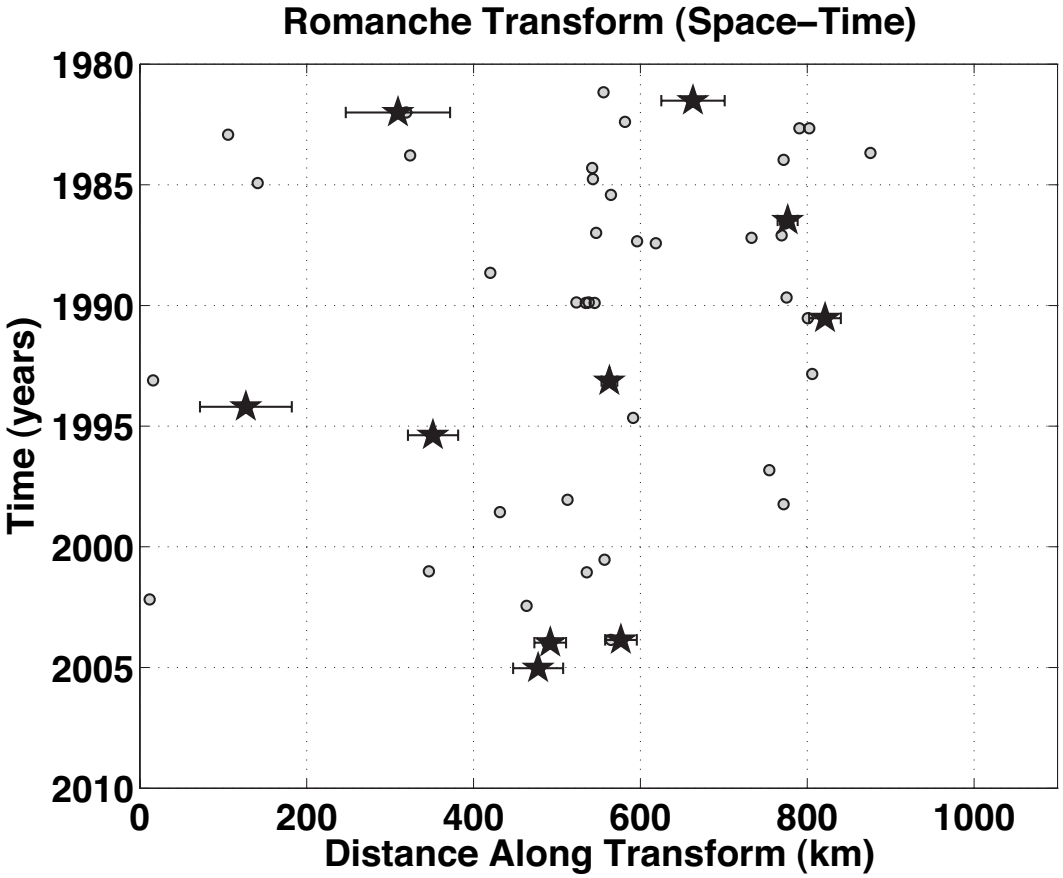

Figure 2.13. Space-time seismicity plot for the Romanche OTF.

probably does not need statistical support. Ruptures from one event often seem to initiate near the end of an earlier event (within a rupture length), although the time between the events varies from months to more than a decade. With the exception of a pair of events on the Chain transform, most of these adjacent ruptures are separated by at least a year. All seven transforms show a number of moderate-size events within close temporal and spatial proximity on the STSDs. Perhaps the most energetic in this regard is the Tharp, (the central segment of the Eltanin), which shows a westward migrating cluster of moderate-magnitude activity between 400 and 600 km, and the years 2000 and 2005. Three particularly tight sub-clusters reside within the larger sequence. A small percentage of moderate-to-large magnitude earthquake doublets can be observed on the STSDs. A doublet is defined as events within 100 km and 30 days of each other, with a

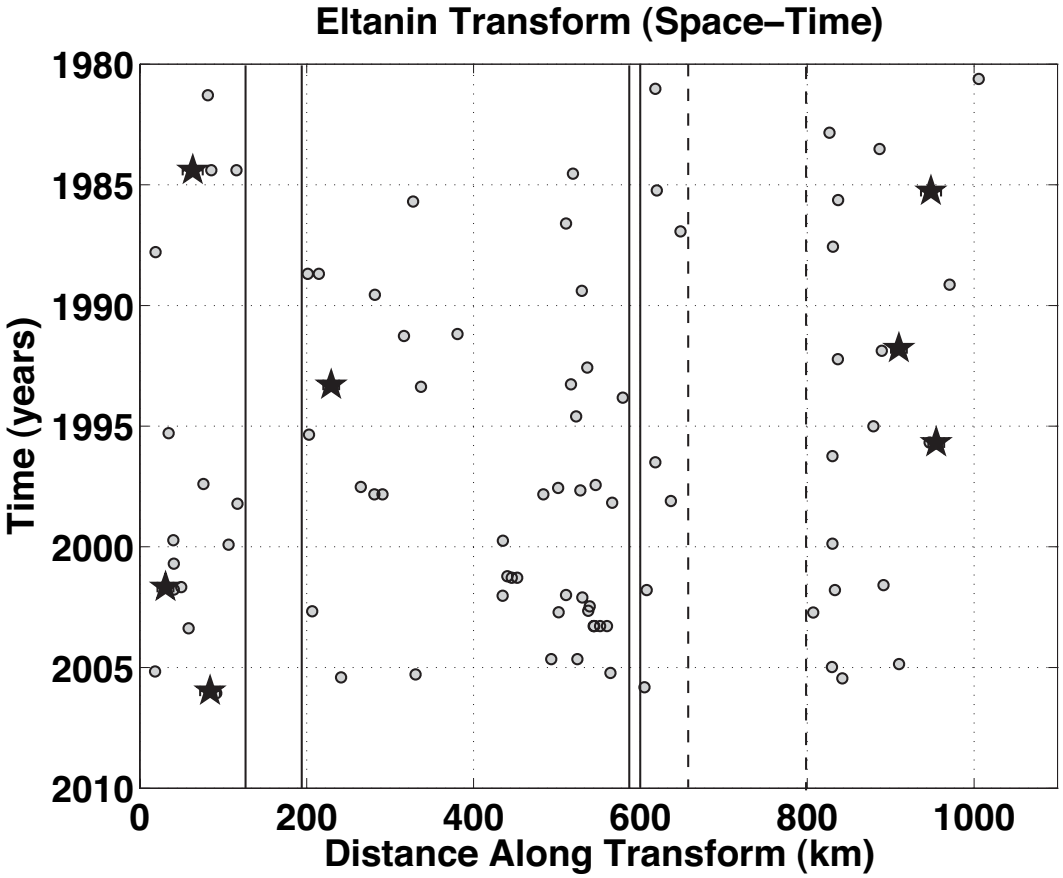

Figure 2.14. Space-time seismicity plot for the Eltanin OTF. Solid lines delineate spreading ridge boundaries, while dashed lines delineate gaps in moderate- and larger-size earthquake activity.

magnitude difference of no more than 0.3 (*e.g.* Lay and Kanamori, 1980). The greatest percentage of doublets occurs on the Romanche with 20% of the relocated events being a doublet; all other values range from 0 to 13%.

We investigated the moderate-size event interaction pattern since it may shed some light on how common earthquakes interact. To help avoid the pitfalls in our analysis, we used random space-time diagrams to investigate the likelihood that certain patterns are probable even from a uniformly random interaction of events. For example, one common observation is a number of close association of events on the diagrams (events nearby in space and time). We used random simulations to construct an ensemble with 100,000 realizations of random space-time seismicity distributions for each OTF (we used the same number of events and fault lengths

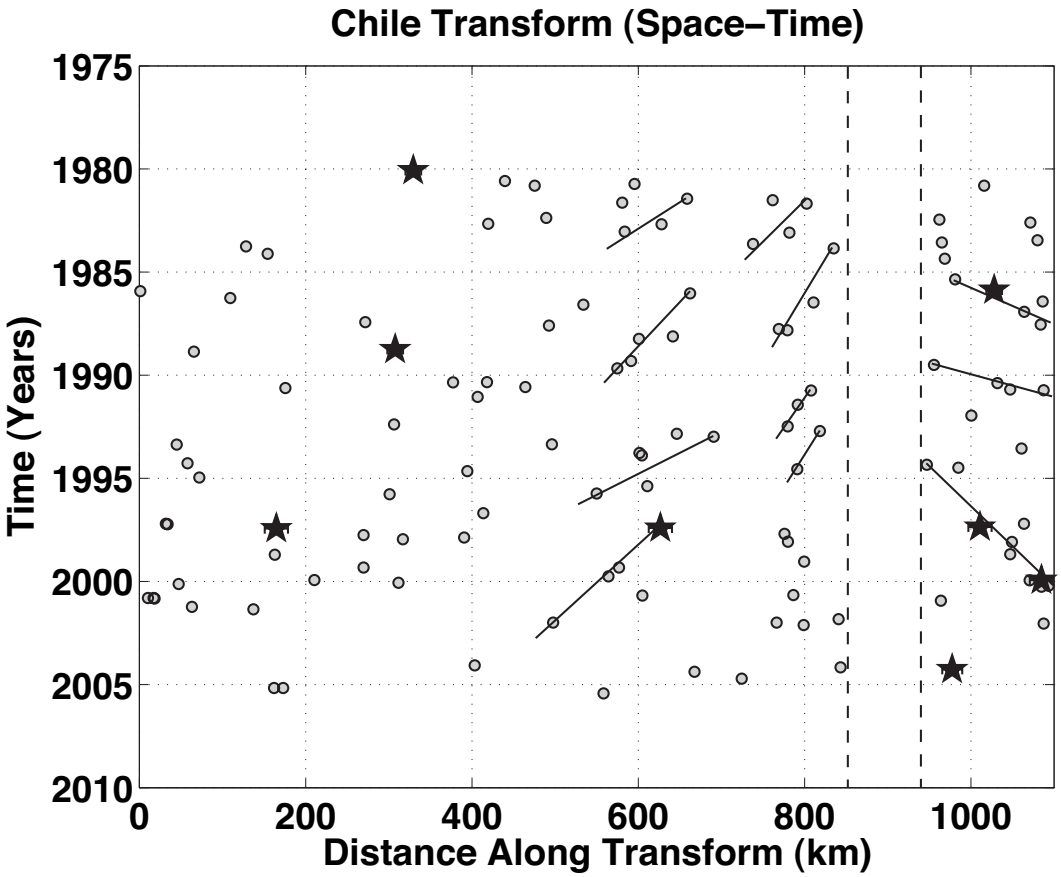

Figure 2.15. Space-time seismicity plot for the Chile OTF. Dashed lines delineate gaps in moderate- and larger-size earthquake activity.

as observed on each transform). For both observed and simulated activity, we defined the fraction of interacting events as the number of events located within a variable time window and a variable distance window (effectively counting events that lie within a box surrounding each event). We ran our observations through the same algorithm to determine the number of interacting events on each transform. We find from these results, which are summarized in Table A.1, that earthquake interactions are indeed not a random process. We note that 93% of our confidence rates for all time and distance windows on our studied transforms are 90% or better that the number of observed event interactions is not a random process. This allows us to make reasonable assumptions concerning event migration that we observe in our space-time plots.

Migrating Seismicity A number of transforms show patterns that suggest repeating along-strike seismicity migrations. The phenomenon is most clearly observed along the eastern segment of the Blanco Transform system (Figure 2.12). Three of the four clear migrating sequences initiate with a large event located near the edge of the quiet central segment, which has hosted no recent moderate-or-large activity. The moderate-size activity migrates at a rate of about 15-20 km/yr. All last on the order of 5 years, spread across about 100 of the segment, and repeat with approximately the same schedule. The larger events in these sequences are located in close proximity and may include repeated failure two or three asperities since the plate motion rates can account for the amount of slip likely released during these events. Perhaps the systematic migration of the moderate-size activity reflects a deeper deformation that sweeps from west to east, loading the shallower asperities than fail in succession. The oldest of the large events on this segment does not initiate a sequence, but this might be a result of seismic network limitations We highlighted on possible migratory pattern along the Balleny Transform (Figure 2.12), but we certainly can't be sure with one observation. The migration occurs at a rate between 40 and 80 km/yr. We see a number of similar sequences along the easter segment of the Chile Transform system, which are not as clear as those along the Blanco. Migration rates for the highlighted sequences are on the order of 10-30 km/yr. For the more clear patterns on the east, like the Blanco they seem to emanate from a region with little if any moderate-size activity. One explanation for the patterns is a process in which stable deformation loads one or perhaps several asperities adjacent to the stably sliding region and causes each to re-rupture regularly. The patterns are not without complexity some of which could come from activity at different depths. The deformation rates appear to be much more rapid than the episodic slip seen along subduction zones, which appear to migrate 10's of km per day or week, and have a much shorter duration (*e.g.* Dragert *et al.*, 2001).

2.4 Discussion

Although the time window for which we have sufficient seismic waveforms is relatively short, by improving the relative locations of the available data we have been

able to identify a number of interesting patterns in OTF seismicity. Our focus has necessarily been on transforms that include many moderate-and larger-size earthquakes. The seven transforms behave differently, and different segments along each transform also vary in character.

The question of how much moment deficiency (aseismic slip) and where on the fault this moment deficiency is most prevalent is key to our understanding of OTF earthquake behavior (*e.g.* Boettcher and Jordan, 2004). Earlier workers have suggested that aseismic slip can either occur at depth, subjacent to frictionally unstable lithosphere, or in adjacent aseismic gaps where frictionally stable serpentinite zones may slip easily thereby loading the unstable lithosphere (Ihmle and Jordan, 1994; Abercrombie and Ekstrom, 2001). The large moment-rate deficiencies (Chapter 1) or small seismic coupling factors (*e.g.* Boettcher and Jordan, 2004) suggest that large amounts of aseismic deformation occurs along OTFs. Viewed another way, low seismic coupling suggests that the simple thermal models used to estimate the seismogenic zone area for the coupling calculations, based on an approximation of the 600° isotherm, produce over-estimates for all but the slowest moving transforms. Since the 600° isotherm cutoff is seismically derived, more friction work is needed to understand whether the problem lies in the assumption, or in grossly inadequate thermal models.

Among the transforms we analyzed, only the Chile, Eltanin (Heezen), and Blanco OTF systems have significant moderate-size and larger seismicity gaps, possibly indicating long segments dominated by stable sliding. A particularly interesting aseismic segment appears along the Eltanin system from approximately 600 to 800 km (Figure 2.14). This section ends abruptly on the space-time diagram by what may be a repeating sequence or sequences of moderate-size events located near 830 km in Figure 2.14. Further into the seismogenic segment, larger events have occured, suggesting that we may be seeing a lateral gradient increasing the area of frictionally unstable material as we move out from the seismic gap.

The epicentroid locations derived in this work show that while a few segments along the transforms appear to be devoid of moderate-size earthquakes, most of the transforms studied have moderate activity along most of their length. If we are to produce a low seismic coupling along the structure, this means that the corresponding seismogenic zone depth is most often overestimated by the depth of

the 600° isotherm. Transforms moving bounding plates moving at relatively slow to relatively fast velocities have hosted large events, which suggests that at least part of all classes of transforms have some segments for which unstable sliding occurs relatively deeply.

The key elements of our analysis are summarized in an OTF asperity model (Figure 2.16), which incorporates our ideas from thermal modeling, and observations from a Gutenberg-Richter analysis, moment deficiency calculations, and our improved relative locations. The model shows clustering of large and moderate seismicity divided by gaps of smaller magnitude seismicity or aseismicity. All seven transforms have hosted events with $M_W \geq 6.0$ so all have at least a few larger asperities. We reflect the large coupling of the transforms separating slow-moving plates by extending the seismogenic region deeper. Identifying seismogenic regions isolated by regions of stable sliding may allow us to infer slower deformations, and more information on the depth distribution of the moderate activity will help better investigate the relative fraction of stable to unstable frictional regimes as a function of depth.

2.5 Conclusions

Precise, Rayleigh-wave epicentroid locations provide an opportunity to explore patterns in OTF seismicity and quantitatively evaluate moderate and large magnitude earthquake interactions along transform plate boundary systems. Seismicity patterns along the seven seismically active transforms studied exhibit a range of behavior. Specific short-term earthquake interactions occur, but do not dominate the moderate magnitude activity. Events larger than $M_W \sim 6.0$ appear to interact on most of the transforms, but their small numbers make a quantitative statistical analysis difficult. Moderate-size activity appears to regularly migrate along segments of several transforms at a rate of 10-30 km/yr, perhaps driven by slow deformation at depth. Low seismic coupling coefficients and the spread in moderate-size earthquake activity along most of the transforms, suggest that estimates of the seismogenic zone depth using a 600° isotherm (from simple thermal models) may be too large. But the existence of large events on each transform requires at least part of transform to have relatively deep seismogenic zones.

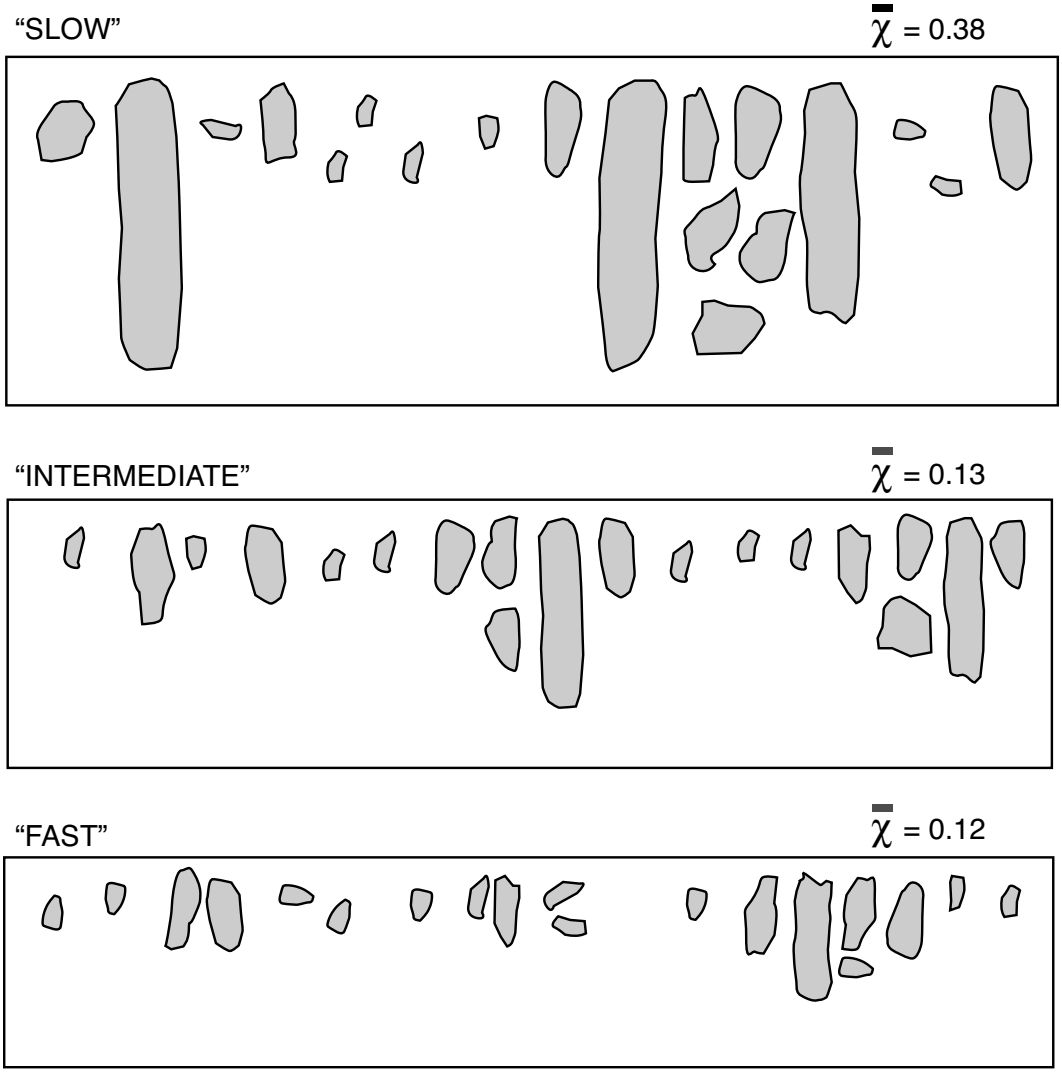

Figure 2.16. Asperity models for oceanic transform faults based on relative plate velocity. OTFs separating plates of all speeds can host large events, but the coupling is largest for the OTFs separating plates moving more slowly. Vertical exaggeration for all three models is about 12:1.

Appendix A

Supplementary Information Tables

In this appendix I tabulate information related to discussions in the main body of the thesis. Included are descriptive statistics on OTF aftershocks, epicentroid locations from the double-difference location procedure, details on the projections used for the space-time seismicity diagrams, and a summary of the random pattern simulation experiments.

A.1 Earthquake Re-location Tables

I tabulate origin time and location shifts in tables A.1 through A.1. The sum of time shifts for any cluster is zero, so these are relative time shifts and should not be applied directly to the NIEC locations - they must be applied jointly, with the epicentroid shifts. *Lat* and *Lon* are the initial locations (NEIC hypocenters) and *ddLat* and *ddLon* are the double-difference epicentroid latitude and longitude. The values δT_0, Δ, and ϕ represent the origin time shift, and the distance and azimuth of the epicentroid from the NEIC hypocenters.

A.2 STD Projection Parameters

Table A.2 is a list of the origins and azimuths used in the space-time seismicity diagrams of Chapter 2. Latitudes and longitudes were projected using the GMT

Table A.1. Blanco OTF - Table of oceanic transform earthquakes relocated with Rayleigh Wave Double-Difference Method.

					Origin Shift		
eventName	Lat	Lon	ddLat	ddLon	δT_0	Δ	ϕ
E1980 03 30 13 49	43.430	-127.120	43.430	-127.120	0.000	0.0	0.0
E1980 12 24 13 29	42.370	-125.730	42.370	-125.730	0.000	0.0	0.0
E1981 11 03 13 47	43.540	-127.710	43.566	-127.680	0.474	3.8	40.6
E1981 11 22 11 37	43.600	-127.340	43.522	-127.377	-0.692	9.2	198.9
E1982 11 13 15 44	44.410	-129.510	44.410	-129.510	-0.000	0.0	0.0
E1985 03 13 19 35	43.510	-127.560	43.557	-127.534	-0.084	5.7	21.7
E1986 01 30 07 15	43.600	-127.340	43.522	-127.335	-2.324	8.6	177.5
E1986 10 05 21 57	43.490	-127.250	43.476	-127.216	-1.590	3.1	119.2
E1987 06 27 06 01	43.490	-127.090	43.443	-127.089	-1.026	5.3	179.1
E1987 12 07 17 48	43.510	-127.250	43.445	-127.144	-2.305	11.2	130.3
E1988 10 23 13 48	44.420	-129.460	44.439	-129.616	-8.682	12.6	279.5
E1989 05 16 12 21	43.560	-127.630	43.557	-127.486	-1.889	11.6	91.4
E1990 01 16 12 57	43.560	-127.400	43.526	-127.306	0.065	8.5	116.1
E1990 01 17 12 05	43.590	-127.440	43.547	-127.422	-1.571	5.0	163.1
E1990 02 12 13 44	44.130	-128.930	44.160	-128.921	-6.236	3.4	12.3
E1992 08 04 14 27	43.470	-127.010	43.482	-127.141	0.668	10.6	277.3
E1994 02 28 21 52	44.700	-129.890	44.521	-129.972	68.793	20.9	198.2
E1994 10 27 17 46	43.510	-127.430	43.656	-127.743	6.076	30.0	302.8
E1996 04 15 12 29	43.660	-127.500	43.550	-127.432	-2.584	13.4	155.9
E1996 11 04 22 54	43.520	-127.360	43.539	-127.328	-0.851	3.3	50.2
E1996 12 08 03 48	44.210	-129.370	44.265	-129.310	-6.915	7.8	38.1
E1997 07 11 02 03	44.270	-129.360	44.324	-129.322	-6.270	6.7	26.5
E1997 10 11 15 54	44.550	-129.730	44.487	-129.724	-6.855	7.0	175.9
E1998 03 23 02 28	43.440	-127.090	43.439	-127.062	-1.503	2.2	93.2
E1999 03 09 17 48	43.450	-127.070	43.447	-127.108	-1.963	3.1	264.5
E2000 01 20 09 41	43.650	-127.260	43.579	-127.468	1.289	18.5	244.7
E2000 06 02 11 13	44.510	-130.080	44.549	-129.941	-4.843	11.9	68.6
E2002 05 15 07 06	43.410	-127.080	43.437	-127.032	-1.123	4.9	52.3
E2002 07 09 18 40	43.520	-127.170	43.477	-127.180	-1.645	4.8	189.9
E2003 01 16 00 53	44.280	-129.020	44.267	-129.120	-4.361	8.1	259.6
E2003 01 16 02 25	44.280	-129.350	44.299	-129.266	-4.782	7.0	72.3
E2003 03 07 22 11	43.530	-127.120	43.454	-127.100	-1.864	8.6	169.3
E2003 12 27 15 23	43.520	-127.350	43.533	-127.300	-1.410	4.3	69.8
E2005 03 07 02 34	42.510	-126.570	42.710	-126.588	-1.687	22.3	356.2
E2005 03 07 02 48	42.530	-126.530	42.727	-126.565	-2.313	22.1	352.6

Table A.2. Chain OTF - Table of oceanic transform earthquakes relocated with Rayleigh Wave Double-Difference Method.

eventName	Lat	Lon	ddLat	ddLon	δT_0	Shift Δ	ϕ
E1982 10 01 05 35	-1.630	-15.610	-1.552	-15.408	-0.811	24.1	69.0
E1984 12 05 13 39	-1.270	-13.950	-1.117	-13.946	0.947	17.0	1.6
E1984 12 07 10 19	-1.420	-15.060	-1.403	-14.889	-0.109	19.1	84.2
E1985 02 27 22 57	-1.320	-14.570	-1.311	-14.562	0.216	1.3	38.8
E1987 06 30 10 59	-1.070	-13.050	-1.206	-14.208	-3.662	129.6	263.3
E1988 02 22 01 58	-1.100	-13.920	-1.228	-14.019	-1.792	18.0	217.8
E1988 09 30 03 00	-1.290	-14.470	-1.290	-14.470	0.000	0.0	0.0
E1988 11 21 05 30	-1.370	-15.090	-1.448	-15.142	1.417	10.4	214.0
E1988 12 06 19 42	-1.460	-15.240	-1.414	-15.052	-0.020	21.5	76.2
E1989 07 09 09 46	-1.580	-15.550	-1.548	-15.358	-0.864	21.6	80.6
E1990 08 05 17 42	-1.080	-13.890	-1.165	-14.098	3.338	24.9	247.8
E1992 08 28 18 18	-0.960	-13.560	-1.124	-13.794	0.512	31.7	235.2
E1993 11 25 20 24	-0.960	-13.260	-1.106	-13.592	-0.716	40.3	246.3
E1996 02 16 09 44	-1.500	-15.280	-1.462	-15.126	0.549	17.6	76.1
E1996 02 18 23 49	-1.270	-14.270	-1.207	-14.157	1.341	14.4	60.8
E1996 02 19 02 28	-1.200	-14.230	-1.176	-14.211	-0.079	3.4	38.1
E1998 04 10 16 40	-1.320	-15.650	-1.494	-15.207	1.309	52.9	111.4
E2001 11 15 01 03	-1.590	-15.580	-1.486	-15.219	1.244	41.8	74.0
E2002 08 03 14 18	-1.510	-14.370	-1.262	-14.450	1.390	28.9	342.0
E2003 09 21 23 15	-1.010	-14.060	-1.105	-13.896	3.415	21.1	120.1
E2003 10 11 23 08	-1.410	-15.050	-1.515	-15.305	-2.743	30.6	247.8
E2004 05 12 23 23	-1.610	-15.290	-1.417	-15.102	-2.400	30.0	44.3
E2005 01 29 21 01	-1.630	-15.520	-1.515	-15.354	-2.480	22.4	55.4

"project" command. Values in the direction of the azimuth are positive.

Table A.3. Chile OTF - Table of oceanic transform earthquakes relocated with Rayleigh Wave Double-Difference Method.

eventName	Lat	Lon	ddLat	ddLon	δT_0	Shift Δ	ϕ
E1980 01 27 16 38	-35.380	-105.870	-35.229	-105.741	9.762	20.5	35.0
E1980 08 03 13 42	-35.580	-104.630	-35.418	-104.547	5.856	19.5	22.8
E1980 09 26 20 26	-35.900	-102.940	-35.798	-102.881	2.263	12.6	25.0
E1980 10 22 22 59	-36.490	-98.610	-36.305	-98.245	-9.160	38.7	57.9
E1980 10 22 23 27	-35.110	-104.080	-35.110	-104.080	0.000	0.0	0.0
E1981 06 10 04 06	-35.800	-102.170	-35.800	-102.170	0.000	0.0	0.0
E1981 07 06 08 25	-36.230	-101.090	-36.230	-101.090	-0.000	0.0	0.0
E1981 08 22 23 47	-35.830	-103.300	-35.752	-103.037	4.507	25.2	70.1
E1981 09 06 16 43	-36.170	-100.700	-36.061	-100.604	-5.827	14.9	35.6
E1982 05 17 02 39	-35.350	-103.840	-35.547	-104.019	3.695	27.2	216.4
E1982 06 15 01 20	-36.520	-98.650	-36.351	-98.854	-9.914	26.2	315.6
E1982 08 08 04 40	-36.240	-97.610	-36.240	-97.610	0.000	0.0	0.0
E1982 08 27 03 56	-35.460	-104.850	-35.410	-104.772	8.529	9.0	52.0
E1982 09 09 06 40	-35.550	-102.420	-35.691	-102.491	-0.444	16.9	202.2
E1983 01 13 09 23	-35.810	-102.630	-35.803	-103.013	8.955	34.6	271.1
E1983 01 28 23 11	-36.230	-100.970	-36.084	-100.839	-4.636	20.1	36.1
E1983 06 17 11 33	-36.380	-97.520	-36.357	-97.530	-10.735	2.7	341.3
E1983 07 26 04 14	-36.280	-98.810	-36.280	-98.810	-0.000	0.0	0.0
E1983 08 20 08 30	-36.250	-101.540	-36.060	-101.326	-2.106	28.6	42.5
E1983 10 02 23 02	-34.320	-107.760	-34.320	-107.760	0.000	0.0	0.0
E1983 11 09 01 57	-36.190	-100.240	-36.155	-100.256	-6.865	4.2	339.3
E1984 02 12 18 58	-34.880	-107.630	-34.892	-107.618	9.603	1.7	138.7
E1984 05 10 09 51	-36.270	-98.890	-36.338	-98.782	-11.445	12.2	128.0
E1985 05 06 07 33	-36.410	-98.870	-36.354	-98.641	-11.024	21.5	73.2
E1985 11 12 03 34	-36.500	-98.160	-36.343	-98.114	-9.373	18.0	13.3
E1985 12 05 08 25	-35.250	-109.440	-35.250	-109.440	0.000	0.0	0.0
E1986 01 12 14 00	-36.010	-102.210	-36.034	-102.173	-6.693	4.3	129.0
E1986 04 09 01 44	-34.880	-108.120	-34.880	-108.120	-0.000	0.0	0.0
E1986 06 05 09 01	-36.350	-97.380	-36.325	-97.455	-10.076	7.3	292.0
E1986 06 24 23 53	-36.080	-100.470	-36.129	-100.522	-7.866	7.2	220.2
E1986 08 01 14 09	-35.880	-103.700	-35.739	-103.557	2.034	20.3	39.4
E1986 12 05 01 45	-36.470	-97.630	-36.342	-97.709	-9.218	15.9	333.3
E1987 06 09 22 46	-35.280	-106.670	-35.151	-106.370	9.508	30.8	62.5
E1987 07 21 13 27	-36.290	-97.250	-36.331	-97.485	-11.030	21.6	257.7
E1987 08 09 08 24	-35.140	-104.060	-35.565	-103.985	5.802	47.6	171.8

eventName	Lat	Lon	ddLat	ddLon	δT_0	Shift Δ	ϕ
E1987 10 06 14 39	-36.090	-101.170	-36.139	-100.992	-6.169	16.9	108.8
E1987 10 28 18 24	-36.080	-100.840	-36.115	-100.870	-8.004	4.7	215.3
E1988 02 11 02 56	-35.620	-102.270	-35.834	-102.368	1.524	25.4	200.4
E1988 03 28 18 36	-36.040	-102.840	-35.791	-102.817	2.992	27.7	4.3
E1988 10 01 09 43	-35.310	-106.050	-35.187	-105.975	11.488	15.2	26.8
E1988 11 13 23 40	-34.830	-108.600	-34.830	-108.600	0.000	0.0	0.0
E1989 04 22 04 48	-35.580	-102.930	-35.802	-102.929	0.870	24.6	179.8
E1989 07 07 12 27	-36.260	-99.250	-36.332	-98.928	-11.940	30.0	105.6
E1989 09 06 09 10	-36.090	-103.170	-35.786	-103.112	6.180	34.2	8.8
E1990 05 06 16 46	-35.250	-104.140	-35.334	-104.773	4.884	58.3	260.7
E1990 05 07 16 46	-35.250	-105.210	-35.250	-105.210	-0.000	0.0	0.0
E1990 05 22 13 25	-36.300	-97.880	-36.324	-98.069	-13.408	17.1	261.1
E1990 07 28 13 59	-36.420	-104.520	-35.500	-104.289	13.542	104.3	11.6
E1990 08 19 17 44	-34.600	-107.780	-34.986	-107.409	9.780	54.7	141.8
E1990 09 13 07 08	-36.540	-97.690	-36.337	-97.894	-10.272	29.0	320.9
E1990 09 24 21 37	-36.290	-97.530	-36.321	-97.443	-9.151	8.5	113.7
E1990 09 26 15 40	-36.190	-100.790	-36.128	-100.555	-5.070	22.2	71.9
E1991 01 16 23 26	-34.990	-104.400	-35.313	-104.891	5.650	57.3	231.1
E1991 06 05 16 43	-36.040	-100.730	-36.107	-100.728	-7.172	7.5	178.5
E1991 12 15 06 12	-36.490	-98.520	-36.315	-98.416	-9.557	21.6	25.7
E1992 05 22 13 06	-35.340	-105.890	-35.188	-105.990	8.660	19.1	331.7
E1992 06 23 11 21	-36.100	-101.220	-36.102	-100.865	-3.165	32.0	90.4
E1992 09 15 04 19	-36.280	-100.220	-36.126	-100.434	-6.808	25.7	311.5
E1992 11 04 04 53	-35.790	-102.280	-35.848	-102.318	3.284	7.3	207.9
E1992 12 27 23 58	-35.970	-101.910	-35.895	-101.830	0.959	11.0	41.0
E1993 05 10 02 01	-35.540	-103.950	-35.608	-103.955	3.003	7.5	183.6
E1993 05 16 16 09	-34.330	-108.940	-35.000	-108.880	6.022	74.6	175.8
E1993 07 21 13 03	-35.970	-97.980	-36.314	-97.742	-9.074	43.8	150.8
E1993 10 08 06 36	-35.900	-102.780	-35.804	-102.813	4.179	11.0	344.3
E1993 11 21 00 16	-35.960	-102.890	-35.797	-102.780	2.571	20.6	28.9
E1994 04 13 14 19	-33.970	-108.800	-34.702	-108.652	6.192	82.4	170.6
E1994 05 08 14 49	-35.730	-99.200	-36.326	-99.022	-10.637	68.1	166.5
E1994 06 27 04 10	-36.240	-98.190	-36.329	-98.597	-7.269	37.9	254.7
E1994 07 24 14 24	-36.180	-101.040	-36.114	-100.739	-5.720	28.1	74.9
E1994 08 24 22 05	-35.480	-104.890	-35.305	-105.031	8.614	23.2	326.4
E1994 12 19 13 08	-34.460	-108.230	-34.759	-108.509	8.904	41.9	217.5
E1995 05 21 15 47	-35.940	-102.650	-35.804	-102.710	1.988	16.0	340.3
E1995 09 29 13 32	-35.860	-103.400	-35.764	-103.381	1.602	10.8	9.0
E1995 10 12 23 41	-35.290	-106.270	-35.171	-106.044	11.345	24.5	57.3
E1996 09 09 03 21	-35.400	-104.640	-35.294	-104.812	9.750	19.6	307.0

eventName	Lat	Lon	ddLat	ddLon	δT_0	Shift Δ	ϕ
E1997 03 13 06 27	-36.470	-97.670	-36.321	-97.709	-9.023	16.9	348.1
E1997 03 14 09 42	-34.130	-109.530	-34.349	-108.842	9.888	67.8	111.2
E1997 03 23 04 26	-34.150	-109.340	-34.325	-108.816	8.815	52.0	112.1
E1997 05 11 22 16	-36.380	-97.700	-36.320	-98.302	-3.411	54.4	276.9
E1997 05 29 17 02	-35.960	-102.510	-35.810	-102.533	4.137	16.7	352.9
E1997 06 10 21 53	-35.810	-108.140	-35.586	-107.685	11.910	48.1	58.9
E1997 09 11 22 20	-36.230	-101.030	-36.106	-100.910	-5.393	17.5	38.2
E1997 10 04 18 31	-35.290	-106.710	-35.121	-106.387	11.082	34.9	57.5
E1997 11 12 03 26	-35.600	-105.040	-35.211	-105.052	10.387	43.2	358.5
E1997 12 16 20 40	-35.500	-105.920	-35.184	-105.870	10.224	35.4	7.4
E1998 01 26 13 02	-36.070	-100.970	-36.103	-100.865	-5.907	10.1	111.2
E1998 01 31 23 30	-35.760	-97.060	-36.304	-97.869	-12.481	94.6	230.1
E1998 09 07 00 39	-36.240	-97.710	-36.332	-97.898	-9.180	19.7	238.8
E1998 09 14 04 43	-34.750	-107.980	-34.969	-107.544	15.839	46.7	121.5
E1999 01 16 00 19	-35.870	-100.600	-36.131	-100.648	-6.881	29.4	188.5
E1999 04 28 06 34	-35.220	-106.510	-35.055	-106.371	10.943	22.2	34.7
E1999 04 29 18 26	-35.780	-102.900	-35.789	-103.088	1.813	17.0	266.7
E1999 10 05 02 59	-35.840	-103.280	-35.776	-103.229	2.266	8.4	32.8
E1999 12 09 08 34	-34.560	-106.940	-35.002	-107.019	6.957	49.6	188.3
E1999 12 10 18 38	-36.210	-97.320	-36.320	-97.608	-8.619	28.6	244.6
E1999 12 10 20 06	-36.230	-97.420	-36.266	-97.465	-4.020	5.7	225.1
E1999 12 11 09 03	-36.210	-97.400	-36.313	-97.630	-11.524	23.6	240.9
E2000 01 27 02 49	-34.810	-105.460	-35.186	-105.929	5.929	59.8	225.5
E2000 02 17 18 26	-34.940	-109.280	-34.867	-108.813	9.329	43.4	79.3
E2000 03 14 06 18	-36.270	-96.890	-36.295	-97.255	-10.176	32.9	265.0
E2000 03 20 08 42	-36.510	-97.230	-36.427	-97.391	-10.512	17.1	302.6
E2000 04 04 10 59	-36.370	-97.170	-36.392	-97.481	-10.345	28.0	264.9
E2000 09 01 00 07	-36.140	-100.750	-36.105	-100.788	-4.377	5.2	318.8
E2000 09 09 12 18	-35.880	-103.060	-35.808	-102.776	6.661	26.8	72.8
E2000 10 25 05 26	-34.600	-109.650	-34.619	-109.162	12.759	44.8	92.8
E2000 10 25 19 00	-34.680	-109.460	-34.620	-109.083	11.192	35.2	79.1
E2000 10 26 14 08	-34.570	-109.370	-34.592	-109.062	10.917	28.4	95.0
E2000 12 09 22 49	-36.390	-98.760	-36.336	-98.833	-8.064	8.9	312.5

eventName	Lat	Lon	ddLat	ddLon	δT_0	Shift Δ	ϕ
E2001 03 30 07 31	-34.730	-109.010	-34.730	-108.600	9.726	37.5	90.2
E2001 05 11 06 06	-34.920	-108.070	-34.944	-107.828	10.244	22.2	96.8
E2001 11 04 15 39	-36.200	-100.300	-36.146	-100.187	-5.153	11.8	59.6
E2001 12 28 21 31	-36.100	-100.640	-36.111	-101.017	-5.735	34.0	267.7
E2001 12 29 17 29	-35.020	-103.310	-35.630	-103.943	3.411	88.8	220.2
E2002 01 16 18 45	-36.230	-97.110	-36.307	-97.440	-11.152	30.8	253.7
E2002 02 15 01 46	-36.230	-100.300	-36.107	-100.651	-4.160	34.4	293.4
E2004 01 29 01 25	-35.420	-104.670	-35.297	-104.931	7.028	27.4	299.8
E2004 03 01 13 56	-36.170	-100.130	-36.086	-100.148	-7.459	9.5	350.3
E2004 04 08 04 57	-36.260	-97.830	-36.340	-98.681	-1.815	76.9	263.1
E2004 05 22 20 14	-35.910	-101.700	-35.989	-102.103	-3.853	37.4	256.4
E2004 09 21 17 55	-36.230	-101.480	-35.982	-101.468	-5.838	27.6	2.3
E2005 02 28 01 24	-34.920	-107.860	-34.969	-107.556	11.069	28.3	101.2
E2005 02 28 09 39	-34.990	-107.850	-34.971	-107.432	8.287	38.2	86.9
E2005 06 08 13 37	-35.900	-102.910	-35.772	-103.292	-0.403	37.3	292.2

Table A.4. Eltanin OTF - Table of oceanic transform earthquakes relocated with Rayleigh Wave Double-Difference Method.

eventName	Lat	Lon	ddLat	ddLon	δT_0	Shift Δ	ϕ
E1980 08 14 05 06	-56.010	-121.500	-56.192	-121.662	-3.696	22.7	206.4
E1981 01 09 23 34	-55.420	-127.620	-55.591	-127.796	-8.471	22.0	210.3
E1981 04 19 10 11	-54.030	-135.520	-54.377	-135.930	5.903	47.0	214.5
E1982 11 02 18 38	-55.730	-124.170	-55.641	-124.432	4.199	19.2	301.1
E1983 07 05 05 58	-55.850	-123.400	-55.903	-123.532	5.844	10.1	234.3
E1984 05 25 23 18	-54.510	-136.300	-54.510	-136.300	-0.000	0.0	0.0
E1984 05 25 23 54	-54.980	-135.690	-54.605	-135.987	1.270	45.9	335.3
E1984 05 26 02 44	-54.870	-135.410	-54.737	-135.570	-1.174	18.0	325.1
E1984 07 16 12 27	-55.470	-129.000	-55.230	-129.258	3.030	31.3	328.4
E1985 03 30 15 39	-55.620	-127.580	-55.721	-127.801	-9.376	17.9	230.9
E1985 04 07 00 19	-56.390	-122.310	-56.147	-122.584	4.612	32.0	327.8
E1985 08 18 15 25	-55.710	-124.160	-55.702	-124.285	6.607	7.9	276.5
E1985 09 11 18 23	-54.320	-132.000	-54.378	-131.988	-0.980	6.5	172.9
E1986 08 06 13 56	-55.290	-128.980	-55.194	-129.378	-2.850	27.5	292.8
E1986 12 06 16 55	-55.040	-126.780	-55.260	-127.201	-2.654	36.3	227.4
E1987 07 26 23 17	-55.010	-124.330	-55.659	-124.377	6.705	72.4	182.3
E1987 10 19 15 33	-54.090	-137.260	-54.195	-136.851	1.484	29.2	113.9
E1988 09 10 21 38	-54.180	-134.160	-53.933	-133.582	2.069	46.7	54.3
E1988 09 11 13 36	-53.890	-134.070	-53.891	-133.768	-2.081	19.8	90.4
E1989 02 16 16 37	-56.400	-121.960	-56.210	-122.235	3.309	27.2	321.1
E1989 05 25 07 24	-54.980	-129.200	-55.242	-129.095	-2.809	30.0	167.1
E1989 07 22 12 52	-54.410	-132.680	-54.214	-132.641	-2.493	22.0	6.7
E1991 03 09 01 01	-54.880	-131.530	-54.608	-131.234	-1.515	35.8	32.3
E1991 04 05 18 35	-54.590	-132.520	-54.342	-132.141	-1.404	37.0	41.8
E1991 10 13 18 12	-56.100	-122.630	-55.983	-123.173	5.212	36.3	290.9
E1991 11 19 13 21	-56.120	-123.370	-55.893	-123.488	5.580	26.3	343.8
E1992 03 24 18 20	-55.510	-124.360	-55.687	-124.289	7.198	20.2	167.3
E1992 07 29 01 54	-55.350	-128.440	-55.281	-128.999	-3.456	36.3	282.0
E1993 04 10 13 31	-54.130	-129.650	-55.211	-129.289	-2.786	122.6	169.2
E1993 04 18 14 10	-53.960	-133.870	-54.000	-133.375	0.387	32.8	98.1
E1993 05 15 20 39	-54.710	-131.930	-54.447	-131.860	-3.105	29.6	8.8

eventName	Lat	Lon	ddLat	ddLon	δT_0	Shift Δ	ϕ
E1993 10 24 15 36	-55.620	-128.040	-55.439	-128.367	-0.721	28.8	314.3
E1994 08 05 19 41	-55.370	-128.150	-55.242	-129.203	-0.207	68.3	281.7
E1995 01 04 06 28	-56.060	-123.230	-55.865	-123.642	5.467	33.6	310.0
E1995 04 18 16 23	-54.240	-136.600	-54.371	-136.691	-0.957	15.7	202.2
E1995 05 09 12 29	-53.970	-134.300	-53.898	-133.748	-1.330	37.1	77.8
E1995 09 08 00 27	-56.200	-122.270	-56.103	-122.600	5.307	23.1	297.6
E1995 09 08 01 15	-56.200	-122.270	-56.182	-122.488	8.873	13.7	278.5
E1996 03 30 09 57	-55.850	-125.670	-55.665	-124.381	5.072	83.5	76.2
E1996 06 30 22 27	-55.180	-127.080	-55.134	-127.637	-1.920	35.8	278.1
E1997 05 27 06 10	-54.920	-136.170	-54.558	-136.122	1.007	40.4	4.4
E1997 06 08 10 48	-55.150	-128.650	-55.322	-128.855	-1.745	23.2	214.1
E1997 07 08 13 18	-54.150	-133.450	-54.166	-132.887	-3.218	36.8	92.9
E1997 07 21 02 05	-54.860	-129.620	-55.154	-129.516	-1.590	33.4	168.5
E1997 09 03 06 22	-55.190	-128.990	-55.241	-129.121	-2.710	10.1	235.6
E1997 10 26 13 55	-54.120	-132.970	-54.241	-132.506	5.284	33.2	114.1
E1997 10 26 18 14	-55.370	-129.480	-55.053	-129.765	-0.220	39.7	332.7
E1997 10 27 00 55	-54.270	-133.370	-54.206	-132.646	-1.711	47.7	81.7
E1998 02 07 23 16	-55.160	-126.860	-55.185	-127.356	-1.893	31.7	264.8
E1998 03 05 01 16	-55.100	-128.510	-55.375	-128.553	-2.072	30.8	185.1
E1998 03 21 01 29	-54.640	-135.360	-54.725	-135.546	-1.063	15.3	231.6
E1999 09 23 23 51	-54.160	-136.490	-54.405	-136.621	0.332	28.6	197.3
E1999 10 04 06 26	-54.580	-130.860	-54.890	-130.479	-1.626	42.3	144.8
E1999 11 16 13 44	-55.820	-125.130	-55.662	-124.383	3.651	50.1	69.7
E1999 11 27 14 37	-54.850	-136.380	-54.694	-135.700	-0.482	47.0	68.6
E2000 09 13 22 29	-54.110	-136.820	-54.394	-136.602	1.425	34.6	155.9
E2001 03 24 02 14	-54.700	-130.620	-54.904	-130.401	-2.301	26.7	148.2
E2001 04 14 10 14	-54.630	-130.320	-54.696	-130.228	-2.735	9.4	141.0
E2001 04 15 11 26	-54.700	-130.310	-54.717	-130.139	-2.757	11.2	99.8
E2001 08 05 20 01	-55.850	-123.280	-55.875	-123.448	5.032	10.9	255.3
E2001 09 02 10 06	-54.360	-137.020	-54.357	-136.746	-0.554	17.8	89.0
E2001 09 02 11 13	-54.370	-136.620	-54.438	-136.486	0.056	11.5	131.0

eventName	Lat	Lon	ddLat	ddLon	δT_0	Shift Δ	ϕ
E2001 10 09 14 36	-54.220	-136.690	-54.382	-136.600	-0.175	18.9	162.1
E2001 10 14 15 44	-55.760	-124.290	-55.673	-124.341	9.330	10.2	341.7
E2001 10 18 12 55	-55.090	-126.910	-55.110	-127.795	-4.032	56.5	267.4
E2002 01 01 10 39	-55.210	-129.000	-55.198	-129.376	-1.762	23.9	273.0
E2002 01 11 03 02	-54.890	-130.620	-54.889	-130.481	-2.582	8.9	89.0
E2002 02 06 19 55	-55.190	-128.940	-55.265	-129.089	-1.366	12.6	228.5
E2002 04 24 11 00	-56.130	-122.310	-56.126	-122.485	6.234	10.9	272.3
E2002 06 22 01 58	-55.460	-128.370	-55.299	-128.959	0.933	41.4	295.4
E2002 08 26 13 57	-55.230	-128.640	-55.273	-128.982	-2.664	22.2	257.4
E2002 09 04 03 45	-53.750	-134.680	-53.918	-133.696	-2.602	67.4	106.5
E2002 09 16 07 49	-55.130	-129.440	-55.158	-129.507	-2.192	5.3	234.0
E2002 09 21 05 03	-55.580	-124.960	-55.590	-124.740	3.231	13.9	94.7
E2003 04 16 19 22	-55.370	-129.050	-55.327	-128.773	-2.560	18.2	74.9
E2003 04 16 20 24	-55.360	-128.840	-55.356	-128.651	-2.360	12.0	88.1
E2003 04 17 03 46	-55.270	-128.920	-55.308	-128.875	-3.059	5.1	146.2
E2003 04 18 08 35	-55.040	-128.700	-55.313	-128.888	-1.839	32.6	201.4
E2003 05 18 08 23	-54.200	-136.550	-54.486	-136.366	-0.224	34.0	159.5
E2004 08 24 20 07	-55.180	-128.920	-55.247	-129.176	-4.569	17.9	245.3
E2004 08 26 10 24	-54.560	-129.790	-55.106	-129.631	-2.245	61.7	170.5
E2004 11 08 04 44	-55.790	-123.000	-55.996	-123.176	3.328	25.4	205.5
E2004 12 22 21 03	-55.940	-125.000	-55.657	-124.389	2.026	49.6	50.8
E2005 03 03 05 37	-54.420	-137.170	-54.295	-136.917	-2.859	21.5	49.9
E2005 03 04 09 54	-54.100	-137.020	-54.306	-136.922	-2.634	23.8	164.5
E2005 03 21 07 38	-55.420	-128.420	-55.373	-128.582	-3.846	11.5	297.0
E2005 04 16 12 18	-54.990	-132.100	-54.394	-131.946	-1.625	67.1	8.6
E2005 05 30 10 04	-54.070	-133.960	-54.034	-133.204	-3.609	49.6	85.7
E2005 06 12 02 27	-55.240	-123.840	-55.710	-124.205	2.435	57.2	203.7
E2005 10 27 06 01	-55.030	-127.830	-55.097	-127.835	-3.341	7.5	182.4
E2005 12 22 12 20	-54.720	-135.870	-54.597	-136.009	1.878	16.3	326.7
E2006 01 24 04 27	-55.220	-135.580	-54.619	-135.905	-1.497	70.1	342.6

Table A.5. Romanche OTF - Table of oceanic transform earthquakes relocated with Rayleigh Wave Double-Difference Method.

eventName	Lat	Lon	ddLat	ddLon	δT_0	Shift Δ	ϕ
E1981 03 03 09 21	-0.410	-19.780	-0.410	-19.780	0.000	0.0	0.0
E1981 07 07 21 10	-0.170	-18.840	-0.170	-18.840	0.000	0.0	180.0
E1982 01 03 14 09	-0.970	-21.870	-0.941	-21.938	4.751	8.2	292.9
E1982 01 05 13 44	-0.890	-21.920	-0.919	-21.852	-4.751	8.2	112.9
E1982 05 26 20 04	-0.320	-19.330	-0.518	-19.527	11.158	31.0	225.0
E1982 08 30 08 39	0.000	-17.600	0.000	-17.600	-0.000	0.0	0.0
E1982 08 30 11 20	-0.030	-17.700	-0.030	-17.700	0.000	0.0	0.0
E1982 12 02 03 20	-1.200	-23.750	-1.200	-23.750	0.000	nan	180.0
E1983 09 08 20 36	0.170	-16.960	0.170	-16.960	0.000	0.0	180.0
E1983 10 13 13 06	-0.850	-21.820	-0.850	-21.820	0.000	0.0	180.0
E1983 12 21 07 09	-0.050	-17.870	-0.050	-17.870	0.000	0.0	180.0
E1984 04 22 06 14	-0.540	-19.860	-0.458	-19.896	-2.178	9.9	336.3
E1984 10 09 11 23	-0.560	-19.790	-0.531	-19.874	-2.196	9.9	289.1
E1984 12 08 12 24	-1.070	-23.450	-1.070	-23.450	-0.000	0.0	0.0
E1985 06 04 12 06	-0.380	-19.540	-0.361	-19.705	-4.047	18.5	276.6
E1986 06 24 06 56	-0.090	-17.820	-0.090	-17.820	-0.000	0.0	0.0
E1986 08 11 19 43	-0.080	-17.850	-0.080	-17.850	0.000	nan	0.0
E1986 12 29 12 39	-0.590	-19.830	-0.590	-19.830	0.000	0.0	0.0
E1987 02 01 06 56	-0.110	-17.790	-0.148	-17.878	-0.185	10.6	246.5
E1987 03 12 23 10	-0.270	-18.150	-0.280	-18.185	-0.414	4.0	254.2
E1987 05 05 10 50	0.000	-19.150	-0.494	-19.400	-0.546	61.3	206.9
E1987 06 07 14 48	-0.380	-19.080	-0.444	-19.201	-0.683	15.2	242.2
E1988 08 27 16 52	-0.940	-20.930	-0.940	-20.930	-0.000	0.0	180.0
E1989 08 31 11 04	-0.170	-17.800	-0.171	-17.820	0.924	2.2	266.0
E1989 11 15 04 00	-0.580	-19.990	-0.599	-20.043	-2.987	6.3	250.5
E1989 11 15 04 15	-0.500	-19.810	-0.563	-19.916	-2.748	13.8	239.4

eventName	Lat	Lon	ddLat	ddLon	δT_0	Shift Δ	ϕ
E1989 11 21 20 36	-0.640	-19.790	-0.605	-19.944	-1.980	17.6	282.7
E1989 11 22 05 46	-0.560	-19.710	-0.570	-19.848	-2.369	15.4	266.0
E1990 07 14 05 54	0.000	-17.380	-0.056	-17.417	1.416	7.4	213.5
E1990 07 14 07 24	-0.070	-17.520	-0.112	-17.597	1.068	9.7	241.4
E1992 11 04 20 31	-0.590	-17.470	-0.590	-17.470	-0.000	0.0	180.0
E1993 02 04 18 04	-1.290	-24.280	-1.305	-24.553	-8.779	30.4	266.9
E1993 02 18 10 10	-0.460	-19.450	-0.554	-19.692	2.034	28.8	248.9
E1994 03 14 04 30	-1.080	-23.930	-1.171	-23.562	12.617	42.1	103.9
E1994 03 14 04 30	-1.280	-23.570	-1.173	-23.560	4.472	11.9	5.5
E1994 08 29 17 36	-0.400	-19.170	-0.360	-19.465	-4.534	33.1	277.7
E1995 05 18 00 06	-0.890	-22.000	-0.793	-21.579	0.220	48.0	77.0
E1996 11 01 14 38	-0.230	-18.010	-0.197	-18.004	0.645	3.8	10.5
E1998 01 19 12 30	-0.650	-20.110	-0.632	-20.138	-1.511	3.7	303.1
E1998 03 29 07 14	-0.240	-17.930	-0.187	-17.848	3.008	10.9	57.3
E1998 07 26 03 38	-0.770	-20.960	-0.735	-20.860	-2.592	11.8	70.6
E2000 07 15 03 13	-0.440	-19.590	-0.323	-19.783	-2.515	25.1	301.2
E2001 01 05 11 54	-0.660	-22.070	-0.817	-21.621	-3.212	52.9	109.2
E2001 01 24 05 34	-0.600	-19.860	-0.549	-19.938	-1.569	10.4	303.1
E2002 03 07 07 10	-1.320	-24.480	-1.316	-24.589	-8.310	12.2	272.0
E2002 06 12 19 52	-0.680	-20.720	-0.560	-20.596	-3.080	19.1	46.1
E2003 11 09 19 52	-0.670	-19.690	-0.533	-19.569	4.080	20.3	41.6
E2003 11 09 22 56	-0.470	-19.690	-0.470	-19.690	-0.000	0.0	0.0
E2003 12 21 07 40	-0.770	-20.600	-0.629	-20.325	6.946	34.3	63.0
E2003 12 23 05 58	-0.700	-20.330	-0.665	-20.351	-2.123	4.5	328.5
E2005 01 12 08 40	-0.880	-21.190	-0.629	-20.457	9.971	86.1	71.2

Table A.6. Balleny OTF - Table of oceanic transform earthquakes relocated with Rayleigh Wave Double-Difference Method.

eventName	Lat	Lon	ddLat	ddLon	δT_0	Shift Δ	ϕ
E1981 06 13 01 26	-60.170	154.710	-60.469	154.575	12.365	34.1	192.6
E1983 04 27 01 39	-62.510	155.500	-62.375	155.200	-2.377	21.6	314.1
E1985 04 25 09 06	-60.690	154.330	-60.636	153.839	4.061	27.5	282.5
E1985 05 08 13 30	-62.840	155.690	-62.562	155.387	-0.770	34.7	333.3
E1985 08 08 22 26	-61.560	154.350	-61.400	154.350	0.019	17.8	360.0
E1986 03 01 08 47	-62.690	155.110	-62.408	155.200	-1.228	31.7	8.4
E1986 07 23 07 35	-61.930	154.770	-61.801	154.720	-0.551	14.6	349.5
E1987 01 28 20 14	-61.090	153.860	-61.177	154.167	-1.735	19.1	120.5
E1987 04 06 07 19	-62.640	155.400	-62.561	155.336	-3.412	9.4	339.4
E1988 01 16 05 46	-60.370	154.210	-60.821	153.945	-2.856	52.3	196.0
E1988 09 08 11 06	-60.940	154.070	-60.938	154.000	2.901	3.8	272.8
E1989 05 17 16 12	-62.100	154.630	-62.007	154.872	-1.562	16.3	50.8
E1989 08 10 10 44	-61.900	154.620	-61.857	154.755	-2.233	8.5	56.1
E1989 09 17 05 48	-61.440	153.990	-61.491	154.416	-1.072	23.4	104.3
E1989 11 09 22 05	-61.450	154.310	-61.433	154.362	-0.757	3.4	55.9
E1991 12 17 03 41	-62.550	155.050	-62.116	154.935	2.127	48.7	352.9
E1992 06 15 14 16	-60.770	154.040	-61.088	154.100	-5.263	35.6	174.8
E1992 09 24 18 17	-61.220	154.360	-61.245	154.235	0.615	7.2	247.4
E1992 11 04 01 59	-61.540	154.570	-61.620	154.566	1.180	8.9	181.5
E1993 06 29 07 07	-60.440	152.770	-61.058	154.100	6.499	99.9	134.1
E1993 11 07 20 24	-62.190	154.360	-61.924	154.802	-1.557	37.5	38.2
E1994 01 23 00 20	-60.730	154.360	-60.833	154.005	-1.068	22.5	239.2
E1995 02 03 02 31	-62.710	155.670	-62.451	155.246	3.543	36.1	322.8
E1995 03 23 10 14	-62.590	155.500	-62.353	155.163	-1.582	31.6	326.5
E1995 05 02 23 52	-60.430	154.040	-60.548	153.789	3.795	19.0	226.3
E1995 06 21 15 28	-61.670	154.770	-61.772	154.685	1.660	12.3	201.4
E1998 06 29 23 37	-60.350	153.140	-60.593	153.796	3.254	45.1	127.2
E2000 07 15 10 22	-61.190	154.600	-61.369	154.322	-4.616	24.9	216.7
E2001 11 17 22 10	-60.590	154.090	-60.851	153.965	-1.364	29.8	193.2
E2002 04 07 01 41	-60.940	154.250	-61.178	154.186	2.808	26.7	187.4
E2002 08 09 11 44	-61.450	154.950	-61.491	154.423	0.424	28.5	260.5
E2003 07 29 19 33	-61.310	154.800	-61.385	154.326	-0.155	26.7	251.5
E2003 09 26 15 22	-62.670	153.870	-62.271	154.919	-2.152	70.0	51.0
E2004 04 14 08 10	-60.710	153.580	-60.721	153.858	-2.157	15.2	94.9
E2004 10 24 05 37	-62.090	154.620	-62.037	154.879	-4.150	14.8	66.4
E2005 05 31 09 06	-62.830	155.780	-62.522	155.308	-2.637	42.0	324.6

Table A.7. Udintsev OTF - Table of oceanic transform earthquakes relocated with Rayleigh Wave Double-Difference Method.

eventName	Lat	Lon	ddLat	ddLon	δT_0	Shift Δ	ϕ
E1982 07 19 14 53	-56.610	-141.760	-56.653	-141.836	-0.992	6.7	224.0
E1982 11 26 17 45	-55.890	-144.240	-55.910	-144.158	2.020	5.6	113.3
E1984 01 02 22 09	-56.740	-142.650	-56.574	-142.532	-0.414	19.9	21.4
E1984 08 18 03 33	-56.780	-141.030	-56.780	-141.030	-0.000	0.0	0.0
E1986 02 25 21 50	-57.090	-141.960	-56.812	-141.878	-1.327	31.3	9.2
E1986 06 06 04 00	-56.810	-140.960	-56.933	-141.256	0.493	22.7	232.6
E1988 07 04 03 35	-56.750	-140.600	-56.909	-141.392	1.366	51.5	249.5
E1990 10 29 06 42	-55.980	-143.240	-56.289	-143.179	-0.601	34.6	173.7
E1990 11 01 01 56	-56.000	-143.200	-56.308	-143.364	-1.655	35.7	196.5
E1991 02 01 17 14	-57.070	-141.110	-56.863	-141.628	2.294	39.0	306.0
E1991 05 31 22 17	-56.840	-140.930	-56.935	-141.364	0.632	28.4	248.1
E1992 12 09 06 27	-56.560	-142.560	-56.502	-142.666	0.874	9.1	314.5
E1994 10 06 15 42	-56.630	-141.920	-56.631	-142.243	-0.436	19.8	269.7
E1994 11 16 06 54	-56.170	-142.610	-56.467	-142.650	-1.187	33.2	184.2
E1995 10 09 07 50	-56.060	-144.210	-56.059	-143.919	-0.716	18.1	89.6
E1995 12 11 06 48	-56.460	-142.310	-56.590	-142.465	-0.732	17.3	213.4
E1997 04 28 20 43	-55.930	-143.880	-56.311	-143.048	0.625	66.9	129.7
E1998 05 11 13 22	-57.290	-142.360	-56.778	-141.926	-3.795	62.9	25.0
E1998 10 11 23 36	-56.910	-142.620	-56.443	-142.824	4.079	53.5	346.4
E1999 03 27 21 02	-56.800	-141.050	-56.922	-141.430	1.774	26.8	239.4
E1999 08 08 15 15	-56.440	-143.020	-56.391	-143.061	-1.105	6.1	335.1
E1999 10 09 14 11	-56.380	-144.220	-56.205	-143.342	-1.491	57.7	70.7
E2000 09 21 17 45	-56.510	-141.830	-56.729	-142.027	0.751	27.3	206.2
E2000 12 04 22 16	-56.230	-143.540	-56.258	-143.248	-1.277	18.4	99.9
E2001 05 07 01 56	-55.950	-144.540	-55.984	-144.109	-1.156	27.2	98.2
E2002 07 19 06 43	-56.620	-140.690	-56.892	-141.518	6.149	58.9	238.8
E2002 10 18 11 16	-57.190	-142.750	-56.532	-142.535	2.453	74.5	10.2
E2003 02 19 00 42	-56.940	-142.800	-56.584	-142.366	-1.351	47.7	33.9
E2003 08 28 17 41	-56.100	-143.600	-56.229	-143.281	0.520	24.5	126.1
E2004 02 19 05 53	-55.960	-143.350	-56.273	-143.270	-2.252	35.2	171.9
E2004 07 17 15 26	-56.650	-141.940	-56.744	-141.955	-2.765	10.5	184.9
E2004 10 03 18 34	-56.560	-141.910	-56.740	-141.982	-0.779	20.5	192.4

Table A.8. Starting positions and azimuths used to create oblique projections and space-time seismicity diagrams for the seven studied OTFs.

Transform	Origin		Azimuth
	Lon	Lat	c (°)
Balleny	153.5	-60.0	163
Blanco	-130.4	44.5	113
Chain	-15.8	-1.6	77
Chile	-109.3	-34.7	103
Eltanin	-137.1	-54.1	108
Romanche	-24.7	-1.3	81
Udintsev	-144.8	-55.8	120

Table A.9. A table of interacting earthquakes from our OTFs using varying maximum distance and time window. Our observations (Obs) and the percent confidence level (Conf), which is the percent confidence observations are not random.

Max Distance (km)		Max Time Difference (days)					
		7		30		365	
		Obs.	Conf.	Obs.	Conf.	Obs.	Conf.
	Blanco	L=400 km		nEvents / 100 km =4.5			
10		1	98%	1	99%	4	92%
5		0	-	0	-	1	97%
	Balleny	L=350 km		nEvents / 100 km =9			
10		0	-	0	-	1	41%
5		0	-	0	-	0	-
	Chile	L=1,100 km		nEvents / 100 km =11			
10		3	100%	5	99%	12	96%
5		1	98%	2	98%	7	90%
	Eltanin	L=1,000 km		nEvents / 100 km =8.6			
10		7	100%	8	100%	20	100%
5		2	100%	2	99%	5	96%
	Romanche	L=900 km		nEvents / 100 km =4.8			
10		3	100%	3	100%	5	98%
5		2	100%	2	99%	4	99%
	Udintsev	L=330 km		nEvents / 100 km =9.4			
10		1	99%	1	98%	3	65%
5		0	-	0	-	2	90%

Appendix B

OTF Foreshock and Aftershock Characteristics

I analyzed 106 $Ms \geq 6.0$ earthquakes that occurred on 21 transforms to explore mainshock-aftershock patterns using the USGS National Earthquake Information Center Epicenter Catalog. The specific sequences included in the analysis, along with foreshock and aftershock counts are listed in Table A.1. Foreshocks and aftershocks were defined as an event that occurs within 100 km and 30 days of the mainshock and greater than 0.2 units of magnitude less than the mainshock. Events that are within the same temporal and spatial parameters but no more than 0.2 units of magnitude difference are considered doublets (Lay and Kanamori, 1980). Although clearly an oversimplification in some instances, these criteria enable both foreshocks and aftershocks to be easily distinguished from background seismicity. Only 37% of the events had detectable aftershock sequences, 26% had detectable foreshock sequences, and less than 4% meet the loose definition of a doublet. Fifteen transforms had at least three large events, and of those 15, only the remote Balleny-AAN OTF had no detected aftershocks; three did not have foreshock sequences.

The Blanco and Romanche transforms had the greatest percentage of aftershocks - 80% of their large events produced a detectable sequence. Event detection capabilities should be high for the Blanco OTF, since it lies off the U.S. western seaboard. The largest aftershock sequence occurs on the Blanco with 17 after shocks occurring after M_w 6.2 on 16 January, 2003. More than half of the

considered events did not produce a single detected aftershock and 70% of all the aftershock sequences only contain one detected event. Although it could be posited that magnitude 6 earthquakes may not produce detectable aftershocks on remote transforms, a number of large, $M_W \approx 7.0$ size events produced no detectable aftershock activity. Without a detailed investigation of detection thresholds, little can be said at this point, other than aftershock sequences along OTFs appear to have few large aftershocks.

The Menard and Bode Verde transforms have had the greatest percentage of detected foreshock sequences with 50% and 67% of the large events preceded by detected seismic activity. Again, interpretive caution is warranted without detailed information on detection results. However, this result may be biased by the crude 100km spatial parameter since both of these transforms are 200 km long. Two models are generally considered to describe a foreshock sequence, both of which were outlined by Dodge *et al.* (1996): The first is a cascade or rupture-controlled model, where an initial event triggers a sequence of events that culminate in the mainshock. In this view, large and small events initiate in the same way, but event size is controlled by the area of the rupturing asperity or the distance to a fault heterogeneity capable of stopping the rupture. A mainshock is a rupture that grows into a larger earthquake. The second foreshock model is the nucleation or pre-slip model, where aseismic slip occurs within the region of the hypocenter. This slip continues until the unstable, dynamic rupture of the mainshock is initiated. Pre-seismic slip has been studied in rock mechanic experiment and is known as the critical slip distance (D_C), which is observed to decrease with decreasing stress (Marone and Kilgore, 1993). The nucleation-controlled model may seem to make sense for oceanic transforms, since these faults fail primarily by aseismic slip.

B.1 OTF Mainshock/Aftershock Descriptive Statistics

I include the table of aftershock numbers for each OTF, as discussed in 1. Foreshocks and aftershocks were defined as an event that occurs within 100 km and 30 days of the mainshock and greater than 0.2 units of magnitude less than the

mainshock. Events that are within the same temporal and spatial parameters but no more than 0.2 units of magnitude difference are considered doublets (Lay and Kanamori, 1980).

Table B.1. List of oceanic transform earthquakes (M≥6) and associated foreshock and aftershock sequences from the USGS earthquake catalog (1963-2006).

Date	Time	Ms	Latitude	Longitude	No. Foreshocks	No. Aftershocks
Blanco-JDFR						
1981-11-03	13:47:34	6.2	43.542	-127.706	0	2
1985-03-13	19:34:57	6.3	43.510	-127.561	0	4
1994-10-27	17:45:58	6.0	43.515	-127.427	0	5
2000-06-02	11:13:49	6.0	44.513	-130.080	1	0
2003-01-16	00:53:15	6.0	44.284	-129.024	1	17
Bode Verde-MAR						
1970-11-29	06:01:18	6.0	-11.681	-14.087	1	1
1975-09-24	11:03:00	6.1	-11.960	-14.486	1	0
1998-06-18	04:17:54	6.1	-11.572	-13.894	0	0
Charlie Gibbs-MAR						
1974-10-16	05:45:09	6.9	52.636	-32.070	1	2
1998-02-16	23:53:19	6.6	52.718	-33.677	6	2
Chain-MAR						
1990-08-05	17:42:32	6.3	-1.080	-13.887	1	0
1992-08-28	18:18:46	7.0	-0.965	-13.562	0	0
1996-02-16	09:44:58	6.4	-1.496	-15.279	1	0
1996-02-18	23:49:28	6.5	-1.266	-14.273	0	1

Date	Time	Ms	Latitude	Longitude	No. Foreshocks	No. Aftershocks
2001-11-15	01:03:06	6.0	-1.587	-15.578	0	1
Chile-EPR						
1975-04-20	11:40:39	6.2	-36.403	-98.794	0	0
1979-04-14	10:00:24	6.5	-36.007	-102.601	0	0
1979-06-10	06:32:50	6.0	-36.280	-97.953	0	0
1997-05-29	17:02:38	6.1	-35.964	-102.511	0	0
1997-06-10	21:53:55	6.1	-35.815	-108.135	0	1
1999-12-10	18:38:30	6.2	-36.206	-97.316	0	2
Doldrums-MAR						
1977-04-04	17:52:19	6.0	7.301	-34.857	0	0
1979-06-10	06:49:51	6.0	8.106	-38.086	1	0
1984-11-01	04:48:50	7.1	8.185	-38.794	0	1
2004-01-16	18:07:55	6.0	7.641	-37.704	0	0
Eltanin-PAR						
1969-08-18	01:04:04	6.4	-56.022	-123.367	0	1
1971-04-04	10:15:37	6.6	-56.245	-122.459	0	0
1971-03-26	09:08:06	6.0	-55.439	-129.100	0	0
1972-05-07	22:06:30	6.3	-53.713	-134.214	0	0
1973-09-18	13:32:51	6.4	-54.518	-132.624	0	0
1979-03-12	06:38:11	6.1	-56.077	-122.440	0	0
1991-10-13	18:12:20	6.2	-56.097	-122.633	0	0
1993-04-18	14:10:38	6.1	-53.958	-133.868	0	0
1995-09-08	01:15:28	6.3	-56.222	-122.419	0	0
1997-09-03	06:22:44	6.0	-55.190	-128.989	0	0
2001-08-06	03:52:59	6.5	-55.537	-123.422	1	7
2002-04-24	11:00:00	6.0	-56.135	-122.312	0	0
Guafo-ANZ						
1978-05-29	17:20:28	6.0	-44.855	-79.413	0	0
Kangaroo-AAN						
1970-07-02	00:56:15	6.0	-51.035	139.487	0	0
1975-04-11	00:10:35	6.3	-50.803	139.095	0	0

Date	Time	Ms	Latitude	Longitude	No. Foreshocks	No. Aftershocks
1975-05-30	17:46:24	6.1	-50.416	139.351	0	1
1976-04-14	15:26:16	6.2	-51.905	139.471	0	0
1976-05-11	11:29:06	6.1	-51.506	139.678	0	0
1976-05-11	15:50:41	6.6	-51.603	139.683	2	0
1987-09-23	15:14:56	6.1	-50.716	139.279	0	1
1991-01-18	10:45:18	6.3	-51.145	139.415	1	0
1992-02-02	00:31:30	6.3	-51.547	139.704	1	0
1993-01-13	18:50:42	6.3	-50.791	139.505	0	0
2000-06-11	11:55:12	6.4	-50.579	139.550	0	1
2002-04-08	03:48:55	6.1	-51.068	139.269	0	1
2004-06-09	22:52:08	6.3	-51.603	139.615	2	0
Menard-PAR						
1983-01-26	04:43:20	6.0	-49.556	-114.079	1	0
1997-06-26	19:21:08	6.0	-49.692	-114.570	1	1
2003-08-28	04:48:19	6.1	-49.816	-114.811	0	0
2004-01-29	03:52:52	6.0	-50.206	-114.780	0	0
Mendocino-JDF						
1994-09-01	15:15:53	7.0	40.402	-125.680	0	2
N. Sandwich-MAR						
1973-04-07	12:22:47	6.7	-58.302	-13.394	0	1
1984-06-22	15:55:28	6.1	-58.318	-15.786	0	0
2004-02-21	02:34:42	6.5	-58.425	-14.963	0	1
Oceanographer-MAR						
1970-11-18	12:23:18	6.0	35.147	-35.736	1	0
1990-08-14	15:13:28	6.0	35.432	-35.648	0	0
Panama						
1968-06-15	07:08:48	6.0	5.602	-82.570	0	0
1982-08-19	15:59:01	6.5	6.718	-82.680	0	2
1990-05-08	00:01:40	6.3	6.905	-82.622	0	1
1999-03-31	05:54:42	6.1	5.827	-82.616	1	0

Date	Time	Ms	Latitude	Longitude	No. Foreshocks	No. Aftershocks
Romanche-MAR						
1971-08-05	01:58:51	6.3	-0.853	-22.130	0	2
1973-08-28	15:01:59	6.8	-0.189	-18.027	0	0
1981-07-07	21:10:57	6.4	-0.166	-18.837	0	1
1982-01-03	14:09:50	6.5	-0.972	-21.870	0	1
1986-06-24	06:56:54	6.0	-0.085	-17.824	0	1
1990-07-14	05:54:25	6.4	0.003	-17.376	0	1
1992-12-26	19:52:24	6.2	-0.564	-19.318	0	1
1994-03-14	04:30:07	6.0	-1.083	-23.929	1	0
1994-03-14	04:30:15	7.0	-1.278	-23.569	1	0
1995-05-18	00:06:27	6.2	-0.893	-21.996	0	1
2003-11-09	19:52:36	6.0	-0.674	-19.689	1	2
2005-01-12	08:40:03	6.0	-0.878	-21.194	0	1
S. Sandwich-AAN						
1969-10-01	19:53:15	6.0	-60.846	-19.723	0	0
1973-10-06	15:07:37	7.0	-60.823	-21.549	0	0
1977-02-10	22:41:06	6.2	-60.933	-23.090	0	0
1982-05-07	05:38:34	6.7	-60.597	-20.877	0	0
1983-10-22	04:21:35	6.8	-60.665	-25.451	0	9
1983-10-22	05:53:23	6.2	-60.404	-24.865	0	0
1983-10-22	13:07:39	6.1	-60.620	-25.392	0	0
1992-06-22	04:00:41	6.1	-60.728	-21.969	0	1
2006-01-02	06:10:49	7.3	-60.794	-21.480	0	0
St. Paul-MAR						
1972-04-11	02:21:15	6.4	0.967	-28.286	1	0
1973-10-11	02:07:52	6.3	0.636	-29.514	1	0
1975-10-07	08:28:09	6.7	0.898	-26.772	0	1
1985-06-06	02:40:12	6.5	0.932	-28.432	0	0
1985-10-12	22:20:38	6.0	0.917	-29.921	0	0
1993-09-20	10:17:42	6.0	0.750	-29.354	0	1

Date	Time	Ms	Latitude	Longitude	No. Foreshocks	No. Aftershocks
Balleny-AAN						
1971-08-11	14:23:31	6.1	-62.749	155.711	1	0
1974-10-11	08:33:52	6.1	-60.748	153.931	1	0
1981-06-13	01:26:03	6.0	-60.171	154.712	0	0
1991-12-17	03:41:08	6.1	-62.551	155.054	0	0
1992-11-04	01:59:26	6.2	-61.542	154.573	0	0
1995-02-03	02:31:35	6.3	-62.711	155.666	0	0
1995-06-21	15:28:51	6.7	-61.673	154.766	0	0
Tristan da Cunha						
1968-06-16	04:55:57	6.1	-36.175	-15.860	0	1
1979-05-16	02:27:00	6.2	-35.666	-16.242	0	0
1981-06-03	05:47:44	6.4	-35.560	-17.040	0	0
1989-09-13	11:40:46	6.2	-35.577	-17.063	1	1
Udintsev-PAR						
1970-08-24	12:30:19	6.4	-56.587	-142.483	0	0
1984-01-02	22:09:58	6.0	-56.745	-142.655	0	0
Vema-MAR						
1979-08-25	08:44:04	6.6	10.731	-41.688	0	0
1996-06-02	02:52:09	6.9	10.797	-42.254	1	0

Appendix C

Rayleigh-Wave Relative Location Sensitivity Analyses

In this appendix we explore how parameters and assumptions involved in the relative location process may affect the location results. In addition to illustrating the stability of the results, the analyses were used to select the best combination of slowness, correlation threshold, and maximum event-linking distance, and inversion stabilization parameters to insure quality locations. Before moving onto the results of numerical experiments, we present a sample of the waveform quality assignments, which are used to screen seismograms with little signal content from the relocation procedure. Figure C.1 shows an illustration from the four quality groups. Each waveform used in the inversion is examined and assigned one of these grades. Only waveforms with "C" quality or better are included in any of the relocation inversions.

C.1 Event-Linking Distance Sensitivity

The maximum event-linking distance proved to be the most important parameter in the relocation process. The value is used to insure that events only within a certain distance are linked together. We tested linking distances of 25 km, 50 km, and 125 km, and compared the results from each linking distance to observations from the NEIC and Harvard CMT catalogs. We also compared the spatial alignment of our relative locations with known bathymetry of the transform system.

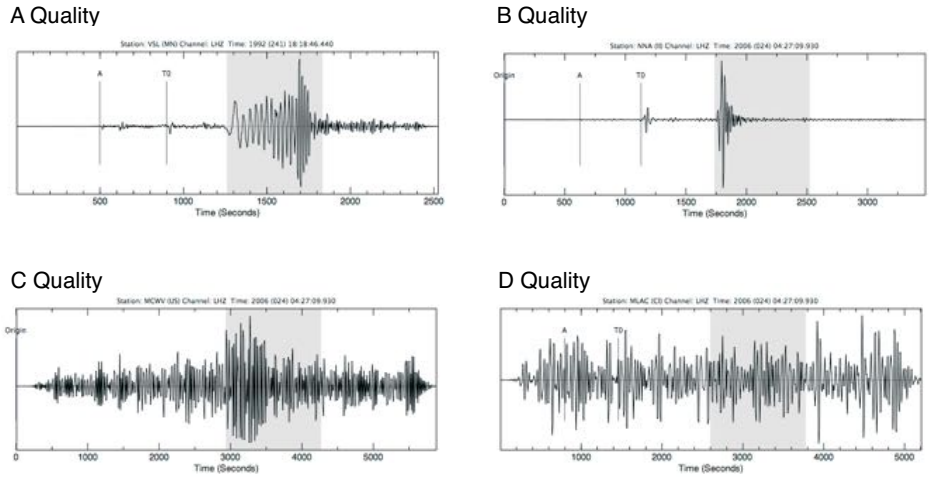

Figure C.1. Examples of the quality of graded event waveforms. "A" is the highest quality, while "F" is the lowest. The "A" quality event has not been filtered, while all others have been band-passed from 30 to 80 s. The better the quality of the waveform the more heavily it is weighted in the inversion. The shaded area highlights the 2.75 to 4.00 km/s group velocity window.

We illustrate the sensitivities using observations from the Eltanin OTF.

Figure C.2 shows locations from the NEIC and Harvard CMT catalogs. The CMT centroid locations appear to define linear features across the region better than the body-wave derived hypocenters of the NEIC. Figure C.3 shows our relative locations at the three prescribed maximum event-linking distances. With a 25 km maximum linking distance, a clearer image of the fault system begins to emerge from the NEIC locations and some of the events start to mimic the bathymetry, however, a good percentage of events remain scattered. Only the tight clusters delineate sharp features. The 25 km linking distance may be less than the uncertainty of the original NEIC locations and the minimal number of links for such a conservative linking distance limits our ability to recover a true picture of the activity. With a 50 km maximum event-linking distance we can the relative relocations delineate the three transforms that make up the Eltanin system. Most locations mimic the OTF bathymetry well. A large offset between two groups of earthquakes on the middle transform (Tharp OTF) is apparent and a smaller offset between to groups of earthquakes on the Hollister transform (westernmost structure). With a 125 km maximum event-linking distance, the relocations produce a

very clean image of the Eltanin system. The locations almost perfectly mimic the bathymetry and azimuthal orientation of the Eltanin transforms. The locations begin and terminate almost exactly at the ridge-transform intersections.

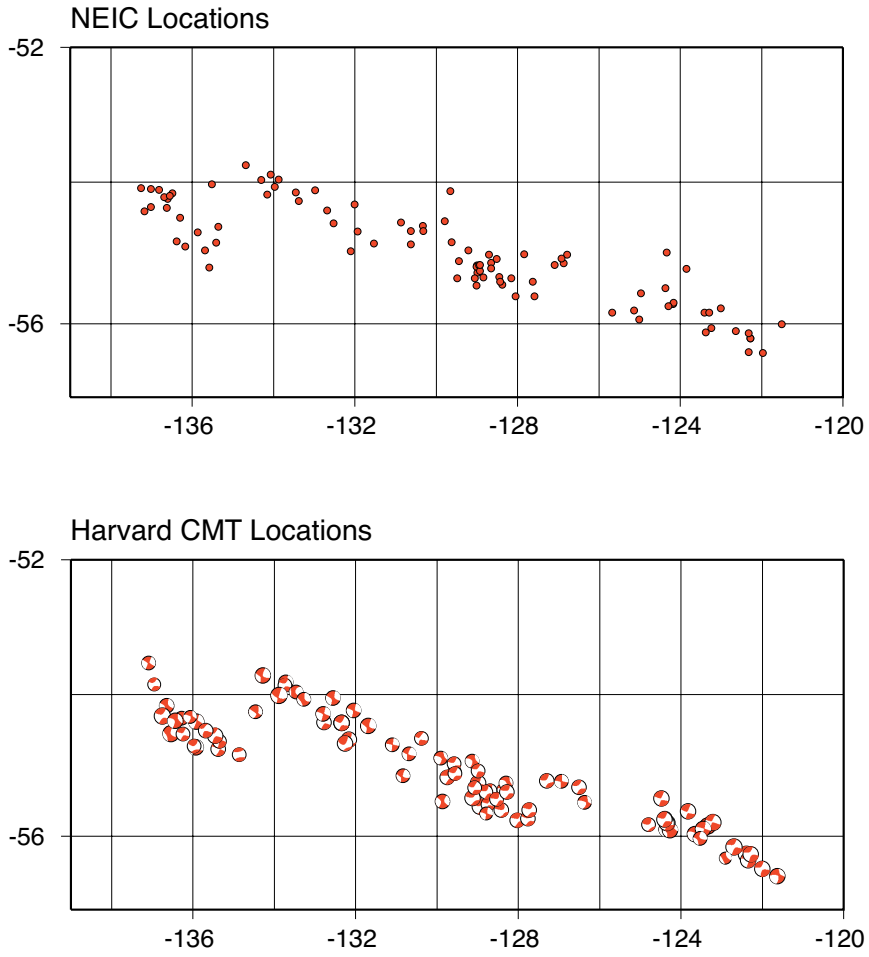

Figure C.2. Event locations from the NEIC and the Harvard CMT catalogs for events on the Eltanin OTF.

C.2 Rayleigh-Wave Slowness Sensitivity

We also conducted experiments to explore the sensitivity of the locations to the assumed Rayleigh wave slowness for the source region. We tested slowness values of 0.255 s/km and 0.300 s/km, which bracket the acceptable range for oceanic lithosphere (Nishimura and Forsythe, 1989). Once again have used our observations

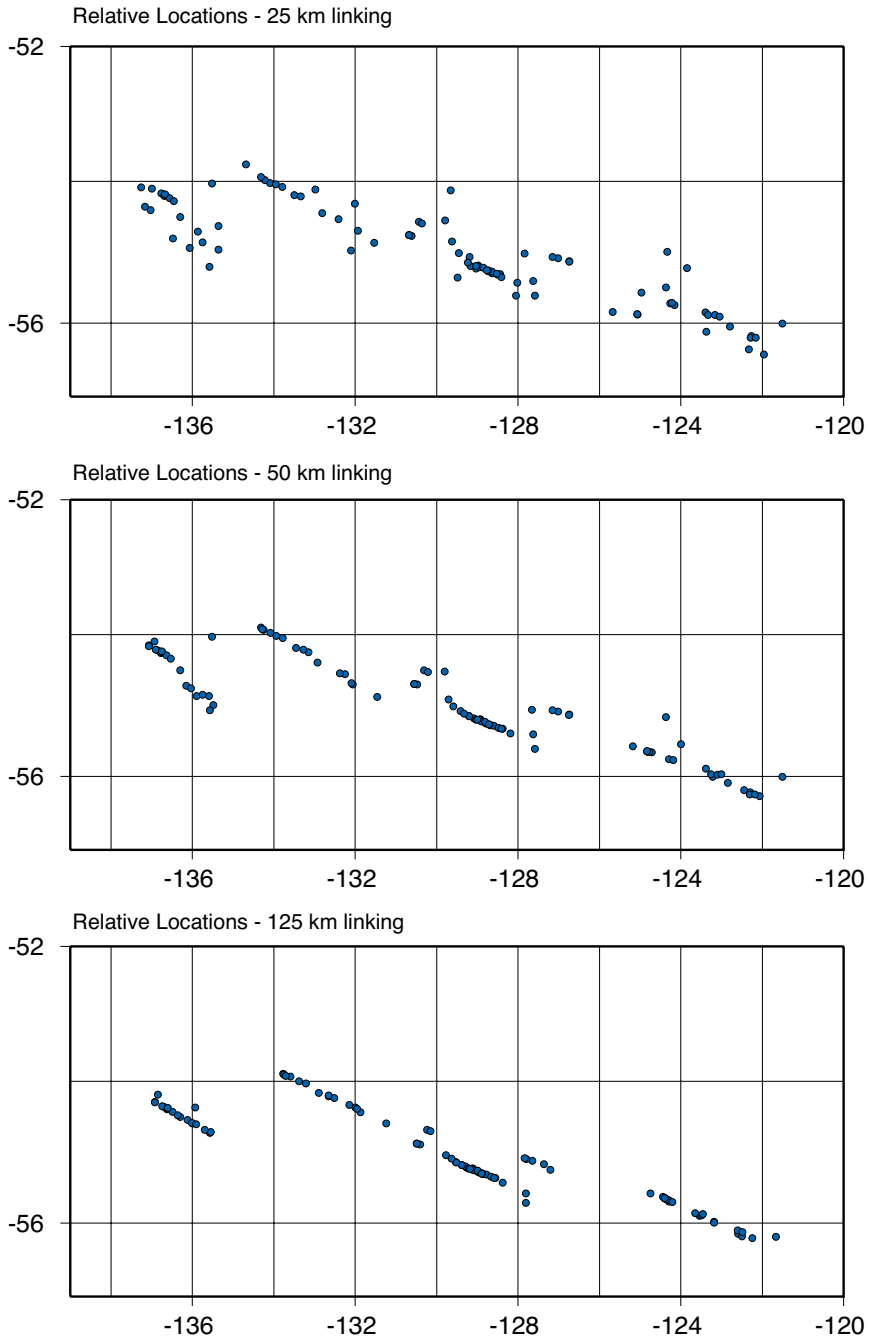

Figure C.3. Linking distance comparison using events from the Eltanin OTF. The 125 km linking distance shows the best conformation to transform morphology.

from the Eltanin OTF to illustrate the experiment results. The results are shown in Figure C.4, where the two patterns were offset to facilitate a convenient comparison. As expected, using the lower slowness value produces a pattern slightly expanded compared with the higher value. The faster the Rayleigh waves, the greater the event separation in the relocations. The most notable difference occurred on the Tharp (middle) transform, which shows the same first-order features regardless of which slowness that we choose.

Figure C.4. Comparison of slowness factor for events on the Eltanin OTF. We see that the greater slowness factor actually compresses the events spatially, however the overall relative pattern remains the same.

C.3 Cross-Correlation Threshold Sensitivity

The cross-correlation threshold is used to discard waveform phase shifts that don't produce a cross correlation equal to or greater than this threshold (as measured by the peak amplitude of the normalized cross correlation). We used a value of 75% for the inversions presented in the main body of the thesis; a typical value assumed in waveform correlation based location methods. In this section we examine the effect of this choice on the results from a test we conducted to see how the level of cross-correlation between waveforms may affect our final locations. We used both 50% and 75% correlation values for this test and our observations come from the Balleny OTF. The results are shown in C.5. Little change occurs in our locations between the two correlation values - no first-order trends in the locations

are notable.

C.4 Minimum Length Weight Sensitivity

Virtually all geophysical inversions require some numerical stabilization. The inversion was constructed in a manner to allow constraints on the size of the correction vector (minimum length constraints). We conducted numerical experiments to see how different values of minimum length weight affect our final locations. The results are shown in Figure C.6. The numbers correspond to a scalar parameter, σ that is used to adjust the importance of a minimum length constraint to equation 2.1.

$$\begin{pmatrix} P \\ \sigma I \end{pmatrix} \delta\mathbf{h} = \begin{pmatrix} \delta\mathbf{t} \\ \mathbf{0} \end{pmatrix} \tag{C.1}$$

The primary result was that using a smaller minimum length weight resulted in a smaller number of iterations necessary before the inversion converged to stable locations and a small misfit. Our observations for this test come from the Balleny OTF (Figure C.6). Higher values produced several outlying event locations. Again, the main results in the locations do not seem to be sensitive to the assumed parameter.

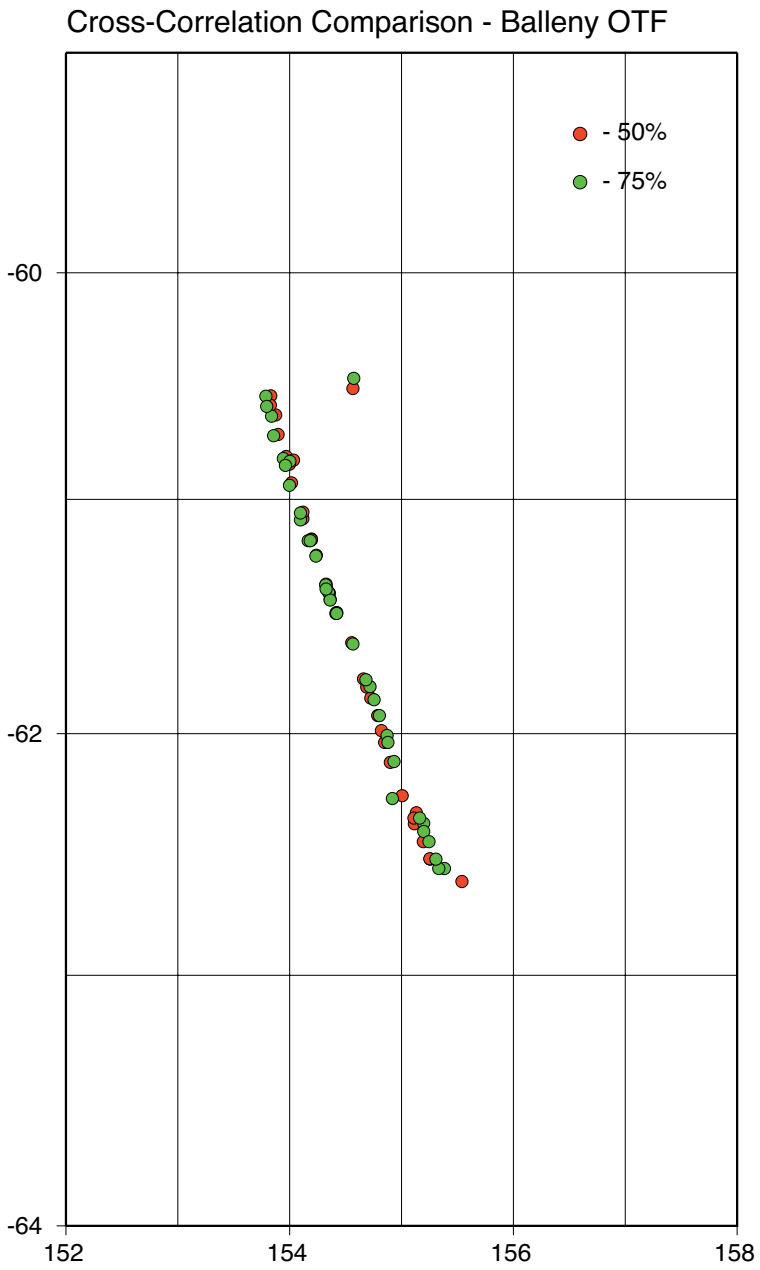

Figure C.5. Comparison of cross-correlation levels for events on the Balleny OTF. We note no major change to relative locations between the 50% and 75% threshold values.

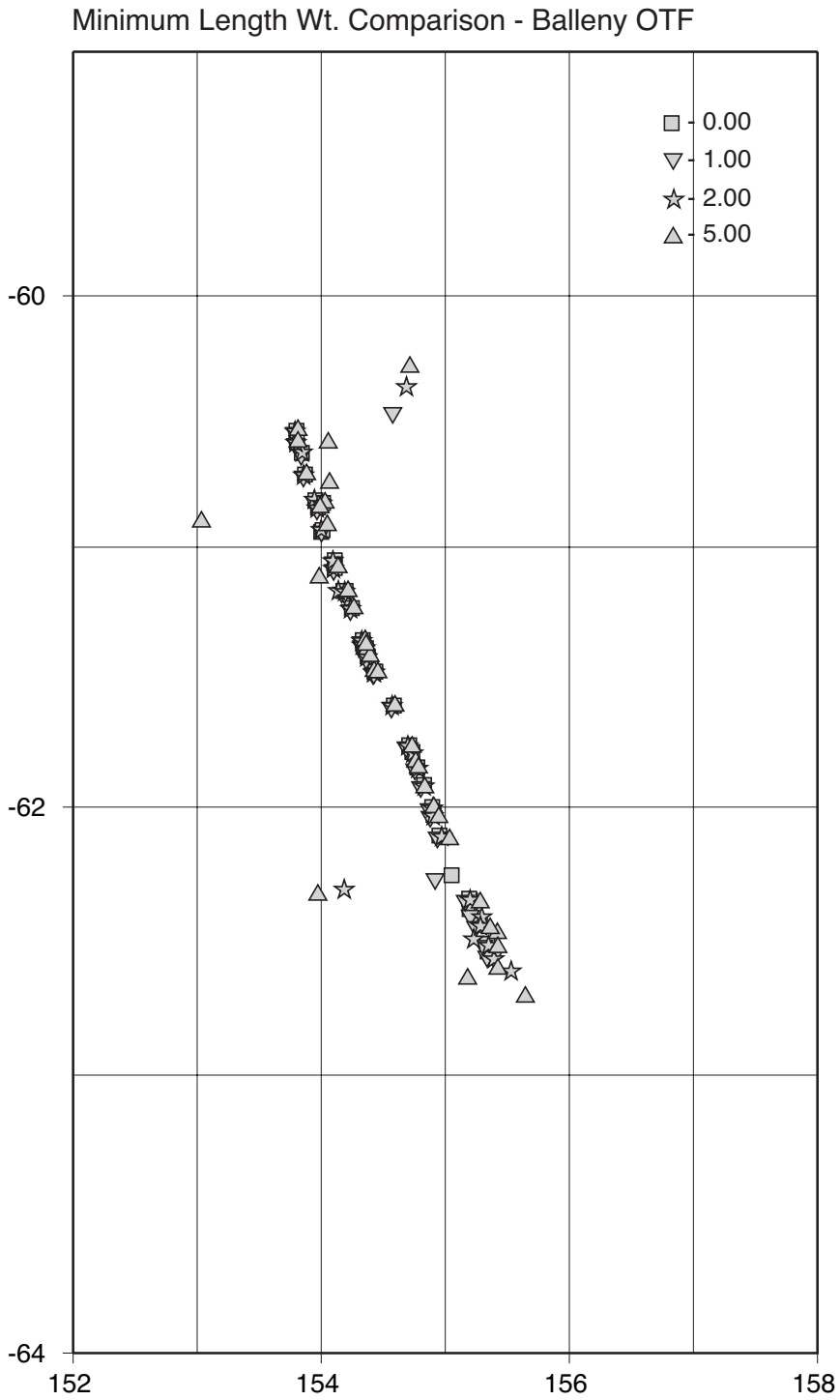

Figure C.6. Comparison of minimum weight length values for events on the Balleny OTF. Values of 2 and 5 increase the number of outlier events.

Bibliography

[1] Abe, K., Reliable estimates of the seismic moment of large earthquakes, *J. Phys. Earth*, **23**, 381-390, 1975.

[2] Abe, K., and H. Kanamori, Magnitudes of great shallow earthquakes from 1953 to 1977, *Tectonophysics*, **62**, 191203, 1980.

[3] Abercrombie, R. E., and G. Ekstrom, Earthquake slip on oceanic transform faults, *Nature*, **410**, 74-77, 2001.

[4] Ammon, C J, Relative Earthquake Location Using Surface Waves, *Eos Trans. AGU, 85(47), Fall Meet. Suppl., Abstract S11B-1015*, 2004.

[5] Anderson-Fontana, S., J. F. Engeln, P. Lundgren, R. L. Larson, and S. Stein, Tectonics of the Nazca-Antarctic plate boundary, *Earth Planet. Sci. Lett.*, **86**, 46-56, 1987.

[6] Bird, P., Y. Y. Kagan, and D. D. Jackson, Plate tectonics and earthquake potential of spreading ridges and oceanic transform faults, in *Plate Boundary Zones*, *Geodynamics Series*, **30**, S. Stein and J.T. Freymueller (Editors), American Geophysical Union, Washington, D.C., 203-218, 2002.

[7] Burr, N., and S. Solomon, The relationship of source parameter of oceanic transform earthquakes to plate velocity and transform length, *J. Geophys. Res.*, **83**, 1193-1205, 1978.

[8] Chen, Y., Thermal model of oceanic transform faults, *J. Geophys. Res.*, **93**, 8839-8851, 1988.

[9] Chen, Y., A mechanical model for the inside corner uplift at a ridge-transform intersection, *J. Geophys. Res.*, **94**, 9,275-9,282, 1989.

[10] DeMets, C., R. G. Gordon, D. F. Argus, and S. Stein, Effect of recent revisions to the geomagnetic reversal time scale on estimate of current plate motions, *Geophys. Res. Lett.*, **21**, 2191-2194, 1994.

[11] Detrick, R. S., R. S. White, G. M. Purdy, Crustal structure of North Atlantic fracture zones, *Rev. Geophys.*, **31**, 439-458, 1993.

[12] Dodge, D. A., G. C. Beroza, and W. L. Ellsworth, Detailed observations of California foreshock sequences: Implications for the earthquake initiation process, *J. Geophys. Res.*, **101**, 22,371-22,392, 1996.

[13] Duda, S. J., Strain release in the Circum-Pacific Belt, Chile: 1960,*J. Geophys. Res.*, **68**, 5531-5544, 1963.

[14] Duda, S. J., Secular seismic release in the circum-Pacific belt, *Tectonophysics*, **2**, 409452, 1965.

[15] Dziewonski, A. M. and D. L. Anderson, Preliminary Reference Earth Model (PREM), *Phys. Earth Planet. Inter.*, **25**, 297-356, 1981.

[16] Dziewonski, A. M., T. A. Chou, and J. H. Woodhouse, Determination of earthquake source parameters from waveform data for studies of global and regional seismicity, *J. Geophys. Res.*, **86**, 2825-2852, 1981.

[17] Engeln, J. F., D. A. Wiens, and S. Stein, Mechanism and depths of Atlantic transform earthquakes, *J. Geophys. Res.*, **91**, 548-577, 1986.

[18] Escartin, J., G. Hirth, B. Evans, Strength of slightly serpentinized peridotites: Implications for the tectonics of the oceanic lithosphere, *Geology*, **29**, 1023-1026, 2001.

[19] Fisk, M. R., R. A. Duncan, C. G. Fox, and J. B. Witter, Emergence and petrology of the Mendocino Ridge, *Mar. Geophys. Res.*, **15**, 283-296, 1993.

[20] Forsythe, D. W., Y. Yang, M.-D. Mangriotis, and Y. Shen, Coupled seismic slip on adjacent oceanic transform faults, *Geophys. Res. Lett.*, **30**, 20-1-20-4, 2003.

[21] Frolich, C. and K. D. Apperson, Earthquake focal mechanisms, moment tensors, and the consistency of seismic activity near plate boundaries, *Tectonics*, **11**, 279-296, 1992.

[22] Frolich, C. and S. D. Davis, Teleseismic values; or, much ado about 1.0. *J. Geophys. Res.*, **98**, 631-644, 1993.

[23] Furlong, K. P., Rheologic complications along large offset transform faults (abstract), *EOS Transactions, American Geophysical Union*, **73**, 550, 1992.

[24] Furlong, K. P., S. D. Sheaffer, and R. Malservisi, Thermal-rheological controls within oceanic transforms, *The Nature and Tectonic Significance of Fault Zone Weakening, Geological Society of London, Special Publications*, **186**, 65-83, 2001.

[25] Godfrey, N. J., A. S. Meltzer, S. L. Klemperer, A. M. Trehu, B. Leitner, S. H. Clarke, and A. Ondrus, Evolution of the Gorda Escarpment, San Andreas Fault and Mendocino triple junction from multichannel seismic data collected across the northern Viscaino block, offshore northern California, *J. Geophys. Res.*, **103**, 22,813-22,825, 1998.

[26] Gomberg, J., P. Bodin, K. Larson, and H. Dragert, Earthquake nucleation by transient deformations caused by the M=7.9 Denali, Alaska, earthquake, *Nature*, **427**, 621-624.

[27] Gomberg, J., Earthquake triggering by seismic wave following the Landers and Hector Mine earthquakes, *Nature*, **411**, 462-466, 2001.

[28] Gudmundsson, A., Dynamics of volcanic systems in Iceland: Example of tectonism and volcanism at juxtaposed hotspot and mid-ocean ridge systems, *Annu. Rev. Earth Planet. Sci.*, **28**, 107-140, 2000.

[29] Gutenberg, B., The energy of earthquakes, *Q. J. Geol. Soc. London*, **112**, 1-14, 1956.

[30] Gutenberg, B. and C. F. Richter, Seimicity of the Earth and Associated Phenomena, Princeton University Press, Princeton, N.J., 2nd Ed., 310 pp., 1954.

[31] Ihmle, P. F., T. H. Jordan, Teleseismic search for slow precursors to large earthquakes, *Science*, **266**, 1547-1551, 1994.

[32] Kanamori, H., Magnitude scale and quantification of earthquakes. In: S. J. Duda and K. Aki (Editors), Quantification of Earthquakes. *Tectonophysics*, **93**, 185-199, 1983.

[33] Kanamori, H. and E. E. Brodsky, The physics of earthquakes, *Rep. Prog. Phys.*, **67**, 1429-1496, 2004.

[34] Kilb, D., A strong correlation between induced peak dynamic Coulomb stress change from the 1992 M7.3 Landers, California, earthquake and the hypocenter of the 1999 M7.1 Hector Mine, California, earthquake, *J. Geophys. Res.*, **108**, 10-17, 2003.

[35] Kisslenger, C. and M. Jones, Properties of aftershock sequences in Southern California, *J. Geophys. Res.*, **96**, 11,947-11,958, 1991.

[36] Lay, T. and H. Kanamori, Earthquake doublets in the Solomon Islands, *Phys. Earth Planet. Inter.*, **21**, 283-304, 1980.

[37] Lay, T., H. Kanamori, and L. Ruff, The asperity model and the nature of large subduction zone earthquakes, *Earthquake Prediction Research*, **1**, 3-71, 1982.

[38] Ligi, M., E. Bonatti, L. Gasperini, and A. N. B. Poliakov, Ocean broad multifault transform plate boundaries, *Geol. Soc. Am.*, **30**, 11-14, 2002.

[39] Lonesdale, P., Structural geomorphology of the Eltanin Fault System and adjacent transform faults of the Pacific-Antarctic plate boundary, *Mar. Geophys. Res.*, **16**, 105-143, 1994.

[40] Marone, C., Shaking faults loose, *Nature*, **408**, 535, 2000.

[41] Marone, C. and B. Kilgore, Scaling of the critical slip distance for seismic faulting with shear strain in fault zones, *Nature*, **362**, 618-621, 1993.

[42] McGuire, J. J., P. F. Ihmle, and T. H. Jordan, Time-domain observations of a slow precursor to the 1994 Romanche transform earthquake, *Science*, **274**, 82-85, 1996.

[43] McGuire, J. J., Immediate foreshock sequences of oceanic transform earthquakes on the East Pacific Rise, *Bull. Seism. Soc. Am.*, **93**, 948-952, 2003.

[44] Menard, H. W., The East Pacific Rise, *Science*, **132**, 1737-1746, 1960.

[45] Okal, E. A. and A. R. Langenhorst, Seismic properties of the Eltanin Transform System, South Pacific, *Phys. Earth Planet Inter.*, **119**, 185-208, 2000.

[46] Pacheco, J., and L. R. Sykes, Seismic moment catalog of large shallow earthquakes, 1900 to 1989, *Bull. Seism. Soc. Am.*, **82**, 1306-1349, 1992.

[47] Parson, L. M. and R. C. Searle, Strike-slip fault styles in slow-slipping oceanic transform faults–evidence from GLORIA surveys of Atlantis and Romanche Fracture Zones, *Journal of the Geological Society, London*, **143**, 757-761, 1986.

[48] Perez-Campos, X., J. J. McGuire, and G. C. Beroza, Resolution of the slow earthquake/high apparent stress paradox for oceanic transform fault earthquakes, *J. Geophys. Res.*, **108**, ESE 15-1-15-8, 2003.

[49] Scholz, C. H., The Mechanics of Earthquakes and Faulting, Cambridge University Press, Cambridge, UK, 2nd Ed., 471 pp., 2002.

[50] Searle, R. C., GLORIA investigations of oceanic fracture zones: comparative study of the transform fault zone, *Journal of the Geological Society, London*, **143**, 743-756, 1986.

[51] Searle, R. C., M. V. Thomas, and E. J. W. Jones, Morphology and tectonics of the Romanche Transform and its environs, *Mar. Geophys. Res.* **16**, 427-453, 1994.

[52] Stein, S., A model for the relation between spreading rate and oblique spreading, *Earth Planet. Sci. Lett.*, **39**, 313-318, 1978.

[53] Stein, S., T. C. Hanks, M6 earthquakes in Southern California during the twentieth century: no evidence for a seismic moment deficit, *Bull. Seism. Soc. Am.*, **88**, 635-652, 1998.

[54] Stein, R. S., The role of stress transfer in earthquake occurrence, *Nature*, **402**, 605-609, 1999.

[55] Stein, S., and M. Wysession, An introduction to seismology, earthquakes, and Earth structure, Blackwell Publishing, Malden, MA, 498 pp., 2003.

[56] , Stoddard, P. R., A kinematic model for the evolution of the Gorda Plate, *J. Geophys. Res.*, **92**, 11,524-11,532, 1987.

[57] Sykes, L. R., Seismicity of the South Pacific Ocean, *J. Geophys. Res.*, **68**, 5,999-6,006, 1963.

[58] Velasco, A. A., C. J. Ammon, and T. Lay, Recent large earthquakes near Cape Mendocino and in the Gorda Plate: Broadband source-time functions, fault orientations, and rupture complexities, *J. Geophys. Res.*, **99**, 711-728, 1994.

[59] Waldhauser, F. and W. L. Ellsworth, A double-difference location algorithm: Method and application to the Northern Hayward Fault, California, *Bull. Soc. Seism. Am*, **90**, 1353-1368, 2000.

[60] Wells, D. L. and K. J. Coppersmith, New empirical relationships among magnitude, rupture length, rupture width, rupture area, and surface displacement, *Bull. Seism. Soc. Am.*, **84**, 974-1,002, 1994.

[61] West, M., J. J. Sanchez, and S. R. McNutt, Periodically triggered seismicity at Mount Wrangell, Alaska, after the Sumatra earthquake, *Science*, **308**, 1144-1146, 2005.

[62] Wilson, D. S., Deformation of the so-called Gorda Plate, *J. Geophys. Res.*, **94**, 3,065-3,075, 1989.

[63] Wilson, J. T., A new class of faults and their bearing on continental drift, *Nature*, **207**, 343-347, 1965a.